E.O. Paton Electric Welding Institute of the National Academy of Sciences of Ukraine

International Scientific-Technical and Production Journal

The Paton WELDING JOURNAL

March **2017**
No. 3

Published since 2000

English translation of the monthly «Avtomaticheskaya Svarka» (Automatic Welding) journal published in Russian since 1948

Founders
E.O. Paton Electric Welding Institute, NASU
International Association «Welding»

Publisher
International Association «Welding»

Translators
A.A. Fomin, O.S. Kurochko, I.N. Kutianova
Editor
N.G. Khomenko
Electron galley
D.I. Sereda, T.Yu. Snegiryova

Address
E.O. Paton Electric Welding Institute,
International Association «Welding»
11 Kazimir Malevich Str. (former Bozhenko Str.),
03680, Kiev, Ukraine
Tel.: (38044) 200 60 16, 200 82 77
Fax: (38044) 200 82 77, 200 81 45
E-mail: journal@paton.kiev.ua
www.patonpublishinghouse.com

State Registration Certificate
KV 4790 of 09.01.2001
ISSN 0957-798X

Subscriptions
$348, 12 issues per year,
air postage and packaging included.
Back issues available.

CONTENTS

SCIENTIFIC AND TECHNICAL

INDUSTRIAL

doi.org/10.15407/tpwj2017.03.01

APPLICATION OF ADDITIVE ELECTRON BEAM TECHNOLOGIES FOR MANUFACTURE OF PARTS OF VT1-0 TITANIUM ALLOY POWDERS

V.M. NESTERENKOV[1], **V.A. MATVEJCHUK**[1], **M.O. RUSYNIK**[1] and **A.V. OVCHINNIKOV**[2]
[1]E.O. Paton Electric Welding Institute, NASU
11 Kazimir Malevich Str., 03680, Kiev, Ukraine. E-mail: office@paton.kiev.ua
[2]Zaporozhye National Technical University
64 Zhukovskogo Str., 09063, Zaporozhye, Ukraine. E-mail: iaov@rambler.ru

The possibility was investigated of application of hydration-dehydration (HDH) titanium powders of domestic production for manufacture of parts using additive electron beam melting on SV-212M installations. HDH powder of commercially pure VT1-0 grade titanium was used for investigations. The elements of technology of part manufacture by 3D layer-by-layer deposition were developed. Part specimens of set shape and 12×12×100 mm size were produced and investigated. Structures of deposited layers were investigated. Absence of porosity and lack of fusion in the produced specimens of the part was noted. The possibility is shown of development of the set shape parts by additive electron beam deposition methods using VT1-0 titanium powder of domestic production. 9 Ref., 1 Table, 12 Figures.

Keywords: *electron beam, layer, additive technologies, titanium powder, structure*

Additive technologies (AT) have found wide application and commercial distribution in manufacture of high-strength volumetric parts of metallic powders. Selective laser melting (SLM) technologies, providing formation of the parts by means of gas-shielded fusion of metal powder using laser beam, and electron beam melting (EBM) technologies, directed on formation of the parts by metal powder using electron beam in vacuum chamber, are mostly used for these purposes.

These technologies are of the great interest for manufacture of complex parts applied in aircraft engine-building. A stable tendency of the last years is implementation of AT in the leading aircraft engine-building companies [1]. «Growing» of the parts using powder materials of titanium alloys [2] for commercial enterprises of domestic machine-building (OJSC «Motor Sich», Gas Turbine Research & Production Complex Zorya-Mashproekt, SE Lutsk Repair Plant «Motor») is a relevant problem in manufacture and repair of gas-turbine engines (GTE), since large number of GDE components are made of these alloys. Traditionally, remelting of titanium alloys for aircraft equipment is carried out in vacuum, laser and gas-shielded arc welding as well as electron beam welding (EBW) are used for welding and surfacing. 3D deposition based on electron beam technologies is good to use in manufacture of aircraft parts of titanium alloys. It allows manufacturing virtually all GDE components providing high-efficient vacuum protection of weld pool deposited metal. Several of engineering solutions [3] are available today. They show the possibility of manufacture of titanium parts using EBW. However, consumables used in these installations, namely titanium alloy powders, have a number of disadvantages. Among them are lack of conformity of powder materials to large number of alloys certified in CIS countries, high price — more than 500 U.S. dollars per 1 kg of powder as well as absence of domestic commercial technologies of their manufacture. Thus, there is a problem of import substitution and supply of raw materials for the equipment used in additive manufacturing.

A relevant problem is a development of installations based on EBW processes using domestic powder materials.

From point of view of EBW technology domestic manufacturers have wide experience of welding and surfacing of titanium alloys, including with complex multi-coordinate system for movement of electron beam guns and deposited parts [3–7]. This provides the background for development of own installations based on electron beam technologies. The problem of application of titanium powder materials of domestic production can be solved applying non-spherical titanium alloys based on hydration-dehydration (HDH) technology [6]. SE SRD Titanium Institute together with STC Titan Zaporozhye ZNTU proposes an innovative technology of manufacture of low prime cost titanium powders from sponge titanium or other titanium containing materials of different quality and fractional composition using hydration-dehydration method [8].

The following problems were solved in this direction, namely providing the necessary chemical and grain-size compositions of powders and possibility of their serial production in Ukraine, which allows forming the price of these materials at the level of 100 U.S. dollars per 1

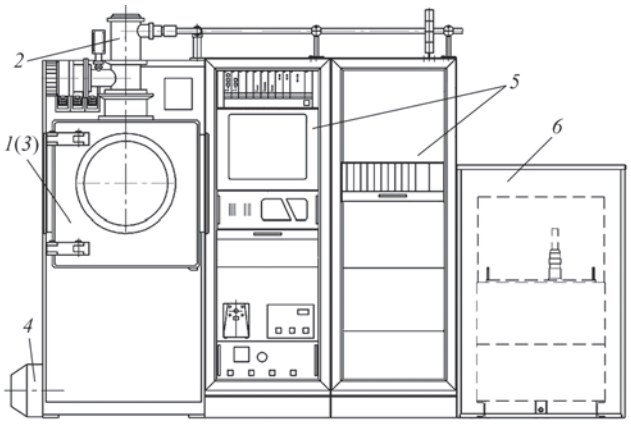

Figure 1. Scheme of SV-212M installation (description *1–6*, see in the text)

kg of powder. However, issues of application of these powder materials for additive processes are still open.

Titanium is a chemically-active metal. Electron beam technologies in vacuum chamber guarantees secure protection of molten and cooling metal, therefore they seem to be the most perspective for development of a technology of direct generation of titanium metallic parts by 3D deposition methods [5].

There are no serially produced domestic installations for this purpose. Foreign manufacturers deliver «key-turn» technology, which does not provide flexibility of manufacture with possibility to replace the raw materials by analogues [7]. The main constraint of commercial development of additive technologies for manufacture and repair of GTE parts in Ukraine is high price of powders [1], therefore application of domestic titanium alloy powders is so perspective.

Aim of the present paper is investigation of possibility of application of titanium alloy powders of domestic production for manufacture of set shape parts by additive electron beam melting.

Non-spherical powder of VT1-0 titanium alloy, provided by STC Titan Zaporozhye ZNTU, was used for manufacture of the parts.

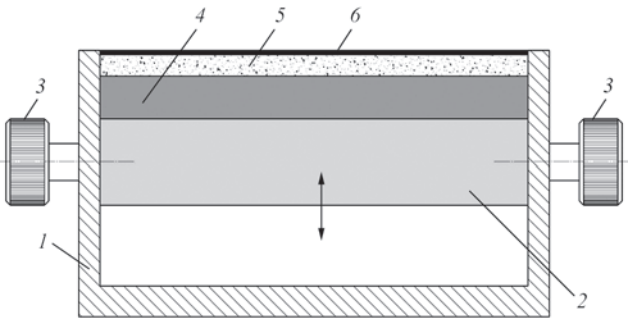

Figure 3. Scheme of modulus for 3D deposition (description *1–7* see in the text); arrow shows direction of table movement

Materials and investigation procedure. The work was carried out on small-size electron beam welding (EBW) installation of SV-212M type with pulse power source 60 kV/60 kW, electron beam gun ELA-60 and application software package for EBW. Equipment and software were developed at the E.O. Paton Electric Welding Institute. Figure 1 presents equipment appearance.

The installation consists of a small-size vacuum chamber *1*, equipped with mobile table and fixed fixture *3* for part growing. Electron beam gun *2* is located on the vacuum chamber. Vacuum system of the installation (pos. 4) provides for value of vacuum in the chamber less than 10^{-4} Torr. Control cabinet *5* contains commercial computer, screen, blocks for control of high-voltage power source and vacuum system. High-voltage source *6* allows obtaining variable voltage to 65 kV and beam current to 1 A.

Figure 2 shows a block diagram of equipment for additive electron beam melting.

A beam of electrons, necessary for heating of the surface with deposited metallic powder, is formed in the electron beam gun (EBG), which is supplied from high-voltage power source. The source is regulated with commercial computer. The systems for control of focusing and beam current are embedded the source. A generator, developing scanning control signals, is

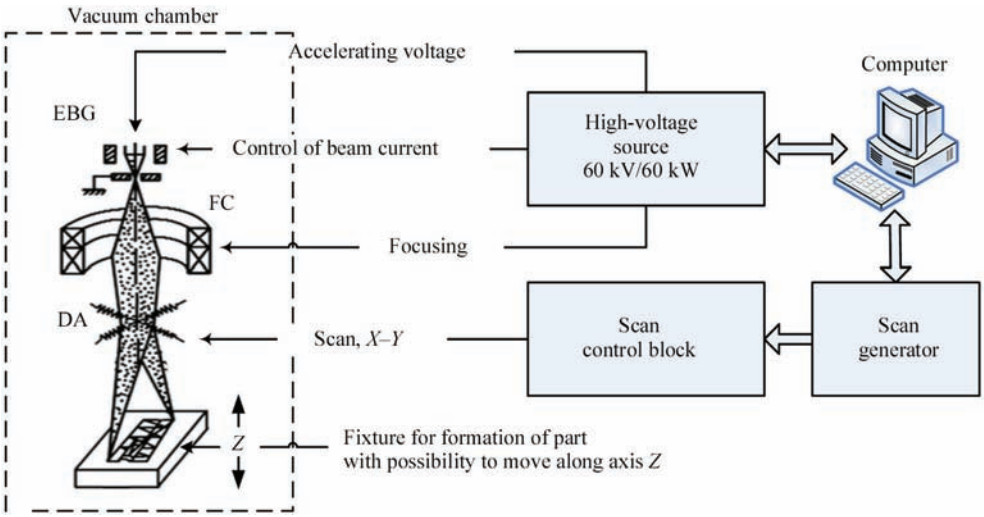

Figure 2. Block diagram of equipment for additive electron beam deposition: EBG — electron beam gun; FC — focusing coil of EBG; DA — EBG deflection-coil assembly

Process characteristics and composition of powder materials of HDH titanium VT1-0

Fraction, μm	Density g/cm^3	Content of additives, wt.%					
		N	C	H	Fe	Si	O
100–160	1.7	≤0.05	≤0.1	0.012	≤0.3	≤0.15	≤0.15
63–100	1.8	≤0.05	≤0.1	0.012	≤0.3	≤0.15	≤0.15

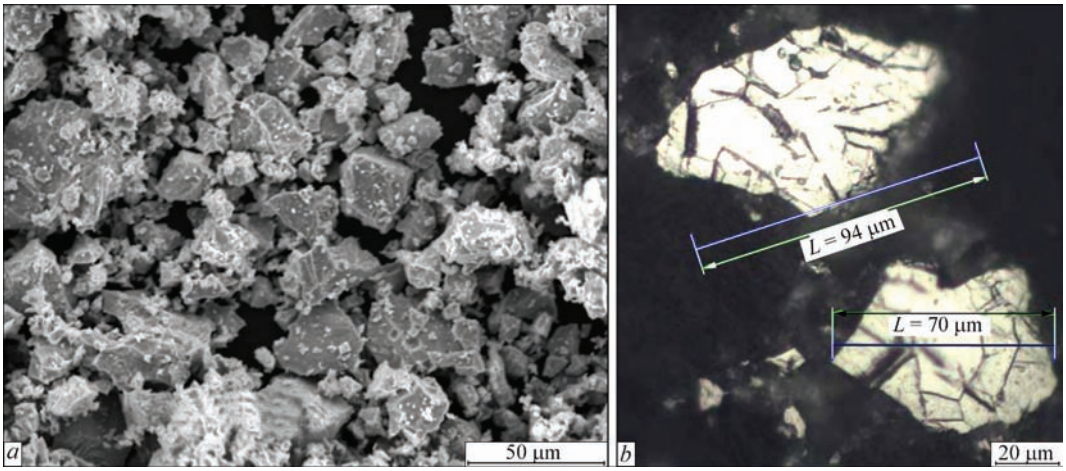

Figure 4. Appearance (*a*) and microstructure (*b*) of HDH powder VT1-0 of 63–100 μm fraction, used for deposition

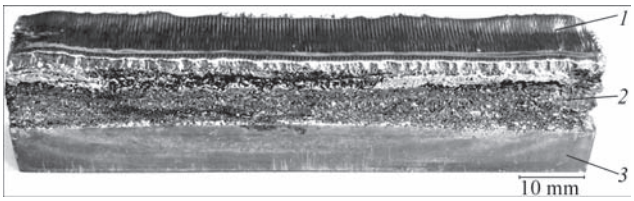

Figure 5. Specimen of part, made by electron beam 3D-deposition method: *1* — upper layer of deposited metal; *2* — interlayer of metal with particles of unmelted powder; *3* — titanium substrate

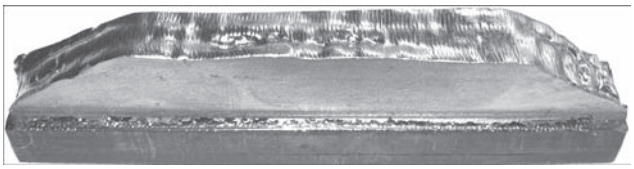

Figure 6. Part after machining

used for melting zone formation. These signals are accelerated in the scanning control block and supplied to EBG deflection coils. The beam of electrons is deflected on *X* and *Y* axes and creates a melting zone of set shape. The process is done following the program in accordance with the process modes. Beam current, focusing current and beam deviation on *X* and *Y* axes are the control objects.

A module of layer-by-layer feeding of powder consumables (Figure 3) was developed to realize the additive processes on standard EBW installation.

This module was installed in a working vacuum chamber. Its structure provided realization of the following process factors, namely change of a layer of powder materials in 50 to 500 μm range; clear formation of 100×15×50 mm working space; application of removable titanium substrate, variation of level of compaction of bulk powder layer. Developed module provides for a possibility of application of spherical as well as pilot non-spherical powder traditionally used in 3D printing machines. An important peculiarity of this device is possibility of powder compaction, which allows rising layer density [9] for non-spherical powders. The module consists of body *1* and table *2* being moved along the vertical line. The table is moved in vertical direction, at that its position is fixed

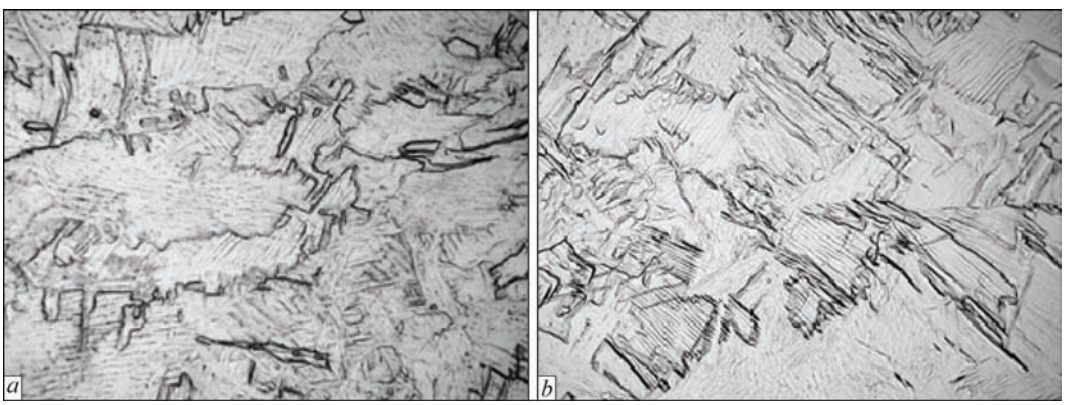

Figure 7. Microstructure (×200) of metal in layer center: *a* — layer up to 100 μm; *b* — layer of more than 100 μm

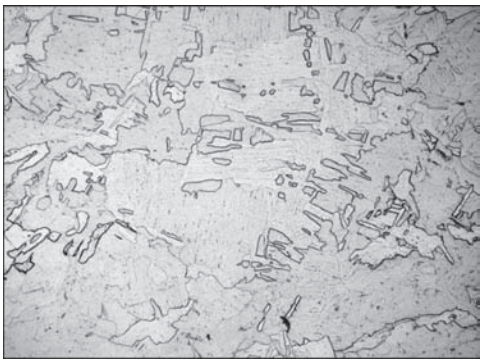

Figure 8. Microstructure (×100) of deposited metal close to fusion line

Figure 10. Microstructure (×100) of metal of deposited outer layers

by screws *3*. Titanium substrate *4* is set on the table and part *5* is built-up on it. The powder is deposited on the substrate with the help of dosing unit. Surpluses are removed by a scrapper, after what the layer is compacted using special forming device if necessary. At that smooth surface with uniformly distributed layer of powder *6* is formed. Before deposition of the next layer, the table is moved down to set value, which is controlled by clockwork type micrometer. At that, distance between an EBM cathode and surface of melting zone is kept fixed and does not change in process of creation of the whole part.

Electron beam melting process takes place in vacuum chamber at vacuum value not less that 1×10^{-4} Torr. Focused beam of the electrons creates a melting zone and forms the part by movement on set trajectory. After melting is finished, the chamber is opened and the next layer of powder is deposited. The part is grown layer-by-layer.

Titanium HDH powders are used as powder materials. They represent themselves VT1-0 titanium alloy granules of non-spherical form with cast microstructure of particles (Figure 4).

Technological characteristics and composition of powder materials of HDH titanium VD1-0 are given in the Table.

Fusion of powders using the scheme given above provided the specimens of parts of set straight shape of 12×12×100 mm (Figure 5).

The photo shows the upper layer of part *1* and substrate *3* with interlayers of deposited metal. Particles of unmelted metallic powder *2* are present on the side surface. This powder is removed later on and metal surface is machined. The specimens for further examinations were received after adjustment of deposition modes taking into account powder fraction, value of layer and size of layers overlapping. Figure 6 shows the part after machining. The surface of deposited metal was milled. Metal structure is homogeneous without obvious damages and inclusions.

Metallographic examinations of microstructure of deposited metal (powder of titanium alloy VT1-0 was made on base of titanium alloy VT-20) were carried out in different sections of the specimen.

The structure of deposited metal consisted of lamellar α-phase. Depending on layer size and powder material fraction there were changes in size of the plates of acicular α-phase as well as α´-phase precipitations were observed. Formation of hardening structures is typical for fractions less than 80 μm that is related with low source energy and fast heat sink in the volume of earlier formed cast metal (Figure 7).

Further the microstructure in the different zones of the specimens made of 63–100 μm fraction powders was examined. Cast structure close to fusion line with substrate differs in size and configuration of α-phase plates. In the first layers of the deposited metal they are coarser and have more polyhedral shape than in the middle part and in the final layers of deposit (Figures 8 and 9). This fact is related with cooling rate, i.e.

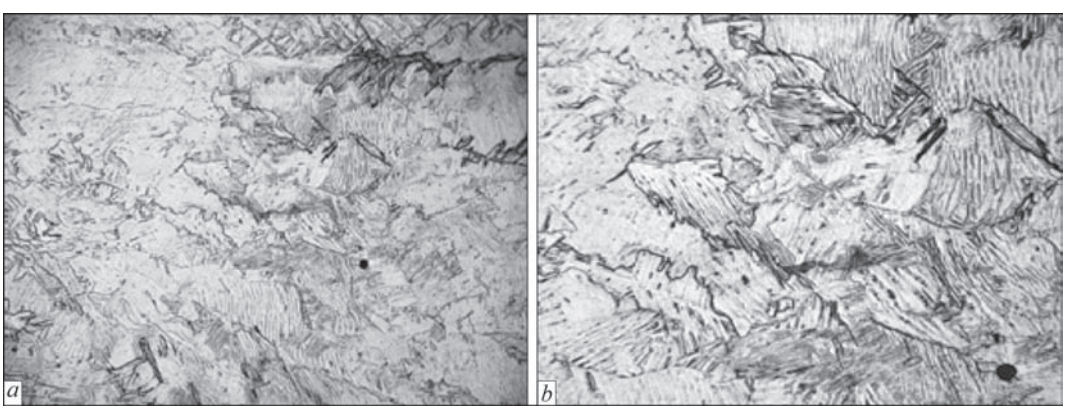

Figure 9. Microstructure of deposited metal in upper part of specimen: *a* — ×100; *b* — ×200

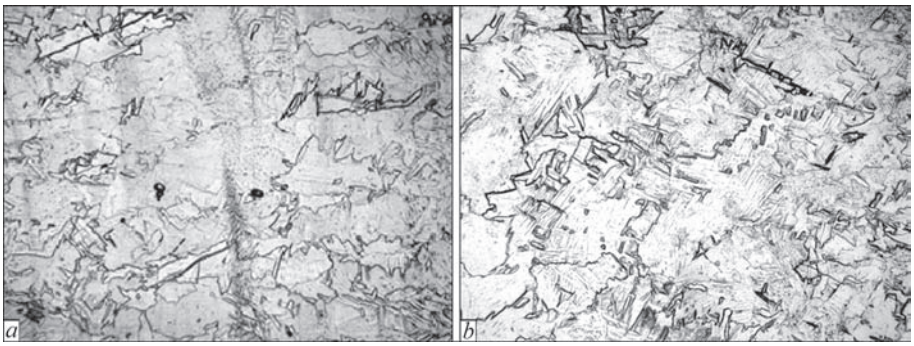

Figure 11. Microstructure of deposition in central part of specimen: *a* — ×200; *b* — ×100

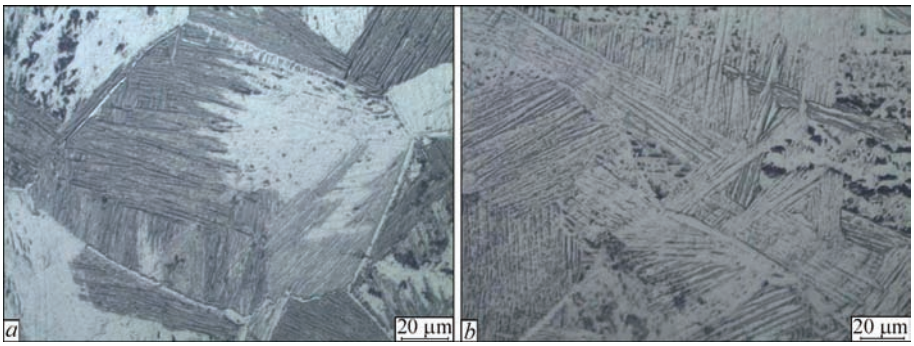

Figure 12. Microstructure of layers: *a* — layer 350; *b* — 120 μm

low rates provide for formation of coarser plates and high ones forms acicular fine α´-structure.

The plates on the outer layers of deposited metal are elongated in a heat sink direction with notched boundaries (Figure 10).

Transition zones of the layers of deposited metal differ by some refining of the plates and rise of amount of acicular α´-phase (Figure 11).

No defects, namely pores and lacks of fusion were found in the structure of examined specimen.

Figure 12 shows the microstructure of layers of built-up metal.

The analysis of microstructures of layers of built-up metal shows that the specimen structure has typical structural zones, size of which depends on their position on deposit height.

Conclusions

1. Quality of fusion of non-spherical shape powders in electron beam 3D deposition was investigated. It is determined that structural differences can be observed in dimensions, structural constituents of α-phase and are the consequence of different rate of layers cooling. It is important to note that structures of the specimens represent themselves α-phase typical for cast titanium alloys independent on powder fraction and layer size. This allows concluding that shape of powder materials, in our case non-spherical, does not affect deposited metal structure.

2. Components of equipment were developed and possibility of manufacture of set shape parts was realized using additive processes by electron beam layer-by-layer build-up method applying HDH powders, which allow getting dense cast structure of deposited metal.

1. Petrik, I.A., Ovchinnikov, A.V., Seliverstov, A.G. (2015) Development of titanium alloy powders for additive technologies applicable to GTE parts. *Aviats.-Kosmich. Tekhnika i Tekhnologiya*, **8**, 11–16.
2. Smurov, I.Yu. et al. *Development of domestic additive technologies for manufacturing and control of critical machine-building parts*: Abstract-presentaion. FGBOU VPO NGTU STANKIN.
3. Nazarenko, O.K. et al. (1987) *Electron beam welding*. Ed. by B.E. Paton. Kiev: Naukova Dumka.
4. Paton, B.E., Nazarenko, O.K., Nesterenkov, V.M. et al. (2004) Computer control of electron beam welding with multi-coordinate displacements of the gun and workpiece. *The Paton Welding J.*, **5**, 2–5.
5. Akhonin, S.V., Vrzhizhevsky, E.L., Belous, V.Yu. et al. (2016) Electron beam 3D-deposition of titanium parts. *Ibid.*, **5/6**, 130–133.
6. Ivasyshyn, O.M. et al. (2011) Surface phenomena in heating of hydride titanium powder. *Fizyka i Khimiya Tverdogo Tila*, 12(**4**), 900–907.
7. Zhukov, V.V., Grigorenko, G.M., Shapovalov, V.A. (2016) Additive manufacturing of metal products. *The Paton Welding J.*, **5**/6, 137–142.
8. (2017) *Manufacturing of powders of hydrated sponge titanium*. SE SRD Titanium Institute. *http*://timag.org/ru_propose.php
9. Olshanetsky, V.E. et al. (2015) Compactibility of powder materials with different shape of particles. *Novye Materialy i Tekhnologii v Metallurgii i Mashinostroenii*, **1**, 130–133.

Received 06.02.2017

doi.org/10.15407/tpwj2017.03.02

MODELLING OF TEMPERATURE FIELDS AND STRESS-STRAIN STATE OF SMALL 3D SAMPLE IN ITS LAYER-BY-LAYER FORMING*

O.V. MAKHNENKO[1], **A.S. MILENIN**[1], **E.A. VELIKOIVANENKO**[1], **N.I. PIVTORAK**[1] and **D.V. KOVALCHUK**[2]
[1]E.O. Paton Electric Welding Institute, NASU
11 Kazimir Malevich Str., 03680, Kiev, Ukraine. E-mail: office@paton.kiev.ua
[2]PJSC SPE «Chervona Khvylya»
15 Kazimir Malevich Str., 03680, Kiev, Ukraine. E-mail: master@chervonahvilya.com

A set of investigations on kinetics of temperature fields and stress-strain state of a tee section was carried out employing mathematical and computer modelling methods in order to optimize a process of layer-by-layer forming of titanium structural elements of aerospace designation by means of current xBeam 3D Metal Printer (xBeam) electron beam technologies. The results of investigations were used for temperature fields optimizing in order to provide uniform distribution on height and length of the product by selection of efficient time between deposition passes of forming beads and source alternating power. Besides, typical stress and strain fields, formed in the product during its manufacture, were shown as well as possibilities of application of processing methods for reduction of residual forming. 26 Ref., 2 Tables, 13 Figures.

Keywords: *layer-by-layer forming, electron beam, temperature field, stress-strain state, optimizing, mathematical modelling*

Currently, the additive technologies are an alternative to traditional manufacture of titanium structural elements with complex geometry, first of all in aerospace industry and medicine [1–9]. It is caused by the fact that cost of remelting of titanium alloy scrap, being a result of machining of medium- and large-size parts, is higher in the majority of cases than the expenses for layer-by-layer forming of such type of objects. In the case with small-size parts this increases productivity of manufacture of the one-of-a kind samples by individual order.

There are several different approaches to production of metallic structures based on principle of layer-by-layer object forming. These approaches differ on types of consumables and used heat sources. They can be divided on two main groups by types of used consumables, namely sintering or fusion of metallic powders [1, 2, 5–10] and deposition with consumable (filler wires etc.) feeding [1, 4, 11–13].

The methods using flux-cored consumables allow producing complex geometry objects with high accuracy of performance, in particular, for manufacture of 3D porous structures [1–3, 5–8, 10, 14–17]. Such types of structures are successfully used in medicine as implants [7, 9, 13, 18]. At that, deposition rate is extremely low that limits application of these technologies for medium- and large-size structures.

A rate of deposition using technology based on filler wires is significantly higher in the majority of cases by order. Besides, in such approaches efficiency of consumables application is also significantly higher and can reach 100 % [1].

The heat sources in approaches using filler wires are laser, electron beam or electric arc. The approaches based on laser technologies are the most popular in current time due to their accuracy [1, 4, 12, 19], nevertheless their energy efficiency is low (2–5 %) [1–4]. Electron beam deposition differs by great efficiency, but requires high vacuum. The results of metal structure examinations show that electron beam deposition allows producing complex-shape parts with homogeneous structure of metal in the deposited layers similar to base metal (substrate) structure [20]. This is a reason why this procedure is the most perspective in aerospace industry [3, 4].

The main disadvantage of the methods using metallic wire deposition is appearance of significant residual stresses and deformations [13]. High residual stresses can significantly reduce service characteristics of produced components, particularly, their dura-

*Based on a report presented at the VIII International Conference «Mathematical Modelling and Information Technologies in Welding and Related Processes», September 19–23, 2016, Odessa, Ukraine.

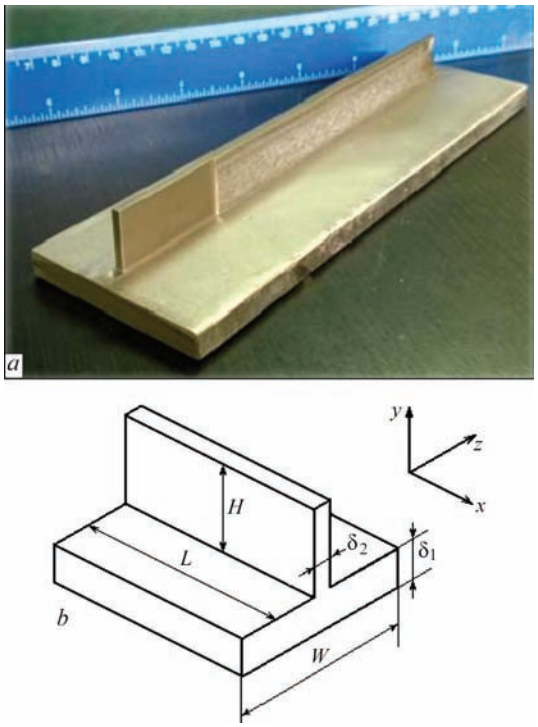

Figure 1. Appearance (*a*) and scheme (*b*) of tee section of titanium alloy, produced by electron beam multilayer forming

bility at cyclic loads, and residual deformations can result in unallowable distortion of shape and rejection of part billets.

Optimizing the additive deposition technologies applying mathematical modelling for decrease of volume of experimental investigations requires substantial computer and time expenses [11, 15]. However, selection of the optimum deposition parameters based on computer prediction is the most promising.

Manufacturing scheme of process of multilayer forming of 3D samples. Figure 2 shows xBeam manufacturing scheme by example of multilayer forming of tee section (Figure 1). The process takes place under conditions of medium vacuum (in the range of 10^{-2} mbar), that, on the one hand, allows eliminating metal contamination due to high affinity with oxygen and/or nitrogen, and on the other hand, provides sufficient focusing of electron beam. Substrate of the product being formed (in considered case it is tee section flange) is located in a pre-stressing fixture, which presses it to movable platform with force *F*, and moves it relatively stationary heat source with set rate V_s in a plate plane and periodically, with deposition of each bead, in normal direction with rate V_d.

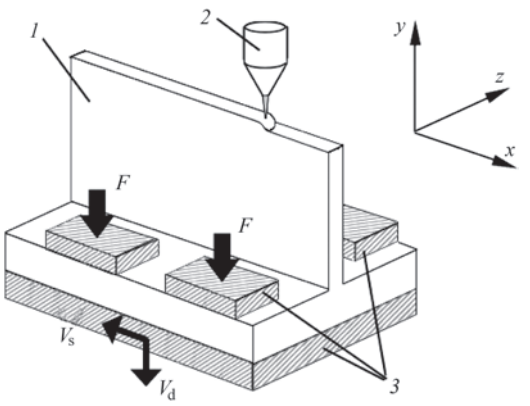

Figure 2. Process scheme of electron beam multilayer forming of tee section samples: *1* — part being formed; *2* — modulus of heating and wire feed; *3* — process fixture

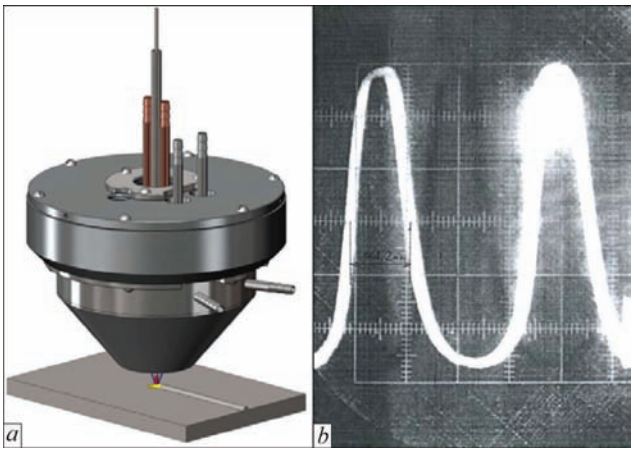

Figure 3. Scheme of electron beam heating (*a*) modulus and experimentally determined distribution of energy flow in electron beam (*b*)

The heat source is a joined complex of systems for generation of electron beam in form of hollow cone, having maximum close convergence on a surface of structure being formed, and filler wire feed (Figure 3, *a*). This allows performing efficient and sufficiently uniform melting of filler wire without its significant overheating as well as forming melt pool on the substrate or earlier deposited layer for quick spread of liquid filler material over the surface. Figure 3, *b* shows experimentally determined distribution of energy flow in such electron beam.

In accordance with laboratory investigations, the product as a result of layer-by-layer deposition got specific residual bending deformation as a consequence of formation of welding shrinkage of metal in the deposition area. Besides, the preliminary experiments showed that the end areas are characterized by irregular structure of section wall as a result of non-uniform heating in deposition. One of the advantages of used xBeam scheme is the possibility of program control of heat input that provides wide possibilities for optimizing the parameters of the considered process. Variation of a delay time between deposition of each bead and reasonable selection of method and level of preheating are also efficient optimizing parameters.

Investigation procedure. Software package WeldPrediction, developed at the E.O. Paton Electric Welding Institute of the NAS of Ukraine for prediction of physical-mechanical processes in welding and related technologies [21–23], was used for prelim-

inary analysis of state kinetics in the sample of tee section of titanium alloy. Solution of the problems of heat conductivity and stress-strain state of metal in preheating, further deposition up to part cooling and removal of process fixture was carried out on joint rectangular partitioning meshes. Shape of the product was changed at each deposition stage in accordance with deposition rate and geometry of beads forming at that. It is reasonable to solve nonstationary thermoplasticity problem in 2D definition by averaging 3D calculation temperature field on thickness. This allows examining development of state of investigated product with sufficient accuracy, and reducing investigation resource intensity.

Thus, finite-difference solution of 3D nonstationary equation of heat conductivity was used for numerical analysis of kinetics of temperature field $T(x, y, z)$ on time t in xBeam deposition of the part, shown in Figure 1:

$$c\gamma(T)\frac{\partial T}{\partial t} = \nabla\left[\lambda(T)\nabla T\right], \tag{1}$$

where $c\gamma$, λ are the specific heat capacity and heat conductivity of material, respectively.

The boundary conditions, necessary for problem solution (1), depend on heat sink from the product surface. Thus, heat sink in the area of contact with process fixture can be described by Newton's law, while on a free surface it is characterized by heat radiation (Stefan–Boltzmann law) with additional energy input from product end being deposited in the case of heat source location in that place. Thus, boundary conditions for solution of heat conductivity problem in the studied case have the following form:

$$-\lambda(T)\frac{\partial T}{\partial n} = \begin{cases} \alpha_T(T - T_C), \\ \text{in the area of contact with fixture} \\ \varepsilon\sigma_{SF}(T^4 - T_C^4) - q, \\ \text{on free surfaces,} \end{cases} \tag{2}$$

where n is the normal to surface; α_H is the heat sink coefficient; T_E is the environment temperature; ε is the material emissivity factor; σ_{SF} is the Stefan–Boltzmann constant; q is the energy flow of electron beam heating.

A relationship between components of stress and strain tensors can be stated by generalized Hooke's law considering temperature volumetric changes and associated law of plastic flow [24, 25]:

$$\begin{cases} \Delta\varepsilon_{ij} = \psi(\sigma_{ij} - \delta_{ij}\sigma_m) + \delta_{ij}(K\sigma_m + \Delta\varepsilon_T) - b_{ij} \\ b_{ij} = \dfrac{1}{2G}(\sigma_{ij} - \delta_{ij}\sigma_m)^* + (K\sigma_m)^* \end{cases} \tag{3}$$
$$(i, j) = (x, y, z),$$

where $K = (1 - 2\nu)/E$; E is the Young's modulus; ν is the Poisson's ratio; $G = E/(2(1 + \nu))$; $\Delta\varepsilon_T$ is the deformation increment, caused by metal thermal expansion; ψ is the function of material state, determined by yield condition, namely:

$$\begin{aligned} \psi &= \frac{1}{2G}, \text{ if } \sigma_i < \sigma_T(T), \\ \psi &> \frac{1}{2G}, \text{ if } \sigma_i = \sigma_T(T), \end{aligned} \tag{4}$$

where

$$\sigma_i = \frac{1}{\sqrt{2}}\sqrt{\begin{aligned}&(\sigma_{xx} - \sigma_{yy})^2 + (\sigma_{xx} - \sigma_{zz})^2 + \\ &+(\sigma_{yy} - \sigma_{zz})^2 + 6(\sigma_{xy}^2 + \sigma_{xz}^2 + \sigma_{yz}^2)\end{aligned}}.$$

Plastic strains are determined from equation

$$\Delta\varepsilon_{ij} = \left(\psi - \frac{1}{2G}\right)(\sigma_{ij} - \delta_{ij}\sigma_m), (i, j = x, y, z). \tag{5}$$

Realization of condition (4) is carried out at each step of tracing, σ_{ij} stresses are presented from (5) at that each ψ iteration in form of

$$\begin{cases} \sigma_{ij} = \dfrac{1}{\psi}\left(\Delta\varepsilon_{ij} + \delta_{ij}\dfrac{\psi - K}{K}\Delta\varepsilon\right) + J_{ij}; \\ J_{ij} = \dfrac{(b_{ij} - \delta_{ij}b) + \delta_{ij}\left(K\sigma^* - \dfrac{\Delta\varepsilon_T}{K}\right)}{\psi}, \end{cases} \tag{6}$$

where

$$\Delta\varepsilon = \frac{\Delta\varepsilon_{xx} + \Delta\varepsilon_{yy} + \Delta\varepsilon_{zz}}{3}, \quad b = \frac{b_{xx} + b_{yy} + b_{zz}}{3}.$$

Relationship between $\Delta\varepsilon_{ij}$ tensor and vector of displacement increment ΔU_i is presented in the following way

$$\Delta\varepsilon_{ij} = \frac{\Delta U_{i,j} + \Delta U_{j,i}}{2}, \tag{7}$$

where coma corresponds to differentiation.

A resolving system of algebraic equations in relation to displacement increment vector in the nodes of finite elements at each step of tracing and ψ iteration is determined as a result of its functional minimizing (Lagrange variation principle)

$$\mathrm{E}_1 = -\frac{1}{2}\sum_V(\sigma_{ij} + J_{ij})\Delta\varepsilon_{ij}V_{m,n,r} + \sum_{S_P} P_i\Delta U_i\Delta S_P^{m,n,r}, \tag{8}$$

where $\sum_V, \sum_{S_P}$ are the operators of sum on internal and superficial finite elements, respectively; P_i is the power vector of external influence ($i = x, y, z$).

Thus, a set of equations, which allows solution in regard to the vector of displacement increments at each step of tracing and ψ iteration for corresponding finite element, looks like:

$$\begin{cases} \dfrac{\partial \Theta_1}{\partial \Delta U_{m,n,r}} = 0; \\ \dfrac{\partial \Theta_1}{\partial \Delta V_{m,n,r}} = 0; \\ \dfrac{\partial \Theta_1}{\partial \Delta W_{m,n,r}} = 0. \end{cases} \tag{9}$$

Table 1. Process parameters of multilayer forming of laboratory titanium alloy sample (working gas — helium)

Parameter	Value	Notes
Consumable (rod)	Diameter 1.6 mm	Titanium of VT1-0 grade
Substrate (plate)	8×30×70 mm	Titanium of VT1-0 grade
Vacuum	$5 \cdot 10^{-1}$ Pa	Vacuum reduced to 1 Pa after start of gas supply
Accelerating voltage	15 kV	–
Electron beam current	300 mA	–
Electron beam power	4.5 kW	–
Consumable feed rate	14 mm/s	–
Rate of substrate movement on axis *X*	14 mm/s	–
Displacement on axis *Y* before each new deposition cycle	0.5 mm	–
Number of deposited layers	37	–

Solution of indicated problems of nonstationary thermal plasticity according to given mathematical description was carried out by means of numerical tracing of elasto-plastic deformations, starting from a stage of substrate preheating, deposition of each bead up to complete cooling of the product and removal of process fixture, in scope of respective finite element description [26].

Modelling results. Considered manufacturing process was modeled based on the results of laboratory investigations on deposition of titanium alloy tee product (Figure 1). Table 1 shows the main parameters of given manufacturing cycle.

Solution of the temperature problem shows (Figure 4) that the temperature fields of studied case have 3D nature, at that temperature in the deposited thin wall of tee section is distributed sufficiently uniform along a cross-section and flange state is characterized by relatively low temperature gradients.

One of the main problems, which was studied at this stage of investigations, lied in study of potential possibilities for achievement of stationary temperature field in the product at each layer deposition. This allows acquiring favorable conditions of bead formation as well as providing uniformity of structural state of metal in all section of the product, and, respectively, homogeneity of its physical-mechanical and service properties. The results of numerical modelling according to procedure mentioned above show absence in bead deposition of significant overheating of liquid metal after coming on the surface of product being formed. This indicates effective heat sink in the metal of product and environment. This allows receiving sufficient heating-through for providing fu-

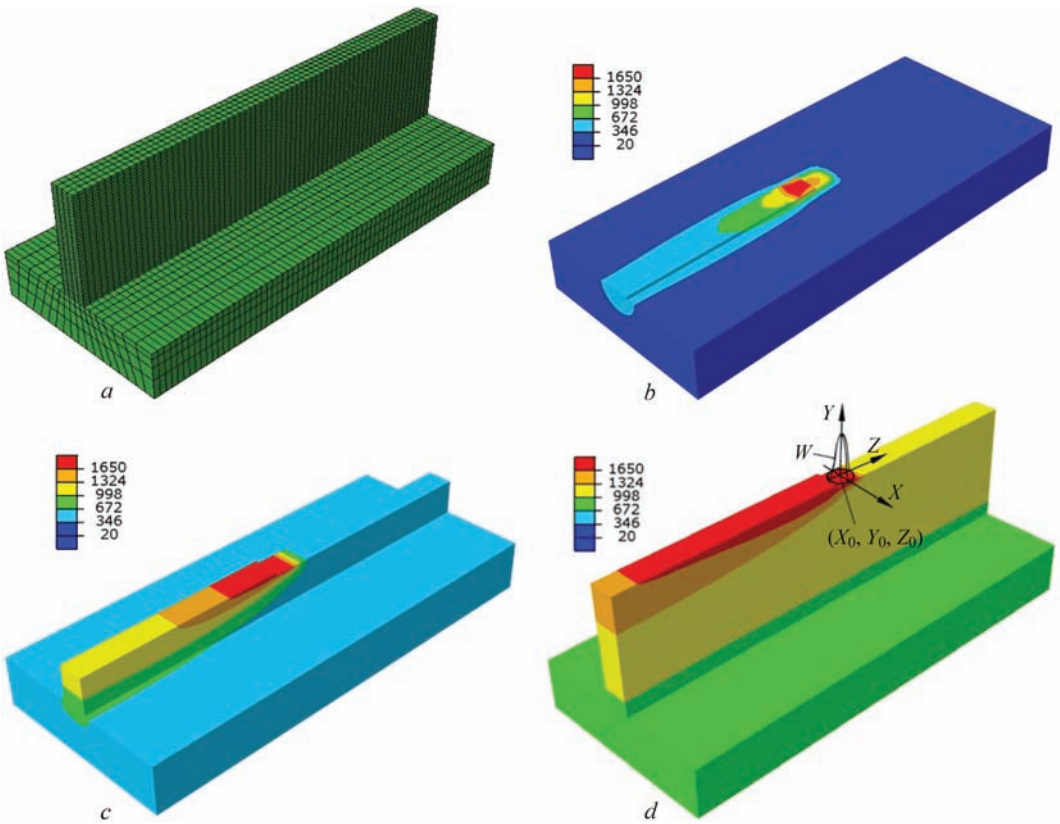

Figure 4. Finite-element model (*a*) and distribution of temperatures in tee sample during layer-by-layer forming: *b* — deposition of the 1st bead; *c* — deposition of the 12th bead; *d* — deposition of the 37th bead and scheme of model of distributed heat source

Table 2. Model modes of bead deposition in process of tee section product forming at alternating power of electron beam heat source

Number of mode	Power of source in different areas of element being deposited, kW (%)		
	0–2 mm	2–68 mm	68–70 mm
1	4.5 (100)	4.5 (100)	4.5 (100)
2	6.3 (140)	4.5 (100)	4.3 (95)
3	7.2 (160)	4.5 (100)	4.3 (95)

sion of beads and preventing overheating and excessive yield of liquid metal.

Typical peculiarity of distribution of the maximum temperatures at deposition area is locally lower temperatures in the beginning of bead and small overheating at the end. This can be balanced, in particular, by alternating power of electron beam heat source on length. Three modes of bead deposition (Table 2) were studied for example, namely basic one (1) and modes of excessive power at the beginning of deposition (2) and reduced at the end (3).

Selected modes use variation of source power at relatively small sections of deposited metal for balancing excessive heat sink in cold part at the beginning of melting and excessive heat accumulation close to end part of the edge, and reaching more uniform distribution of the maximum temperatures (Figure 5 as an example shows calculation distribution of temperatures in deposition of the tenth bead). Further rise of power at the initial stage of formation of tee section wall (more than 160 %) is not reasonable, since it will cause local overheating of given area of the structure.

In addition to provide the homogeneity of metal structural state in bead deposition direction it is also important to keep a temperature mode with the maximum approximation to stationary one in deposition of each wall layer of considered section for metal homogeneity on height. The results of calculations (Figure 6) show that the stationary mode takes place after

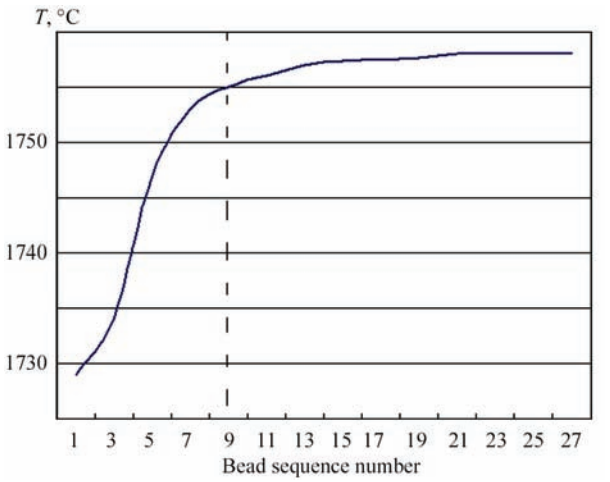

Figure 6. Dependence of space-averaged on bead section maximum temperature of deposited metal in the section central area on bead sequence number

the eighth bead. Temperature averaged on bead area in $2.7 \cdot 10^{-3}$ s after its deposition in the central part of tee section was used as example.

One more important factor, which should to be considered in selection of reasonable parameters for deposition of investigated sample, is the delay time t_r between deposition of each bead. On the one hand, increase of the delay time allows more uniform redistribution of heat from each of deposit beads, on the other hand, decrease of t_r results in reduction of power intensity of studied process and less accumulation of heat energy by section. Figure 7 shows effect of t_r value on value of steady-state temperature in the product central area. It can be concluded from indicated data that overheating of deposited product edge up to remelting of previous deposited layer is observed at $t_r < 25$ s. At $t_r > 40$ s stationary mode is more preferable from point of view of quality of element being formed, but at that initial stage of deposition can be characterized by lack of fusion in the metal layers as

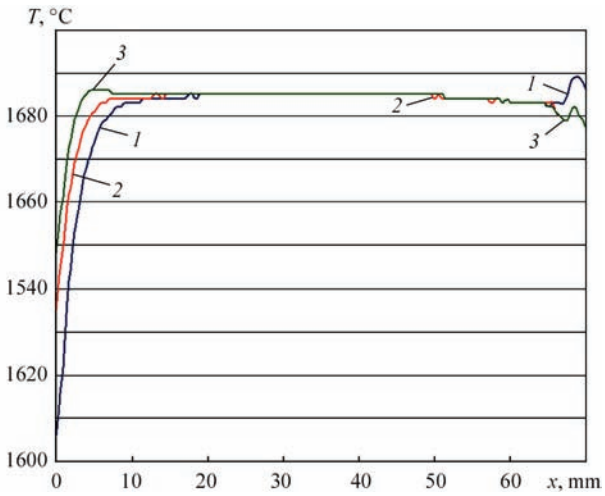

Figure 5. Distribution of maximum temperatures along the whole length of deposited bead for different modes of heat source effect (modes *1–3* according to Table 2)

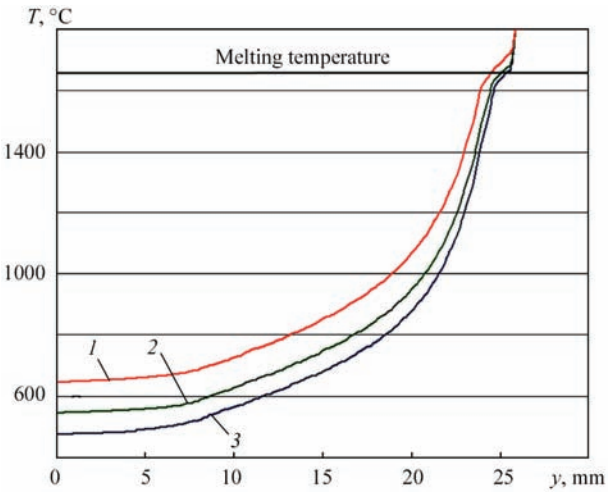

Figure 7. Distribution of maximum temperatures on section height in deposition of the 37th bead for different delay time between beads: *1* — t_r = 20 s; *2* — 30; *3* — 40

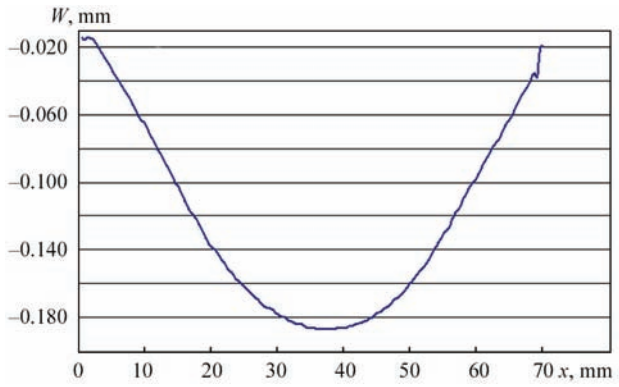

Figure 8. Residual forming of lower plane of product substrate of tee section after EBD ending, complete cooling and removal of pre-stressing fixture

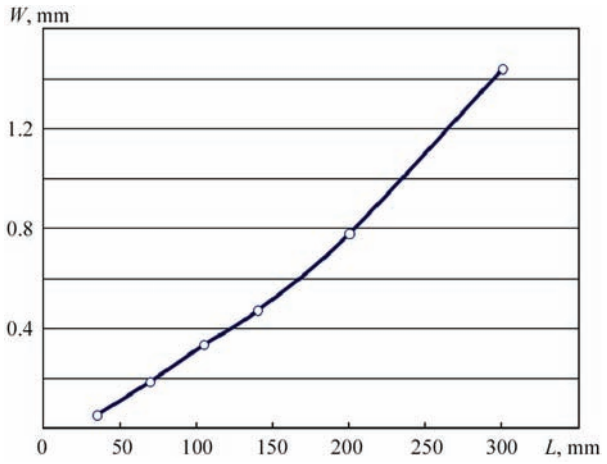

Figure 9. Dependence of residual bending deflection of tee section W on its length L after fixture removal

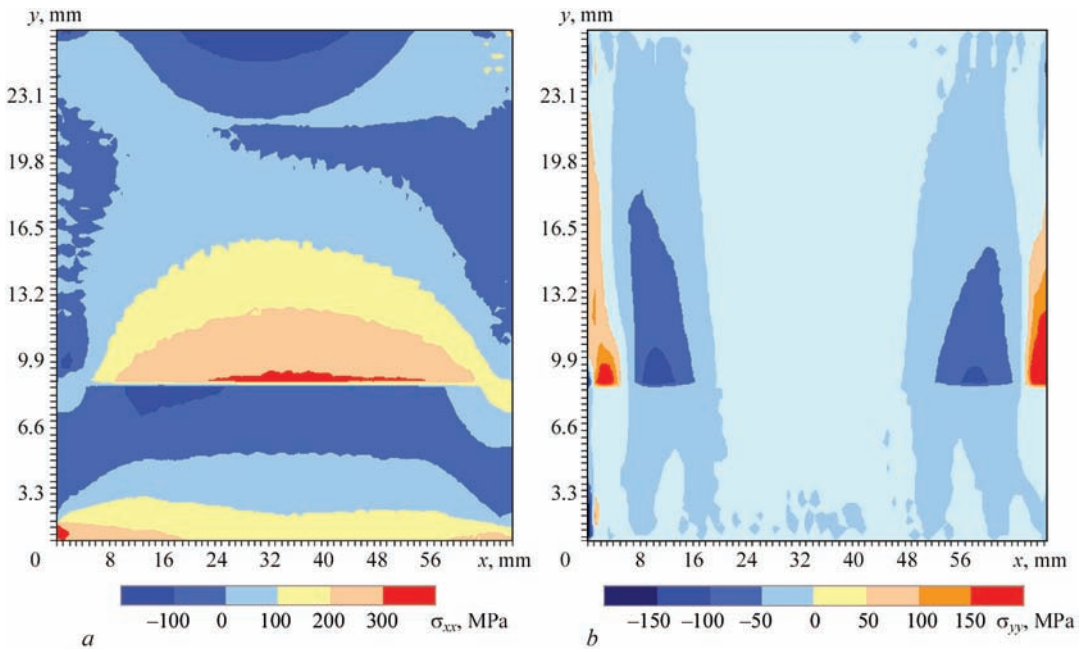

Figure 10. Distribution of residual stresses σ_{xx} and σ_{yy} in product after its forming at mode 1 (see Table 2)

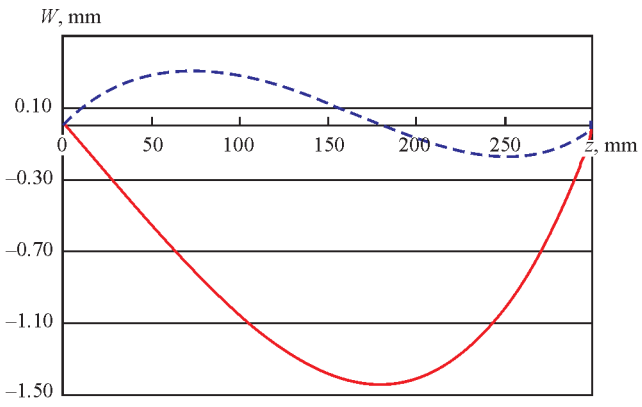

Figure 11. Shape of longitudinal axis of tee deposited sample L = = 300 mm after layer-by-layer forming on initially even substrate (*solid line*) and considering preliminary bending deflection W_0 = 1.5 mm (*dashed line*)

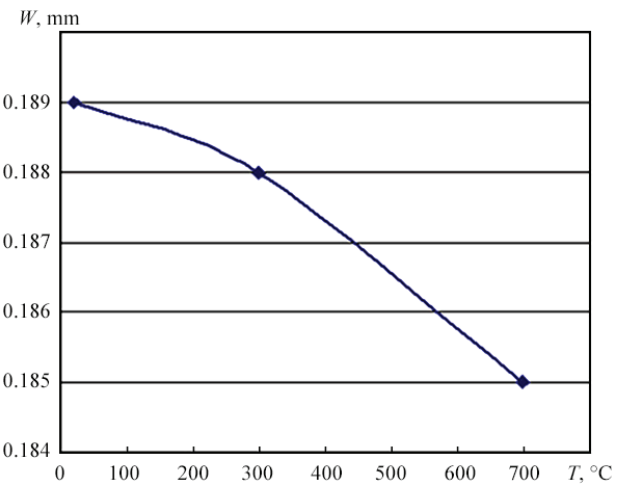

Figure 12. Dependence of residual bending deflection W of deposited sample L = 70 mm after fixture removal on preheating temperature T_0

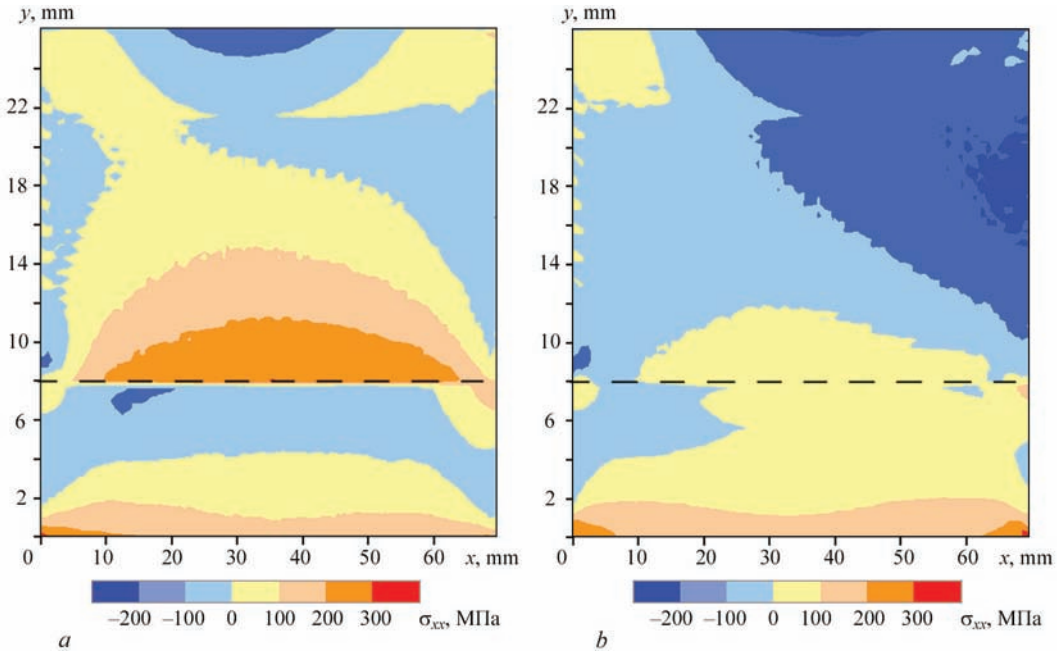

Figure 13. Distribution of longitudinal residual stresses σ_{xx} in product after its forming at substrate preheating to T_0 = 300 (*a*) and 700 °C (*b*)

a result of intensive heat sink in the structure. Therefore, 25 s< t_r <35 s range can be considered as reasonable in selection of a regular delay of deposit of each bead in all height of the element being deposited.

Residual forming and internal stresses in the formed product can be the factors limiting application of considered technology. Irreversible deformations of the substrate of investigated element of tee section as a result of longitudinal shrinkage can exceed the allowances, prescribed by specific design solutions, while high residual stresses depress resistance to fatigue action and increase susceptibility to stress-corrosion fracture. Thermomechanical treatment is mostly used for improvement of service characteristics of the structures, in particular, welded ones. However, additional operating stage of product processing involves increase of prime cost, therefore optimizing the xBeam process taking into account the peculiarities of kinetics of stress-strain state of specific design structure is reasonable. Thus, residual strain on mechanism of longitudinal shrinkage is the most cenfavorable and typical for investigated product of tee section. As a result whole structure bends in longitudinal plane (Figure 8). Due to relatively small length of this element, its residual forming is insignificant (around 0.2 mm), but residual deflection can go beyond the limits of necessary allowances (Figure 9) if rise of structure length is required.

Stressed state in the product plane (Figure 10) is characterized by relatively low level of residual stresses in longitudinal as well as transverse direction. Distinctive feature is some concentration of stresses σ_{yy} as a result of end effects. Besides, area of transition of the tee flange to the wall includes excessive longitudinal stresses σ_{xx}, caused by general structure bend.

An effective processing method for decrease of residual stresses in welded structures is preliminary bending deflection (flexure), which can be realized due to pre-stressing fixture. Figure 11 presents the results of calculation of bending deflection of an axis of tee deposited sample of L = 300 mm length after layer-by-layer forming on initially even substrate and taking into account preliminary bending deflection W_0. It can be seen that the optimum value of preliminary bending deflection can significantly reduce residual deformations of general forming.

The results of evaluation of substrate preheating effect on residual deformations of tee sample of 70 mm length are given in Figure 12. The value of residual bending deflection in substrate heating from room temperature to 700 °C virtually does not change (2 %), and residual stresses in area of flange to wall transition significantly drop at heating temperature increase (Figure 13).

Conclusions

1. A set of mathematical models and software means for their realizing was developed for numerical prediction of kinetics of temperature and stress-strain state of tee section structure of titanium alloy in process of electron-beam deposition by xBeam 3D Metal Printing. Typical peculiarities of temperature field distribution were investigated in terms of basic parameters of manufacture of laboratory samples of tee section. It is shown that specific stabilizing of the temperature cycles on length of deposited wall can be achieved by setting of alternating power of heat source, i.e. up to 160 % of power at initial stage for larger heating of product edge and less than 95 % of power at final

stage for balancing of heat accumulation process at the sample end.

2. Substantial effect of the delay duration between deposit of each of forming beads on nature of temperature distribution was shown, namely reduction of delay duration time less than 20 s results in significant accumulation of heat in the product metal and, as a result, significant overheating and excessive penetration, that can decrease quality of product being formed.

3. Formation of residual longitudinal bending deformations at 0.2 mm level is shown by means of numerical prediction of development of strained state of the product in the process of deposition, further cooling and relieve of fixture forces. At that variation of product length has significant effect on longitudinal bend value, that can require corresponding thermomechanical straightening. An effective processing method for reduction of residual deformations is preliminary bending deflection (flexure), which can be realized due to pre-stressing fixture.

4. Analysis of the results of prediction of residual stressed state of the examined model structure showed formation of excessive tensile longitudinal stresses in the area of tee section flange to wall transition that is caused by total structure bend. Besides, expressed stress concentrators σ_{yy} are formed in area of its ends. The results of evaluation of effect of preliminary substrate heating on stress-strain state of the tee sample showed that residual stresses in the flange to wall transition area essentially drops at rise of heating temperature and high tempering conditions are virtually provided at T_0 = 700 °C.

The authors express gratitude to G.F. Rozynka and D.S. Gavrilov for participation in paper preparation.

1. Ding, D. et al. (2015) Wire-feed additive manufacturing of metal components: Technologies, developments and future interests. *Int. J. of Adv. Manufact. Technology*, 81(**1**), 465–481.
2. Heinl, P. et al. (2007) Cellular titanium by selective electron beam melting. *Adv. Eng. Mater*., **9**, 360–364.
3. Kristofer, Ek. (2014) *Additive manufactured material*: Master of Sci. Thesis, Stockholm.
4. Brandl, E. et al. (2010) Additive manufactured Ti–6Al–4V using welding wire: Comparison of laser and arc beam deposition and evaluation with respect to aerospace material specifications. *Physics Procedia*, December, 595–606.
5. Mandil, G. et al. (2016) Building new entities from existing titanium part by electron beam melting: Microstructures and mechanical properties. *Int. J. of Adv. Manufact. Technology*, Vol. 85, Issue 5, 1835–1846.
6. Murr, L.E. et al. (2010) Characterization of titanium aluminide alloy components fabricated by additive manufacturing using electron beam melting. *Acta Materialia*, Vol. 58, Issue 5, 1887–1894.
7. Marin, E. et al. (2010) Characterization of cellular solids in Ti6Al4V for orthopaedic implant applications: Trabecular titanium. *Mechan. Behaviour of Biomedical Mater*., Vol. 3, Issue 5, 373–381.
8. *Wahyudin P.* Syam et al. (2012) Preliminary fabrication of thin-wall structure of Ti6Al4V for dental restoration by electron beam melting. *Rapid Prototyping J*., April, 230–240.
9. *Leonard F.* et al. (2012) Assessment by X-ray CT of the effects of geometry and build direction on defects in titanium ALM parts. In: *Proc. of Conf. on Industrial Computed Tomography* (ICT), 85–93.
10. Golkovski, M.G. et al. (2013) Atmospheric electron-beam surface alloying of titanium with tantalum. *Mater. Sci. & Engineering, A*, Vol. 578, 310–317.
11. *Yan Ma* et al. (2015) Effect of interpass temperature on in-situ alloying and additive manufacturing of titanium aluminides using gas tungsten arc welding. *Adv. Manufacturing*, **8**, 71–77.
12. *Blanka A.* Szost et al. (2015) A comparative study of additive manufracturing techniques: Residual stress and microstructural analysis of CLAD and WAAM printed Ti–6Al–4V components. *Materials and Design*, Vol. 89, 559–567.
13. Baurfeld, B. et al. (2010) Additive manufacturing of Ti-6Al-4V components by shaped metal deposition: Microstructure and mechanical properties. *Materials and Design*, Vol. 31, 106–111.
14. Edwards, P. et al. (2013) Electron beam additive manufacturing of titanium components: Properties and performance. *J. of Manufact. Sci. and Engineering*, Vol. 135, Issue 6, 061016/1–061016/7.
15. Gong, X. et al. (2013) Powder-bed electron-beam-melting additive manufacturing: Powder characterization, process simulation and metrology. *ASME Early Career Techn. J*., **12**, 59–66.
16. Nai, M.L.S. et al. (2016) Recent progress of additive manufactured Ti-6Al-4V by electron beam melting. In: *Proc. of 27th Annual Int. Solid Freeform Fabrication Symp. — An Additive Manufacturing Conf*., 691–704.
17. Petrovic, V. et al. (2012) Additive manufacturing solutions for improved medical implants. *Biomedicine, InTechOpen*, March, 147–180.
18. Jia, Lv et al. (2015) Electron beam melting fabrication of porous Ti6Al4V scaffolds: Cytocompatibility and osteogenesis. *Adv. Eng. Mater*., 1–8.
19. *Mari Koike* et al. (2011) Evaluation of titanium alloys fabricated using rapid prototyping technologies — electron beam melting and laser beam melting. *Materials*, **4**, 1776–1792.
20. Akhonin, S.V., Vrzhizhevsky, E.L., Belous, V.Yu. et al. (2016) Electron beam 3D-deposition of titanium parts. *The Paton Welding J*., **5/6**, 130–133.
21. Makhnenko, V.I. (2013) Problems of examination of modern critical welded structures. *Ibid*., **5**, 21–28.
22. Makhnenko, V.I., Velikoivanenko, E.A., Olejnik, O.I. (2008) Risk analysis as a method for formalizing decision making on unscheduled repair of welded structures. *Ibid*., **5**, 2–7.
23. Milenin, O.S. (2011) Probabilistic analysis of state of main pipelines with revealed defects and their service life after repair under pressure. *Visnyk Ternopil NTU*, Special Issue, Pt 1, 73–81.
24. Makhnenko, V.I. (1976) *Computational methods of investigation of welding stress and strain kinetics*. Kiev: Naukova Dumka.
25. Makhnenko, V.I. (2006) *Safety service life of welded joints and assemblies of modern structures*. Ibid.
26. Velikoivanenko, E.A. et al. (2014) Methods and technologies of parallel calculations for mathematical modeling of stress-strain state of structures taking into account ductile fracture. *Probl. Upravleniya i Informatiki*, **6**, 42–52.

Received 14.02.2017

doi.org/10.15407/tpwj2017.03.03

FORCE INTERACTION OF ARC CURRENT WITH SELF-MAGNETIC FIELD*

V.F. DEMCHENKO[1], **I.V. KRIVTSUN**[1], **I.V. KRIKENT**[2] and **I.V. SHUBA**[1]
[1]E.O. Paton Electric Welding Institute, NASU
11 Kazimir Malevich Str., 03680, Kiev, Ukraine. E-mail: office@paton.kiev.ua
[2]Dneprosky State Technical University
2 Dneprostrojevskaya Str., 51918, Kamenskoe, Ukraine

Detailed theoretical analysis of force interaction of welding current with self-magnetic field under the conditions of nonconsumable electrode arc welding was performed. Electromagnetic force (Lorentz force) is presented as a sum of vortex and potential forces, from which only the vortex component is capable of exciting the movement of plasma or molten metal. Centripetal vortex force generates magnetic pressure in arc plasma and weld pool metal. The gradient of this pressure induces magnetic force, oriented predominantly in the axial direction. The magnitude of this force is the greater the higher the current density in near-anode region of welding arc (on weld pool surface). Depending on the nature of electric current spreading in the arc column, three possible scenarios of arc plasma movement are considered: by the schematic of right and inverse cone, as well as in the form of two vortices, excited by current channel compression in near-cathode and near-anode regions of the arc. Presented theoretical postulates are illustrated by numerical calculations of distribution of magnetic pressure and magnetic forces in arc column plasma and in weld pool metal. It is established that electric current contraction on the anode intensifies hydrodynamic flows of molten metal, and, therefore, also convective energy transfer from central zone of weld pool surface to its bottom part, promoting an increase of penetrability of the arc with refractory cathode. 14 Ref., 1 Table, 12 Figures.

Keywords: *arc welding, nonconsumable electrode, molten metal, hydrodynamic flows, arc current, magnetic field, arc penetrability*

In arc welding, electromagnetic force, arising as a result of interaction of arc current with self-magnetic field, has an essential influence on the processes of transfer of mass, pulse and energy, both in welding arc column, and in weld pool. In arc plasma Lorentz force is the dominating force factor, determining the structure and intensity of plasma flows. In principle, the nature of gas-dynamic flow of plasma in arc column can vary, depending on its length and transverse dimensions of the regions of arc cathode and anode attachment, which determine the magnitude of ponderomotive force in near-electrode zones of arc column, and, accordingly, structure of gas-dynamic flows of arc plasma as a whole. In the weld pool, alongside electromagnetic force, three more forces are applied to the melt, namely Marangoni thermocapillary force, due to temperature dependence of surface tension factor, and force of viscous friction of arc plasma flow against molten metal surface, acting along weld pool free surface, as well as buoyancy (Archimedean) force, arising due to nonuniformity of the melt temperature field. The latter is the least significant factor in formation of molten metal flows, compared to Lorentz force, Marangoni force and friction force. Dominating role of one of these three force factors depends on welding mode, properties of metal being welded, weld pool dimensions, size of arc attachment region on pool surface, and other welding process characteristics.

As is known, bulk density of electromagnetic force $\vec{F}$ is found from the following formula $\vec{F} = \vec{j} \times \vec{B}$, where $\vec{j}$ is the vector of electric current density; $\vec{B}$ is the vector of magnetic induction. In such a form, electromagnetic force is taken into account in numerous studies (see, for instance, [1–8]), devoted to simulation of the processes of mass, pulse and energy transfer in the arc discharge and in weld pool metal. The given formula for calculation of electromagnetic force allows quite adequate determination of welding current influence on plasma movement in arc column and weld pool hydrodynamics. At the same time, vector field of electromagnetic forces, determined by this formula, does not allow a priori estimation on qualitative level of possible structure of these gas(hydro)

*Based on a report presented at the VIII International Conference «Mathematical Modelling and Information Technologies in Welding and Related Processes», September 19–23, 2016, Odessa, Ukraine.

dynamic flows. The latter can be revealed only a posteriori, after performance of respective calculations of the characteristics of plasma and molten metal flows, initiated by electromagnetic force. This drawback of standard expression for bulk density of electromagnetic force, is due to the fact that this force, similar to bulk force of any other physical nature, is represented as a sum of potential and vortex components, from which only the vortex component of the force is capable of exciting the movement of the medium. Therefore, it is of interest to isolate the vortex component from total electromagnetic force $\vec{F}$, and on this basis to uncover the mechanism and features of action of this important component of the force on arc column plasma and weld pool molten metal. This is exactly the standpoint from which detailed theoretical analysis of force interaction of welding current with self-magnetic field is performed in this paper. This analysis is confirmed by specific calculations of spatial distributions of electromagnetic field characteristics (electric current density, magnetic field intensity, bulk density of vortex component of Lorentz force, magnetostatic pressure) in arc plasma column and in weld pool metal, made for characteristic conditions of nonconsumable electrode welding.

Main theoretical postulates. In arc plasma and in molten metal, magnetic induction vector $\vec{B}$ is connected with magnetic field intensity vector $\vec{H}$ by relationship $\vec{B} = \mu_0 \mu \vec{H}$ where μ_0 is the universal magnetic constant; μ is the magnetic permeability of conducting medium. Then, the formula for bulk density of electromagnetic force can be rewritten as

$$\vec{F} = \mu_0 \mu (\vec{j} \times \vec{H}). \quad (1)$$

In the stationary case the following relationship is in place that relates self-magnetic field intensity $\vec{H}$ with electric current density $\vec{j}$

$$rot\, \vec{H} = \vec{j}. \quad (2)$$

At relatively low speeds of arc movement characteristic for nonconsumable electrode welding, electromagnetic field in arc plasma can be taken to be axisymmetric with good approximation. Such a nature of distribution of field characteristics is preserved also in the volume of metal being welded near the region of anode attachment of the arc. In the cylindrical system of coordinates (r, θ, z) for axisymmetric electromagnetic field we have $\vec{j} = \{j_r, 0, j_z\}$, $\vec{H} = \{0, H_\theta, 0\}$

It follows from equation (2) that

$$-\frac{\partial H_\theta}{\partial z} = j_r; \frac{1}{r}\frac{\partial (rH_\theta)}{\partial r} = j_z$$

then

$$\vec{F} = -\mu_0 \mu \left[H_\theta \frac{1}{r}\frac{\partial}{\partial r}(rH_\theta)\vec{e}_r + H_\theta \frac{\partial H_\theta}{\partial z}\vec{e}_z \right],$$

where $\{\vec{e}_r, \vec{e}_z\}$ are the unit vectors in the direction of the respective coordinate axes. We will transform the resulting expression to the following form

$$\vec{F} = -\mu_0 \mu \left(\frac{1}{2} \text{grad}\, H_\theta{}^2 + \frac{H_\theta{}^2}{r}\vec{e}_r \right). \quad (3)$$

By Helmholtz theorem, any vector field can be represented in the form of a sum of two vector fields $\vec{F}_{pot}$ and $\vec{F}_{rot}$, the first of which is the potential and the second one is the vortex field. In keeping with (3), potential and vortex components of Lorentz force are expressed as follows in terms of the square of azimuthal component of magnetic field intensity:

$$\vec{F}_{pot} = -\mu_0 \mu \frac{1}{2} \text{grad}\, H_\theta{}^2, \ \vec{F}_{rot} = -\mu_0 \mu \frac{H_\theta{}^2}{r}\vec{e}_r. \quad (4)$$

Let us consider the equation of movement of viscous incompressible liquid in the field of electromagnetic force $\vec{F}$

$$\rho \frac{D\vec{V}}{Dt} = -\text{grad}\, P + \eta \Delta \vec{V} + \vec{F}, \quad (5)$$

where ρ is the density; $\vec{V}$ is the vector of medium movement velocity; $D\vec{V}/Dt$ is the substantial derivative; P is the hydrodynamic pressure; η is the dynamic viscosity coefficient. Taking (4) into account, in the case of axisymmetric electromagnetic field, equation (5) can be written in the following form

$$\rho \frac{D\vec{V}}{Dt} = -\text{grad}\, P' + \eta \Delta \vec{V} + \vec{F}_{rot}. \quad (6)$$

Here $P' = P + P_{ms}$, where $P_{ms} = 0,5\mu_0 \mu H_\theta{}^2$ is the magnetostatic pressure. A similar representation for pressure also holds for equations of magnetic gas dynamics of arc plasma. It follows from (6) that in an axisymmetric electromagnetic field the movement of liquid (plasma) proceeds solely as a result of action of centripetal vortex component of force $\vec{F}_{rot} = -\frac{H_\theta{}^2}{r}\vec{e}_r$. Now, the action of potential force $\vec{F}_{pot}$ is limited to creation of magnetostatic pressure P in moving substance volume, compensating the potential component of the force, and not preventing the medium movement under the impact of mass force of another physical nature, for instance, the buoyancy force. Note, that magnetostatic pressure is distributed in a complex manner through the volume of electrically conducting medium.

By the theorem of total current, magnetic field intensity $H_\theta(r, z)$ can be represented in the following form $H_\theta(r, z) = \frac{I(r, z)}{2\pi r}$, where $I(r, z) = \int_0^r j_z(r', z) r' dr'$ is the electric current flowing within a circle of radius r, in arbitrary axial section z. Thus, vortex component of Lorentz force $\vec{F}_{rot}(r, z)$ and magnetostatic pressure P_{ms} can be expressed as current $I(r, z)$ in the following form:

$$\vec{F}_{rot}(r, z) = -\mu_0\mu\frac{I^2(r, z)}{4\pi^2 r^3}\vec{e}_r;$$
$$P_{ms}(r, z) = \frac{\mu_0\mu}{8\pi^2}\frac{I^2(r, z)}{r^2}. \quad (7)$$

Near the axis of symmetry $I(r, z) = 0(r^2)$, so that $\vec{F}_{rot}(r, z) \to 0$, $P_{mag}(r, z) \to 0$ at $r \to 0$. Formulas (7) are similar to those used at description of pinch-effect. At relatively small welding currents (of the order of 100–200 A) arc discharge compression (pinch-effect) is weak, and the action of centripetal force $\vec{F}_{rot}$ is realized by excitation of axial flow of arc plasma or weld pool metal. For qualitative analysis of the mechanism of action of force $\vec{F}_{rot}(r, z)$ on gas(hydro) dynamic flows, let us turn to equations of magnetic hydrostatics. Neglecting inertia and viscosity forces in (5), we will have

$$-\text{grad}\, P' + \vec{F} = 0. \quad (8)$$

In terms of pressure $P'(r, z)$ the system of equations (8), taking into account (3), is written as

$$\begin{cases}\dfrac{\partial P'}{\partial r} = -\mu_0\mu\dfrac{H_\theta^2}{r};\\ \dfrac{\partial P'}{\partial z} = 0.\end{cases} \quad (9)$$

In the context of magnetostatics equations (9), pressure $P'(r, z)$ created by vortex component of Lorentz force, can be interpreted as magnetic pressure, so that further on we will denote it as $P_{mag}(r, z) = P'(r, z)$. Let us integrate the first of equations (9) in the range of $[r, \infty)$, assuming that $P'(r, z)$ vanishes at $r \to \infty$ (due to the fact that $\lim H(r, z) = 0$). We have the following expression for $\vec{P}_{mag}^{\infty}(r, z)$

$$P_{mag}(r, z) = P_{mag}^{(0)} - \mu_0\mu\int_0^r \frac{H_\theta^2(r', z)}{r'}dr', \quad (10)$$

where $P_{mag}^{(0)}(0, z) = \mu_0\mu\int_0^\infty \frac{H_\theta^2(r', z)}{r'}dr'$ is the magnetic pressure on system axis. Magnetic field gradient creates force $\vec{F}_{mag} = \text{grad}\, P_{mag}(r, z)$, which is distributed in a complex way in the bulk of electrically conducting medium. Note that the second of magnetostatics equations (9) is satisfied only when $j_r \equiv 0$ in the current channel. In the general case of axisymmetric Lorentz force, defined by equation (3), the impact of force $\vec{F}_{mag}$ is balanced in equations of magnetic hydrostatics (8) (or equations of magnetic gas(hydro)dynamics) by forces of non-magnetic origin, in which the pressure resulting from dynamic velocity head can have the dominant role.

Force impact of magnetic field of welding current on arc plasma. Intensity and direction of gas-dynamic flows in arc plasma, excited by vortex component of Lorentz force, depend on the ratio of dimensions of current-conducting channels in near-electrode regions of the arc. Let us analyze three characteristic scenarios of plasma flow movement (Figure 1), differing by the nature of electric current spreading in arc column.

Scenario 1. Let us consider straight polarity nonconsumable electrode welding. Let R_a be the radius of anode attachment of the arc; R_c is the radius of cathode attachment. At $R_a > R_c$ electric current in arc column spreads by «right» cone schematic, so that vortex component of Lorentz force $_{rot}$ and magnetic pressure P_{mag} reach the greatest values near the cathode (see Figure 1, *a*), where current density is maximum, and decrease towards the anode. This results in an axial gradient of magnetic pressure in arc column plasma, which causes plasma flow in the axial direction (from cathode to anode) with subsequent formation of bell shape of the arc column.

Scenario 2. In welding over a layer of activating flux (A-TIG process), as a result of arc contraction on the anode, it is anticipated that transverse dimensions of current-conducting channels near the cathode and anode will be commensurate. Then, distribution of vortex component of Lorentz force by column height acquires two maximums, located near the cathode and anode. Magnetic pressure is distributed in a similar

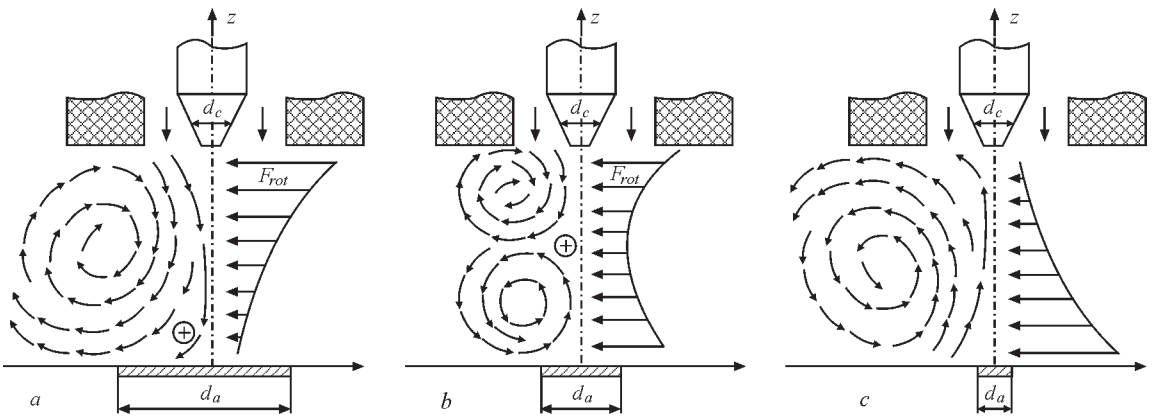

Figure 1. Distribution of vortex component of Lorentz force and plasma flow pattern in welding arc column: *a* — scenario 1; *b* — scenario 2; *c* — scenario 3

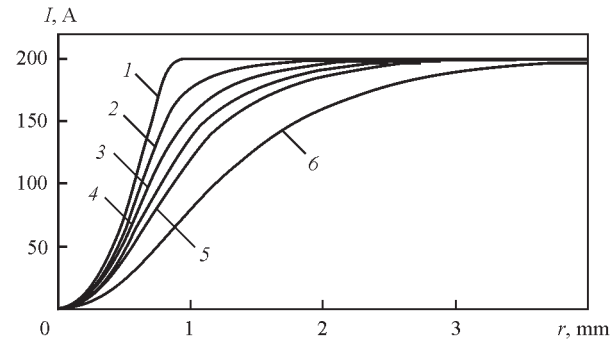

Figure 2. Change of current $I(r)$ in near-cathode region of arc column

fashion. Its gradient causes formation of two opposite vortex flows of plasma in the arc column (see Figure 1, *b*), directed from cathode and anode towards the middle (by height) part of arc column. Their interaction leads to formation of barrel shape of the column. Therefore, gas-dynamic pressure of arc column, as a factor of deformation of weld pool free surface, is in place only under the conditions of scenario 1.

Scenario 3. If $R_c > R_a$, then current spreading proceeds by «inverse cone» schematic. In TIG welding such a scenario is improbable. It, however, can be in place in hybrid laser-arc welding, when plasma flows can be directed towards the cathode (see Figure 1, *c*).

Let us illustrate the features of distribution of vortex component of electromagnetic force and magnetic pressure for free-burning argon arc 3 mm long at current $I = 200$ A (TIG welding). For this purpose we will use the results of numerical simulation [9] of distributed characteristics of arc discharge plasma, performed in keeping with arc model proposed in [10]. During analysis of results, we will prefer near-cathode region of arc column, where the current channel size is the smallest, and, accordingly, the greatest density of electric current is achieved (Figure 2). To illustrate electromagnetic field characteristics in this region, we will single out six cross-sections of arc column, namely: *1* — directly on the column boundary with cathode region; *2–6* — at distances of 0.1; 0.2; 0.3; 0.4; 0.8 mm from this boundary, respectively (in Figures 3–5 the figures on the curves indicate the section

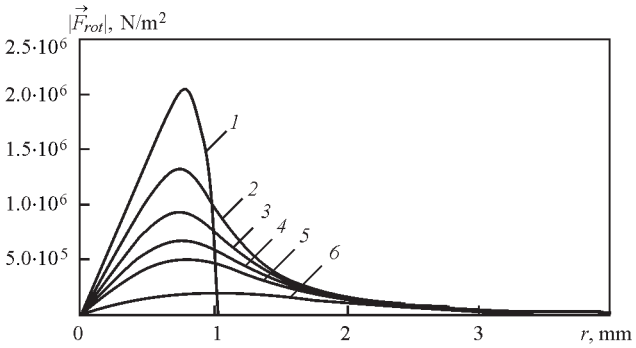

Figure 3. $|\vec{F}_{rot}|$ distribution in cross-sections of near-cathode region of arc column

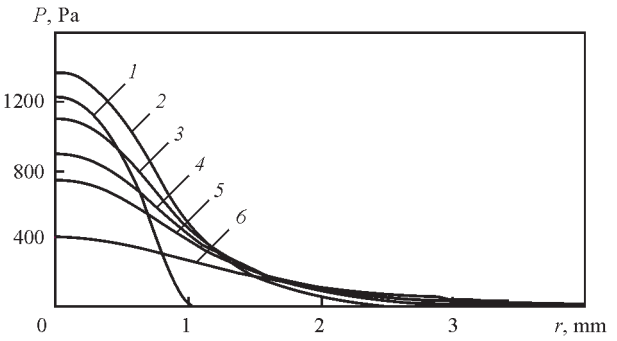

Figure 4. Distribution of magnetic pressure near the cathode

number). Nature of variation of current $I(r, z)$ flowing within a circle of radius r (see Figure 2), is indicative of the fact that in the considered case electric current spreading in arc column occurs by the schematic of «right cone» and, therefore, gas-dynamic processes in the arc discharge develop in keeping with scenario 1.

Modulus of vortex component of Lorentz force $\vec{F}_{rot}$, calculated depending on $I^2(r, z)$ by formula (7), has a maximum (Figure 3) reached in selected arc column sections at $r \approx 1$ mm, this maximum value decreasing rapidly, when moving away from the cathode. The impact of compressive force $\vec{F}_{rot}$ in near-cathode zone of arc column induces magnetic pressure P_{mag}, the maximum value of which is achieved on the arc axis. Magnetic pressure rapidly decreases with increasing distance from the cathode (Figure 4), resulting in formation of high gradient of magnetic pressure $\text{grad}P_{mag} = \vec{F}_{mag}$ in near-cathode plasma, which generates force $\vec{F}_{mag}$ near the cathode, directed predominantly towards the anode. In terms of this calculation of electromagnetic field in arc discharge, axial component $\vec{F}_{mag}$ turns out to be quite significant and is equal to more than $2 \cdot 10^6$ N/m^3.

Force $\vec{F}_{mag}$ excites plasma flow in arc column (Figure 5), predominantly directed towards the anode. This flow has an acceleration section at the distance of about 1 mm from the cathode that corresponds to the region of highest values of the modulus of magnetic pressure gradient. Velocity of plasma flow in the cen-

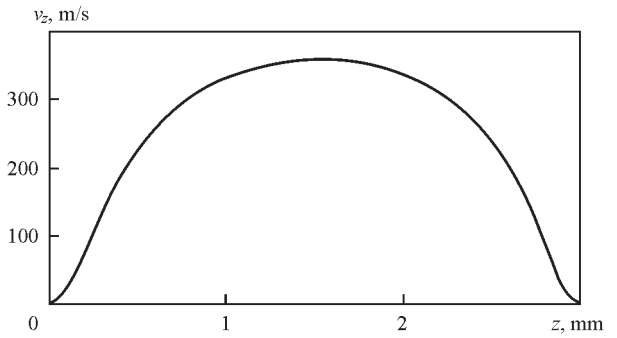

Figure 5. Distribution of velocity of plasma movement along the arc axis (coordinate z is calculated from the cathode region boundary)

tral part of arc axial region is here equal to hundreds of meters per second.

Impact of Lorentz force on weld pool metal. To analyze the force impact of self-magnetic field of arc current on weld pool metal, let us consider the model of charge transfer in the sample being welded (arc anode) of thickness L, in the assumption that electromagnetic field in the metal preserves axial symmetry, inherent to arc plasma. Let $\varphi(r, z)$ be the scalar potential of electric field, and let $\vec{j}(r, z) = -\sigma \text{grad}\,\varphi$ be the density of electric current in the metal, where σ is its specific electric conductivity. Then, we will have the following equation from the law of conservation of electric charge $\text{div}\,\vec{j} = 0$.

$$\frac{1}{r}\frac{\partial}{\partial r}\left(r\sigma\frac{\partial \varphi}{\partial r}\right)+\frac{\partial}{\partial z}\left(\sigma\frac{\partial \varphi}{\partial z}\right)=0. \quad (11)$$

We will integrate equation (11) in the domain of $\Omega = \{0 < r < R,\ 0 < z < L\}$, where we will select a rather large radius of calculation region R for free spreading of current.

Let us formulate boundary conditions. On sample surface $z = 0$, we will assign the distribution of axial component of electric current density by Gaussian law, i.e. we will assume

$$j_z(r, 0) = j_0 \exp(-a^2 r^2), \quad (12)$$

where j_0 is the axial value of current density. Parameters j_0 and a are found from the following conditions: $I = 2\pi\int_0^\infty j_z(r,0)rdr$, $j_z(R_e, 0) = j_0 e^{-2}$, where I is the assigned welding current; $R_e = \frac{\sqrt{2}}{a}$ is the effective radius of current-conducting channel on sample surface (anode).

At $r = 0$ and $r = R$ we will assign the natural boundary conditions as follows:

$$\left.\frac{\partial \varphi}{\partial r}\right|_{r=0} = \left.\frac{\partial \varphi}{\partial r}\right|_{r=R} = 0. \quad (13)$$

On plate lower surface, assuming that the sample being welded is pressed tightly to the copper backing, we will take the potential to be constant and equal to zero

$$\varphi(r, L) = 0. \quad (14)$$

In order to analyze the influence of the size of current-conducting channel in the arc anode region on force interaction of current with self-magnetic field, three effective radii of current-conducting channel were considered: R_e = 1; 2; 3 mm. Respective distributions of current density on the anode surface at current I = 100 A are given in Figure 6.

As specific electric conductivity of metal greatly exceeds that of plasma, the current coming to the metal from arc anode region, quickly spreads through the metal volume. The pattern of current spreading can be traced by distribution of current lines in the sample being welded (Figure 7). Here, the current line refers to a line, outlining the volume of metal, through which current of a specified value flows (Figure 7 shows current lines I = 10; 30; 50; 70 and 90 A). Similar patterns of current spreading in the metal being welded by «right cone» schematic are in place also at other radii of current channel on anode surface.

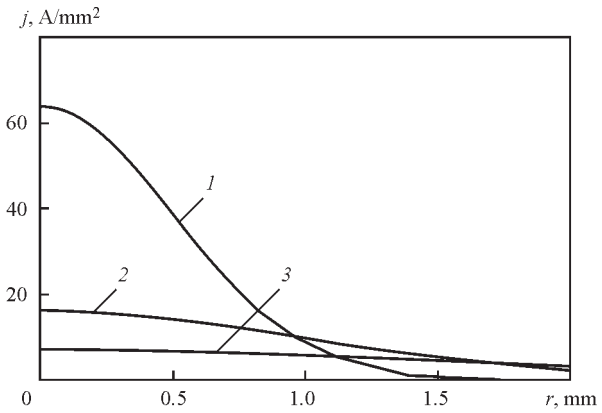

Figure 6. Distribution of current density over the anode surface: *1* — R_e; *2* — 2; *3* — 3 mm

Let us analyze the influence of the size of anode current channel on distribution of electromagnetic field characteristics in the metal being welded. Figure 8 gives for R = 1; 2; 3 mm, radial distributions of azimuthal component of magnetic field intensity H_θ in different sections across sample thickness. In keeping with the theorem of total current, magnetic field intensity as a function of radius, first rises monotonically, reaches a maximum and then decreases to zero at $r \to \infty$ as $1/r$. At the change of R_e in the range of 1–3 mm, H_θ maximum on sample surface and in underlying sections decreases rapidly, and its position shifts towards larger radii.

As the vortex component of electromagnetic force is quadratically dependent on magnetic field intensity, the above-mentioned tendency also holds for $|\vec{F}_{rot}(r, z)|$ distribution in the sample volume (Figure 9) with the only difference that $\max|\vec{F}_{rot}|$ decreases by orders of magnitude at increase of the size of effective radius of current-conducting channel on anode surface from 1 to 3 mm.

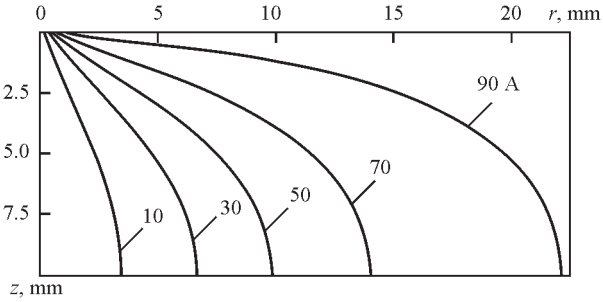

Figure 7. Current spreading in the sample being welded (anode) at R_e = 1 mm

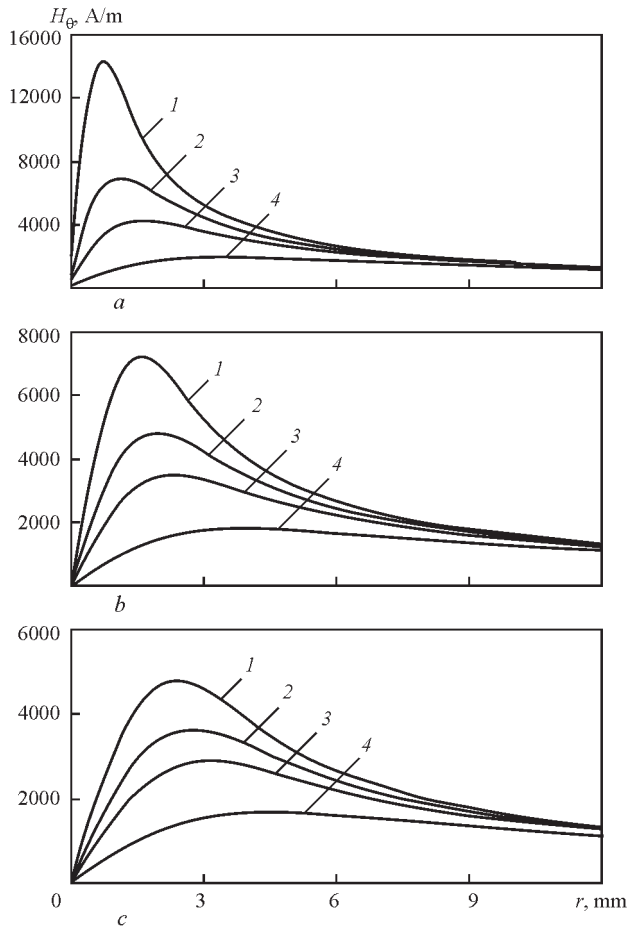

Figure 8. Magnetic field intensity in the sample being welded: *a* — R_e = 1; *b* = 2; *c* — 3 mm (*1* — *z* = 0; *2* — 0.5; *3* — 1; *4* — 2.5 mm)

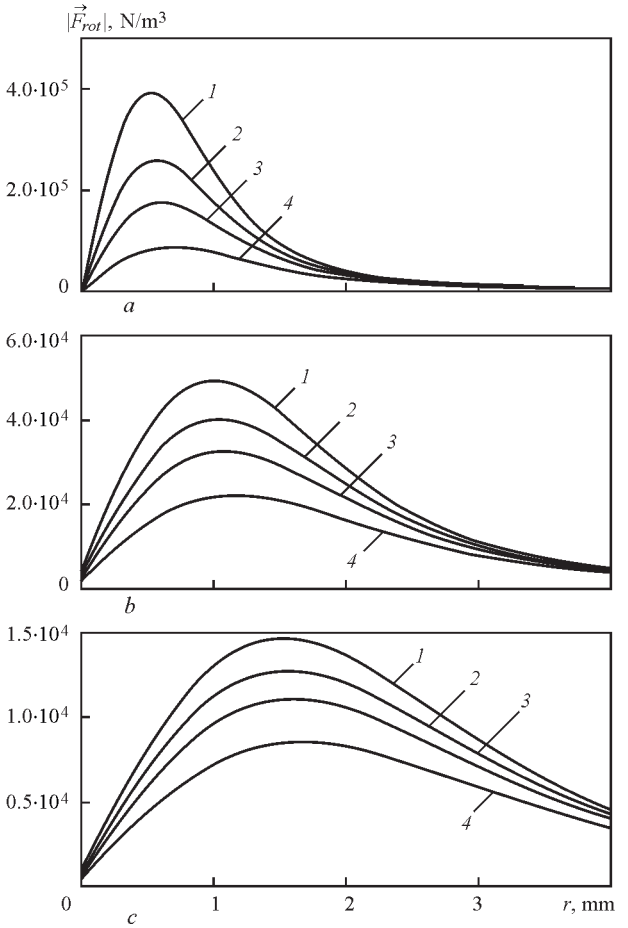

Figure 9. F_{rot} distribution in the sample volume: *a* — R_e = 1; *b* — 2; *c* — 3 mm (*1* — *z* = 0; *2* — 0.5; *3* — 1; *4* — 2.5 mm)

Before we go over to analysis of magnetic pressure distribution in the metal, due to action of force $\vec{F}_{rot}$, let us indicate two fundamental differences of force impact of welding current on arc plasma and on metal being welded. The first of them consists in that current flowing in arc plasma is limited by a region, in which electric conductivity of plasma is different from zero (tentatively, this current-conducting channel in the case of Ar corresponds to the region, where plasma temperature is higher than 5000 K), whereas in the metal being welded current flows freely and the current-conducting channel is not limited in any way. Second difference is connected with formation of magnetic pressure in arc plasma. In arc column magnetic pressure on the axis (see (10)) and in arc plasma, as a whole, is determined by the impact of vortex component of electromagnetic force in the range of $0 \le r < \infty$, while in solid metal $\vec{F}_{rot}$ impact is balanced by the forces of elasticity and does not in any way influence magnetic pressure in the weld pool. Thus, magnetic pressure in the weld pool forms due to force impact of just that part of welding current, which flows through the weld pool, and, therefore, depends on pool shape and dimensions. Taking this feature into account, we will transform expression (10) for magnetic pressure in the weld pool. Let $R^* = R^*(z)$ be the expression, describing the pool shape at a certain moment of time. Integrating the first of equations (9) in the interval of $[0, R^*(z)]$, we will obtain the following expression for magnetic pressure distribution in the weld pool

$$P_{mag}(r, z) = \mu_0 \mu \int_r^{R^*} \frac{H_\theta^2(r', z)}{r'} dr'. \qquad (15)$$

Let us consider this distribution, depending on pool dimensions and effective radius of current channel on anode surface. For qualitative analysis, we will proceed from the assumption that the pool has the shape of a hemisphere of radius R_v. Figure 10 presents the calculated data on magnetic pressure distribution in near-surface region of the pool, depending on effective radius R_e of current-conducting channel at R = = 1; 2 mm.

As the share of welding current flowing through the weld pool, is increased with increase of its size, magnetic pressure on the pool surface and in its volume is essentially increased with R_v increase for all radii of current-conducting channel on the anode (compare the right and left curves in Figure 10). The

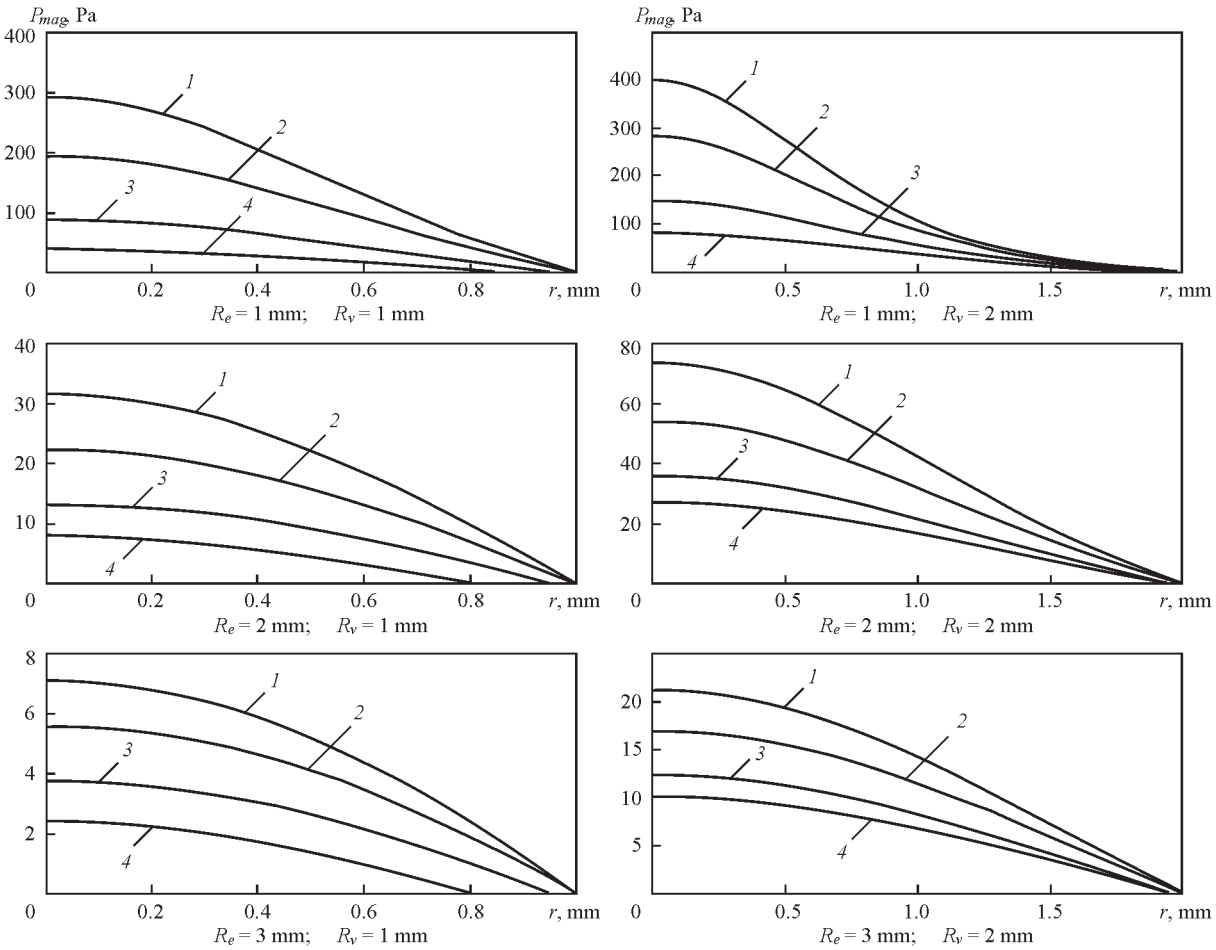

Figure 10. Distribution of magnetic pressure in the weld pool: *1* — $z = 0$; *2* — 0.15; *3* — 0.35; *4* — 0.5 mm

second conclusion which follows from calculated data given in Figure 10, consists in that the magnitude of magnetic pressure in the melt largely depends on the size of current-conducting channel on the anode: with R_e increase, magnetic pressure on the pool surface and in its volume decreases by an order of magnitude. Note that maximum magnetic pressure, reached on the pool surface at R_e = 1 mm; R_v = 2 mm, is equal to 400 Pa. This value is equal to just 0.4 % of atmospheric pressure and, at first glance it seems that magnetic pressure can be neglected. This, however, is not so, as shown by quantitative estimates derived from Bernoulli theorem for incompressible liquid. In keeping with the latter, $P_{mag} + \frac{\rho V^2}{2} = \text{const}$, i.e. in this case magnetic pressure is balanced by velocity head $\rho V^2/2$, where ρ is the metal density, V is the velocity of melt movement (the latter refers to axial component of velocity vector). For numerical estimate, we will select two sections on pool axis $z = 0$, $z = h$, the first of which corresponds to melt surface, and the second is located in-depth of the melt, where magnetic pressure is small ($P(h) \approx 0$ at $h \approx 1$ mm). We will assume $V(0) = 0$, then $V(h) \approx \sqrt{2P_{mag}^{(0)}/\rho}$, where $P_{mag}^{(0)}$ is the magnetic pressure in anode spot center on pool surface. Results of calculations by this formula are given in the Table.

It follows from the data given in the Table, that velocity of melt movement towards weld pool bottom part essentially depends on anode current density and weld pool dimensions, i.e. flow velocities grow with reduction of the radius of current-conducting channel on the anode and the greater, the larger the pool volume.

The above estimates are very approximate, i.e. they are based on unidimensional consideration of liquid metal movement (Bernoulli equation, hydraulic approximation). More accurate calculations should take into account the fact that magnetic pres-

Velocities of melt flows, at which velocity head balances magnetic pressure in the weld pool

R_e, mm	R_v, mm	$P_{mag}^{(0)}$, Pa	V, cm/s	$F_{mag,z}^{(0)}$, N/m^3
1	1	292	27	$1.09\ 10^6$
1	1.5	369	31	$1.26\ 10^6$
1	2	400	32	$1.31\ 10^6$
2	1	32	9	$7.0\ 10^4$
2	1.5	55	12	$1.15\ 10^5$
2	2	74	14	$1.45\ 10^5$
3	1	7	4	$1.11\ 10^4$
3	1.5	14	6	$2.11\ 10^4$
3	2	21	7	$3.09\ 10^4$

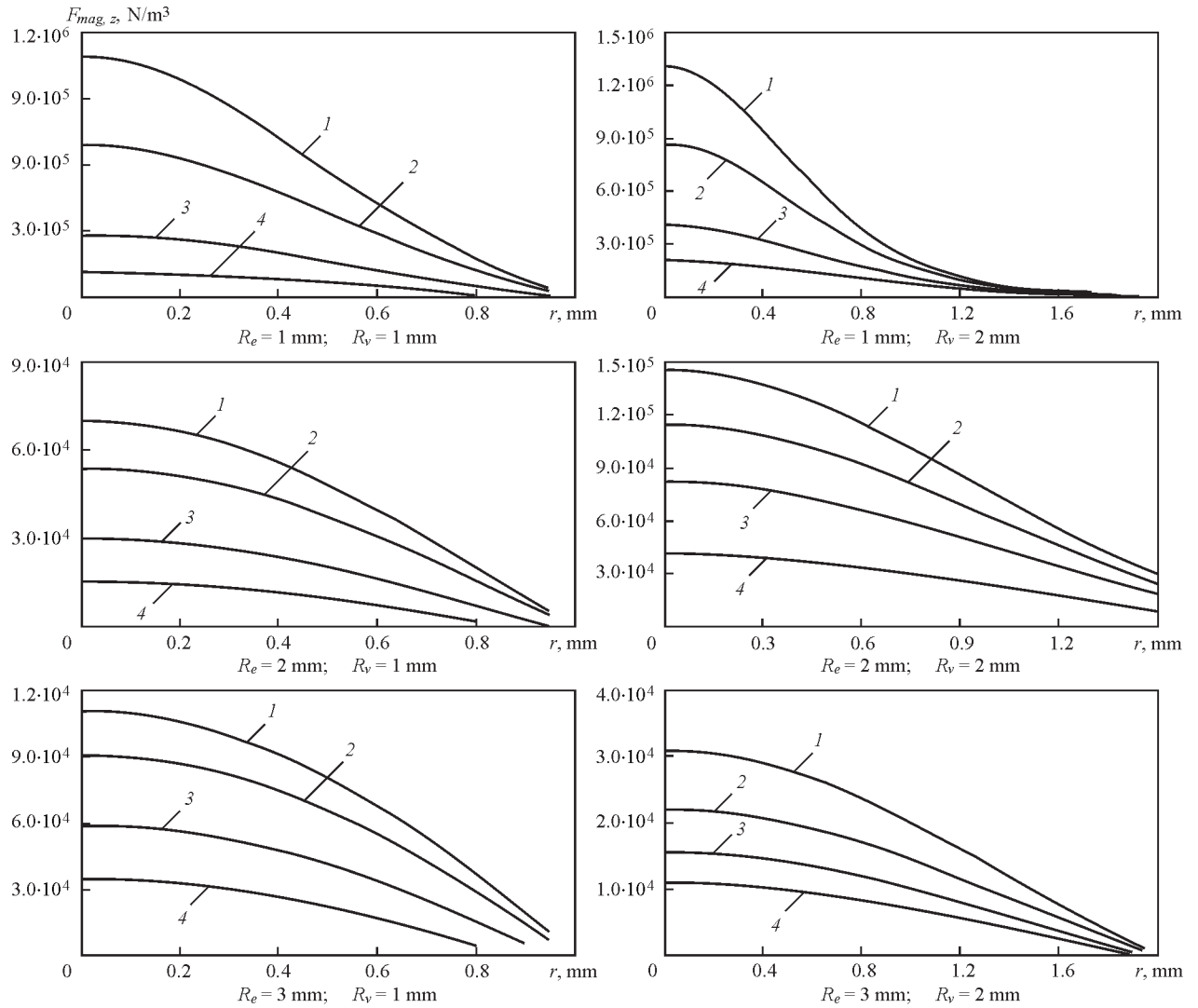

Figure 11. Distribution of F_{mag} in the weld pool: *1* — z =0; *2* — 0.1; *3* — 0.3; *4* — 0.5 mm

sure gradient creates a complexly distributed bulk force $\vec{F}_{mag} = \{F_{mag,r}, F_{mag,z}\}$ in the melt. In keeping with the first of equations (9), $F_{mag.\ r}$ component is equal to $-\frac{H_\theta^2}{r}$, and $F_{mag.\ z}$ component is presented as $F_{mag,z} = \frac{\partial P_{mag}}{\partial z}$.

Let us consider the influence of weld pool and current channel dimensions on the magnitude of axial component of force $F_{mag.\ z}$ (Figure 11). Similar to magnetic pressure (see Figure 10), axial component of magnetic force $\vec{F}_{mag}$ is maximal in anode spot center and rises with increase of current density on anode surface, as well as with increase of molten metal volume (see the last column in the Table). This component of the force has a quite considerable magnitude: at R_e = = 3 mm it is comparable with bulk density of gravitational force (F_{grav} = 7.64 N/m³), applied to the metal, and at R_e = 1 mm it exceeds the gravitational force by more than an order of magnitude. $F_{mag.\ z}$ component decreases rapidly as the function of radius, so that its magnitude at $r > 1$ mm is negligibly small compared to axial values. Contrarily, radial component $F_{mag,\ r}$, rises monotonically at increase of radius and reaches its maximum value (comparable with $F_{mag.\ r}$ by order of magnitude) at $r \approx 1$ mm. Thus, magnetic force F_{mag}, being predominantly axial by its direction, has a centripetal component, which, unlike consideration of the hydrodynamic process in Bernoulli approximation, is capable of increasing the velocity of molten metal flow towards the weld pool bottom part.

In conclusion, one can say that arc plasma interaction with the metal being welded in nonconsumable electrode welding is realized through the arc anode region that determines (see, for instance [9, 10]) such, important in terms of weld formation, characteristics as density of heat flow into the anode and density of anode electric current. Heat flow density distribution in the anode is responsible for heat conductivity mechanism of energy transfer in the metal being welded. It was from exactly such positions that N.N. Rykalin constructed [11] the theory of thermal processes in welding, not taking into account the con-

vective mechanism of heat transfer in the weld pool. Contrarily, the law of current density distribution in the anode, which determines the force impact of arc current on the molten metal, is responsible for the magnitude and direction of hydrodynamic flows in the melt, and, therefore, also for convective heat transfer in the weld pool. To increase the penetrability of the arc with refractory cathode, it is important to organize sufficiently intensive melt flows, directed from overheated near-anode zone of weld pool surface to its bottom part. As shown above, such a nature of liquid metal flow is provided by compressive action of vortex component of Lorentz force. Size of current-conducting channel on anode surface also has an essential influence on magnitude of magnetic force and velocity of downward flow of the melt: the higher the electric current contraction on the anode, the greater the magnitude of axial component of magnetic force, and the higher the speed of melt movement (see Table). This leads to a conclusion, important in terms of practical applications: to increase the arc penetrability in nonconsumable electrode welding, it is necessary to find technological means to reduce the size of current-conducting channel, and to increase anode current density, respectively.

In fundamental terms, the size of anode spot and distribution of current density in it are determined by a combination of factors, related to arcing conditions and thermal state of melt surface: welding current, arc length, plasma gas composition, temperatures of near-anode plasma and melt free surface, distribution of anode potential drop along weld pool surface. At present, welding science has a number of technological measures in its arsenal, which allows regulation (reduction) of the size of current-conducting channel of the arc in the anode. One of such methods is A-TIG welding process based on application of activating fluxes (see, for instance, [12]). Let us give for comparison macrosections of welds (Figure 12, provided by D.V. Kovalenko) in TIG and A-TIG welding in argon of 6 mm stainless steel plate.

As follows from this Figure, at the same values of arc power and length, and welding speed, penetration depth is two higher greater in A-TIG welding, than in TIG welding. This technological result is due to significantly smaller dimensions of the anode spot in A-TIG welding, compared to TIG process (current-conducting channel radius is approximately equal to 2.5 mm and 6 mm, respectively).

We will also point out other possibilities of increasing electric current density in the region of anode attachment of the arc with refractory cathode. In hybrid welding (TIG + CO_2 laser), as shown in Reference

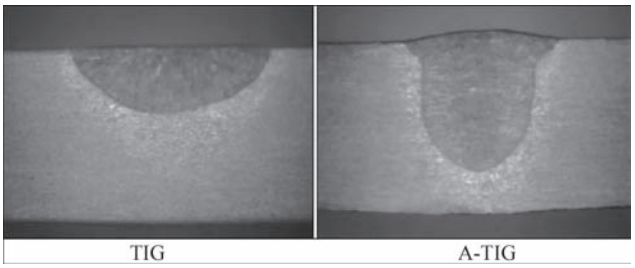

Figure 12. Weld shapes at the same arc power P = 1400 W; arc length l = 1.5 mm and welding speed V = 100 mm/min

[13], the nature of distribution of anode potential drop along weld pool surface changes, due to additional heating of near-anode plasma by laser radiation. This generates the radial component of current density in near-anode plasma, and leads to increase of current density in near-axial portions of the arc anode region.

Application of other shielding gases or their mixtures (He; Ar + H_2) instead of Ar, also leads to reduction of the size of current channel in the arc column, and of the cross-sectional size of the region of anode attachment of the arc, respectively. There is ground to believe [14] that the size of anode current channel decreases, compared to direct current welding, also in welding with high-frequency modulated current. Penetration depth becomes greater at application of the above-listed technological means. Physical mechanisms that cause the effect of anode current contraction are different in all the considered cases, however, the result — increase of arc penetrability by descending melt flows — is the same.

It should be mentioned here that the force impact of welding current on weld pool metal is not the only cause for excitation of hydrodynamic processes running in the pool. Note that the half-width of the weld in TIG welding (Figure 12) noticeably exceeds the penetration depth. The possible causes for such a weld shape can be direct thermocapillary Marangoni convection and viscous friction of arc plasma against the molten metal surface, which form melt flow directed along the pool free surface, which transports overheated metal from the center to pool side surface. The arising subsurface vortex transfers «cold» metal from the melting front to pool center in its reverse flow, reducing the conductive component of heat flow to pool bottom part.

Analysis of the influence of force factors on weld pool hydrodynamics given in this paper, and performed numerical estimates lead to the conclusion that valid calculated prediction of weld pool shape and thermal cycles in welded joint HAZ can be achieved only when convective flow of energy in the weld pool is adequately allowed for. Contrarily, the models based on heat conductivity mechanism of en-

ergy transfer, may lead to quite distorted views about the above-mentioned parameters.

1. Hsu, K.C., Etemadi, K., Pfender, E. (1983) Study of the free-burning high-intensity argon arc. *J. of Appl. Phys*., 54(**3**), 1293–1301.
2. Hsu, K.C., Pfender, E. (1983) Two-temperature modeling of the free-burning high-intensity arc. *Ibid*., 54(**8**), 4359–4366.
3. Fan, H.G., Kovacevic, R. (2004) A unified model of transport phenomena in gas metal arc welding including electrode, arc plasma and molten pool. *J. Phys. D: Appl. Phys*., **37**, 2531, 2544.
4. Nishiyama, H. et al. (2006) Computational simulation of arc melting process with complex interactions. *ISIJ Int*., 46(**5**), 705–711.
5. Hu, J., Tsai, H.L. (2007) Heat and mass transfer in gas metal arc. Pt 1: The arc. *Int. J. Heat and Mass Transfer*, **50**, 833–846.
6. Hu, J., Tsai, H.L. (2007) Heat and mass transfer in gas metal arc. Pt 2: The metal. *Ibid*., **50**, 808–820.
7. *Murphy* Anthony, B. (2011) A self-consistent three-dimensional model of the arc, electrode and weld pool in gas-metal arc welding. *J. Phys. D: Appl. Phys*., **44**, 194009.
8. Mougenot, J. et al. (2013) Plasma-weld pool interaction in tungsten inert-gas configuration. *Ibid*., **46**, 135206.
9. Krikent, I.V., Krivtsun, I.V., Demchenko, V.F. (2012) Modelling of processes of heat-, mass- and electric transfer in column and anode region of arc with refractory cathode. *The Paton Welding J*., **3**, 2–6.
10. Krivtsun, I.V., Demchenko, V.F., Krikent, I.V. (2010) Model of the processes of heat-, mass- and charge transfer in the anode region and column of the welding arc with refractory cathode. *Ibid*., **6**, 2–9.
11. Rykalin, N.N. (1951) *Calculations of thermal processes in welding*. Moscow: Mashgiz.
12. Yushchenko, K.A., Kovalenko, D.V., Kovalenko, I.V. (2001) Application of activators for TIG welding of steels and alloys. *The Paton Welding J*., **7**, 37–43.
13. Krivtsun, I.V., Krikent, I.V., Demchenko, V.F. et al. (2015) Interaction of CO_2-laser radiation beam with electric arc plasma in hybrid (laser + TIG) welding. *Ibid*., **3/4**, 6–15.
14. Zhao, J., Sun, D., Hu, S. (1992) Anode behavior of high frequency pulse TIG welding arc. *Transact. China Weld. Inst*., 13(**1**), 59–66.

Received 14.02.2017

doi.org/10.15407/tpwj2017.03.04

VACUUM DIFFUSION WELDING OF FOIL FROM POWDER NICKEL-CHROMIUM ALLOY

I.A. GUSAROVA[1], **A.M. POTAPOV**[1], **T.A. MANKO**[1], **Yu.V. FALCHENKO**[2], **A.I. USTINOV**[2], **L.V. PETRUSHINETS**[2] and **T.V. MELNICHENKO**[2]

[1]DB «M.K. Yangel Yuzhnoye»
3 Krivorozhskaya Str., 49008, Dnepr, Ukraine. E-mail: info@yuzhnoye.com
[2]E.O. Paton Electric Welding Institute, NASU
11 Kazimir Malevich Str., 03680, Kiev, Ukraine. E-mail: office@paton.kiev.ua

The paper deals with the influence of diffusion welding parameters on formation of joints from foil of Ni–20Cr powder alloy 25 μm thick. It is shown that welding of nichrome alloy in the temperature range of 800–1200 °C without application of interlayers does not allow producing defectfree joints. Features of formation of Ni–Cr alloy joints at application of interlayers from foils, produced by the technology of electron beam deposition and condensation in vacuum were studied. Foil with multilayer structure of Ni–Al, Ti–Cu systems and foil with porous structure from Cu, Ni and Cr was used in the work. Microstructure and chemical composition of the joints were studied, using optical and electron microscopy. Strength properties of metal in the joint zone were assessed by the results of microindentation and tensile testing of flat samples. It is found that application of such interlayers in welding allows producing defectfree microstructure of the joint zone. It is shown that joints with strength properties on the level of those of base metal are formed in welding through an interlayer from copper-based porous foils. 18 Ref., 2 Tables, 9 Figures.

Keywords: *vacuum diffusion welding, Ni–Cr powder alloy, porous foils, multilayer foils, microstructure, microindenting*

Development of a reliable and cost-effective thermal protection structure of windward part of reusable space vehicles is a complex science and technology problem. Development of such promising thermal protection structures with outer metal panel has been conducted in the USA and Europe starting from the middle of the 20th century. However, thermal protection ensuring normal functioning of the space vehicle during the required number of launches is practically non-existent [1].

In Ukraine a thermal protection structure with outer honeycomb panel from high-temperature Ni–Cr-based powder alloy YuIPM-1200 is also being created [2]. At up to 1100 °C temperatures this alloy has the strength of the order of 34 MPa and 30 to 40 % relative elongation at tension that ensures its performance under the conditions of considerable deformations at elevated temperatures [3]. In fabrication of a three-layer honeycomb panel of thermal protection structure the final and most critical operation is joining its elements, namely upper and lower covers with honeycomb core [4].

Various technologies of joining three-layer panel elements are available, namely fusion welding, brazing and pressure welding.

It should be taken into account that to preserve the powder alloy characteristics, welding should be performed in the solid phase that eliminates application of fusion welding: laser and electron beam processes. Moreover, fusion welding of this group of materials is difficult, because of their hot cracking susceptibility. Producing sound joints is possible only at their preheating up to the temperature of 1100–1200 °C [5]. This kind of structures can be produced by brazing. However, high-temperature operation of brazed joints leads to oxide formation in the zone of contact of the metal being joined with braze alloy. This leads to essential intensification of oxidation and intercrystalline corrosion of base material [6].

The most promising method of joining three-layer structure elements into a panel is pressure welding, namely diffusion welding.

Complexity of producing joints of high-temperature nickel-based alloys by diffusion welding consists, primarily, in presence of a heat-resistant oxide layer on their surface and low ductility of this material group. Standard preparation of the surface of samples or items before welding consists in machining, namely grinding and chemical etching that provides removal of surface layer of metal together with oxide films. Such a surface, however, is unstable under atmospheric conditions and it is very quickly covered again by a layer of oxides [7]. Thus, an oxide layer is always present on surfaces being welded, which should be removed during heating prior to conducting the welding process. As a rule, more stringent welding conditions should be applied in welding without interlayers, in view of the presence of a heat-resistant oxide film on the surface of high-temperature nickel alloys.

Table 1. Parameters of porous and multilayer foils

Interlayer	Chemical composition, wt.%					Layer alternation period, μm	Thickness, μm	Porosity, vol.%
	Ni	Al	Ti	Co	Cu			
Ni	100	–	–	–	–	–	25	23
Co	–	–	–	100	–	–	50	25
Cu	–	–	–	–	100	–	30	30
Ni/Al	86.68	13.32	–	–	–	0.40	32	–
Cu/Ti	–	–	48.32	–	51.68	0.86	40	–

Mechanical removal of oxides from the contact zone can also have a positive impact on cleaning of the surfaces to be welded. Owing to differences in plastic characteristics of the alloy and its oxides, surface layer deformation, particularly share deformation, leads to violation of integrity of oxide layer, its cracking and breaking up into fragments. Low ductility of high-temperature nickel-based alloys has a negative impact on formation of physical contact, and, consequently, on the process of adhesion, as well as bulk interaction of the surfaces being joined.

In view of the above-said, in diffusion welding of high-temperature nickel-based alloys, it is recommended to apply enhanced welding modes: temperature T = 1140–1240 °C, pressure P = 20–60 MPa, process time t = 30–120 min [8, 9].

Interlayers are applied in diffusion welding for acceleration of formation of physical contact and activation of surfaces being welded. Interlayers from foil (50–500 μm) produced by the technology of casting and subsequent rolling, are the most widely applied in welding. These foils are relatively inexpensive and adaptable to fabrication, but to ensure interlayer deformation, the welding process should be conducted at increased values of welding pressure. Here, a significant chemical inhomogeneity develops in the joint zone. Application of powder [10] or perforated foils [11] as interlayers in diffusion welding, allows lowering welding temperature and pressure, as well as increasing the uniformity of element distribution in the joint zone. However, their manufacture is a quite complex and labour-consuming process.

In order to decrease chemical inhomogeneity in the butt joint, thinner foils should be applied, capable of plastic deformation during welding. Such foils include rapidly-solidified foils [12], and condensates, produced by spraying processes, in particular, electron beam evaporation and condensation in vacuum [13]. This technology allows producing foils of different chemical composition and structural state: multilayer, porous, and gradient. A feature of both multilayer, and porous foils is the fact that they promote formation of structurally nonequilibrium state, both in the foil proper, and in subsurface layers of metal being welded. Foil heating and application of tensile stresses causes an abrupt increase of their deformation rate, which acquires an exponential dependence that is characteristic for materials at their transition into superplastic state. Application of such condensates as an interlayer in diffusion welding, promotes improvement of the conditions of physical contact formation in the butt and increase of diffusion mobility of atoms [14].

The objective of the work is studying the features of formation of welded joints from Ni–Cr powder alloy, using interlayers of different chemical composition, produced by the method of electron beam evaporation and condensation in vacuum.

Materials and methods of investigation. Studies were performed using experimental alloy YuIPM-1200 (Ni–20Cr–3–4Fe–0.40–0.6Al–0.25–0.35Ti–0.5Y, wt.%), produced by powder technology. Diffusion welding of samples from Ni–Cr alloy foil was performed in a free state in vacuum, using U-394M unit.

Ni–Cr foils of 18×11×0.025 mm size were welded. After welding the samples, sections were prepared for conducting metallographic studies and for more precise determination of the influence of thermodeformational cycle of welding on structure of the produced joints. Parameters of the welding process were

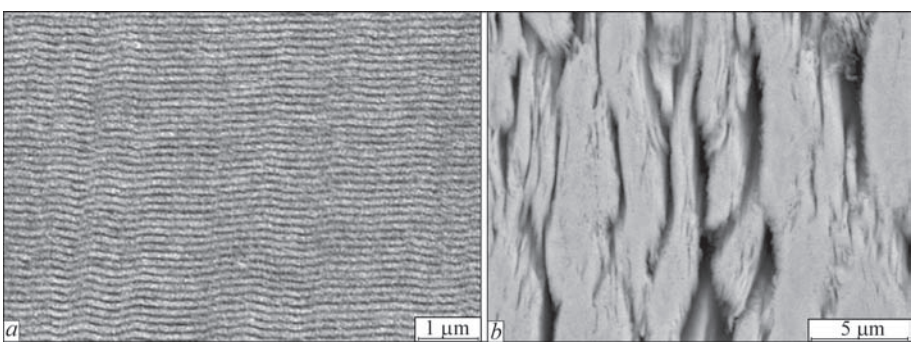

Figure 1. Microstructure of foil cross-section: *a* — multilayer Al/Ni (light layers correspond to nickel, dark layers — to aluminium); *b* — porous foil from Ni

as follows: welding temperature T = 800–1200 °C, welding duration t = 5–30 min, welding pressure P = 5–40 MPa, vacuum in the working chamber was maintained on the level of $1.33 \cdot 10^{-3}$ Pa.

For activation of adhesion at the stage of formation of physical contact, the possibility of application of vacuum condensates (Table 1) with multilayer (Ni/Al, Ti/Cu) (Figure 1, *a*) and porous structures (Ni, Co, Cu) (Figure 1, *b*) as interlayers was studied.

Interlayers for welding were produced by electron beam vacuum deposition by a procedure, described in [15].

Analysis of structural characteristics of interlayers and welded joints was performed, using scanning electron microscope CAMSCAN 4, fitted with energy-dispersion analysis system EDX INCA 200 for determination of local chemical composition on flat samples. For this purpose, transverse sections of foils and welded joints were prepared by a standard procedure, using grinding-polishing equipment of Struers Company.

Mechanical properties of welded joints were assessed by the method of automatic indenting in the plane of welded joint cross-section with recording of the diagrams of indenter loading and unloading in Mikron-gamma unit [216], and tensile testing of flat samples in MTS-810 machine.

Experimental results and discussion. As shown earlier, oxide film is always present on the surface of Ni-Cr alloys [7]. Our results demonstrate that oxygen content on the alloy surface can be higher than 16 % (Figure 2, *a*). Foil surface cleaning with R1000 sand paper to metal lustre and degreasing in alcohol allow reducing the oxide film thickness, and oxygen content on foil surface to 3%, respectively (Figure 2,

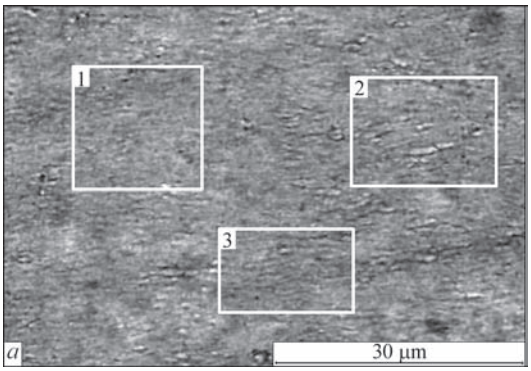

Batch number	Chemical composition of as-delivered foil surface (wt.%)							
	C	O	Al	Ti	Cr	Fe	Ni	Y
1	4.86	16.75	0.66	0.55	18.22	2.27	56.69	–
2	4.60	16.38	0.45	0.18	17.51	2.51	57.66	0.71
3	4.41	16.98	0.53	0.57	18.70	2.57	56.24	–

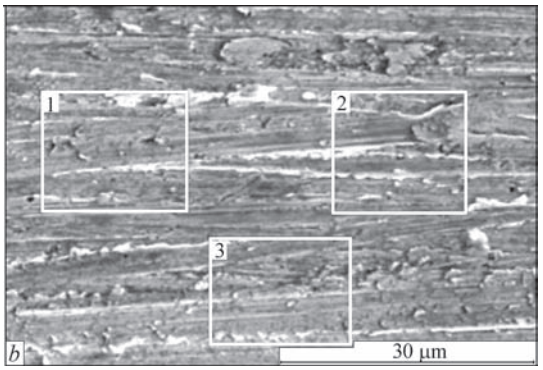

Batch number	Chemical composition of foil surface (wt., %) after mechanical treatment and degreasing							
	C	O	Al	Ti	Cr	Fe	Ni	Y
1	9,29	3,39	–	–	15,87	3,30	68,15	–
2	7,65	3,05	–	–	16,36	3,13	69,81	–
3	6,87	3,17	0,47	0,68	15,98	3,95	68,87	–

Figure 2. Appearance of the surface of foil from Ni–Cr alloy and its chemical composition: *a* — as-delivered; *b* — after mechanical treatment by R1000 sand paper and washing in alcohol

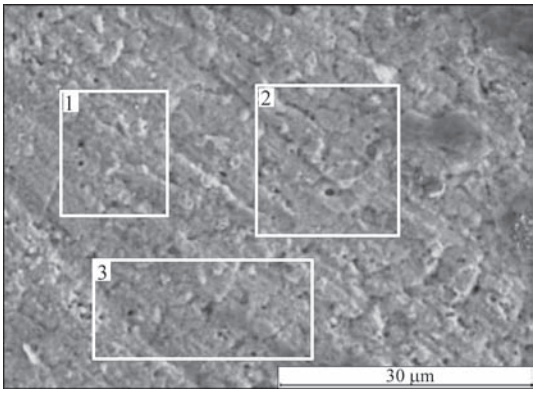

Batch number	Chemical composition of foil surface, wt.%							
	C	O	Al	Ti	Cr	Fe	Ni	Y
1	6.64	12.35	6.70	3.42	15.17	2.46	53.26	–
2	8.62	13.25	6.87	2.18	13.81	1.73	53.54	–
3	10.60	15.13	6.76	2.63	13.71	2.38	48.80	–

Figure 3. Appearance of the surface of Ni–Cr alloy foil and its chemical composition after mechanical cleaning and heating in vacuum

b). Therefore, the sample surfaces were scraped and degreased in alcohol directly before welding.

As shown by our experiments, foil heating in vacuum of $1.33 \cdot 10^{-3}$ Pa at temperature T = 1000 °C for 30 min also leads to oxidation of precleaned surface. Figure 3 gives the foil appearance and its chemical composition. As we see, after heating in vacuum, oxygen content on foil surfaces rises from 3.05–3.39 to 12.35–15.13 wt.%. Note that our data are in agreement with the results of works [8, 17]. The authors of these works recommend applying nickel coatings in welding Ni–Cr alloys that provides protection of the alloy surface during heating.

Investigations of annealing temperature influence on metal structure were conducted to select the parameters of diffusion welding of Ni–Cr alloy.

Sample heating was conducted at temperature T = 1050 °C, pressure P = 5 MPa during t = 5 min in vacuum. At analysis of foil microstructure it was found that reduction of pore content proceeds in it under the impact of temperature and pressure (Figure 4).

It is established that porosity in the foil in the initial condition is equal to 7.7 %, and after annealing it decreases to 5.2 %. Microindentation method revealed that in initial material samples average microhardness value is equal to 3.754 GPa, Young's modulus value is 139.8 GPa, deviation of modulus of elasticity is equal to 4.6 % that is indicative of material homogeneity, as well as uniformity of pore distribution through overall cross-section of foil sample. Foil annealing under vacuum leads to lowering of microhardness values by 1.6 times, compared to material in the initial condition (up to 2.293 GPa) and increase of Young's modulus to 148.7 GPa.

Increase of the modulus of elasticity can be an indication of lowering of material total porosity [18]. However, increase of the range of deviation of its values to 7.1 % can be an indication of a less uniform nature of pore distribution through overall cross-section of the foil, compared to the sample in the initial condition.

A series of experiments to produce joints at temperatures of 800, 900, 1000, 1100, 1200 °C were performed, in order to determine the optimum parameters of welding Ni–Cr alloy. Welding was conducted without application of interlayers. Welding pressure in all the cases was equal to 40 MPa, process time was 20 min.

Microstructures of joints from nichrome alloy, produced at the temperature of 800, 1000 and 1200 °C, are given in Figure 5.

As is seen from Figure 5, welded joint zone defectiveness decreases with increase of welding temperature. However, even at welding temperature of 1200 °C, a string of oxides located along the butt, is preserved in the joint zone.

In welding of Ni–Cr alloy without application of interlayers (T = 1200 °C, P = 40 MPa, t = 20 min), microhardness values in the joint zone, are close to those characteristic for annealed material H = 2.823 GPa. Results of metallographic studies, as well as a broad range of variation of Young's modulus E = 110.7–154.3 GPa lead to the conclusion that influence of high values of welding temperature and pressure results, on the one hand, in pore coagulation in the foil, and on the other hand — in nonuniform redistribution of porosity in the joint zone (Figure 6).

Influence of multilayers on formation of welded joint structure was studied. Analysis of microstructure of the joints produced with application of Al/Ni system interlayers, shows that there are no defects in the butt joint (Figure 7, *a*). Width of the joint zone (JZ) is equal to 20 μm. Depth of aluminium diffusion from interlayer into Ni–Cr alloy is equal to 5–7 μm, proceeding from element distribution (Figure 7, *b*). Chemical element content in the butt joint is equal to: 85.53 Ni; 3.75 Cr; 10.16 Al; 0.56 Fe, wt.%.

Joint zone of samples produced using Al/Ni multilayer, is characterized by higher average values of both microhardness H = 4.340 GPa, and Young's modulus E = 161.3 GPa.

In the case of application of foil of Cu–Ti system, formation of several diffusion zones with different

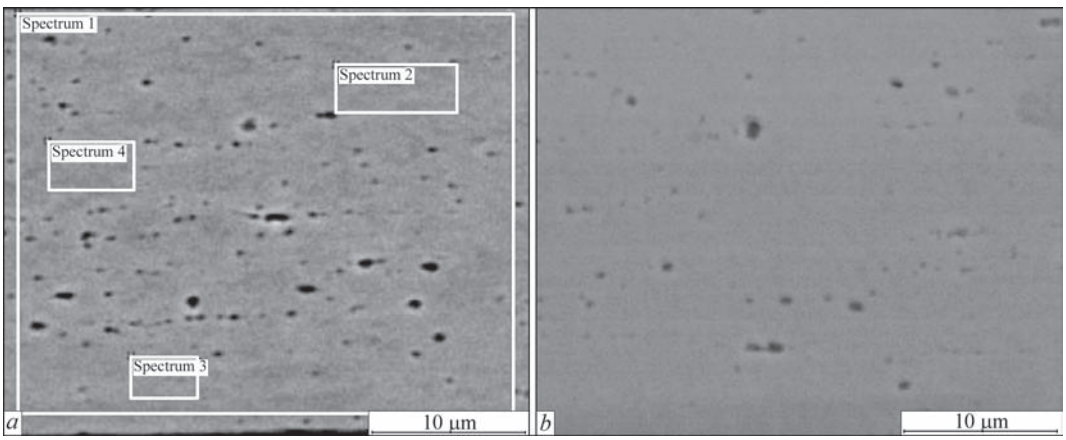

Figure 4. Microstructure of foil from Ni–Cr alloy in the initial condition (*a*) and after heating at temperature T = 1050 °C at the pressure of P = 5 MPa in vacuum (*b*)

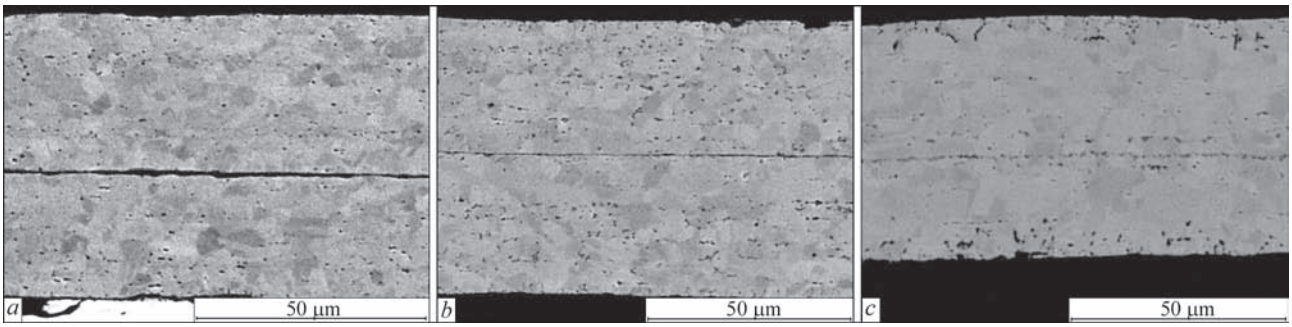

Figure 5. Microstructure of Ni–Cr alloy joints, produced at welding temperature of: *a* — 800; *b* — 1000; *c* — 1200 °C

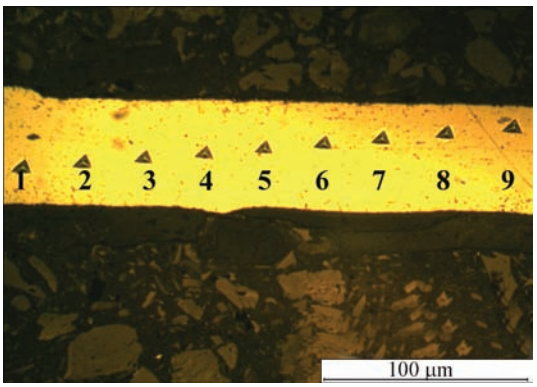

Batch number	*H*, GPa	*E*, GPa
1	2.547	110.7
2	3.029	127.1
3	2.750	112.6
4	2.689	121.4
5	2.804	125.8
6	2.403	131.1
7	2.519	140.4
8	2.707	143.5
9	2.487	154.3
Average value	2.659	129.7

Figure 6. Results of automatic indentation of the joint zone of Ni–Cr foil sample (T= 1200 °C, P = 40 MPa, t = 20 min); imprints obtained by indentation; Table of calculations (indentation was conducted at the same values P = 20 g and V = 2 g/s for all the points)

chemical composition of elements is observed in the butt joint (Figure 7, *c*, *d*). Total width of JZ is equal to 25–30 μm. As follows from graphs of element distribution, during welding nickel diffusion proceeds through the entire interlayer thickness. Depth of titanium diffusion from interlayer into Ni–Cr alloy, is equal to 12–15 μm, proceeding from element distribution (Figure 7, *d*). Nickel concentration in the interlayer is equal to about 40 %. Chromium diffusion from the foil into the interlayer is insignificant, its content in the interlayer being 1.81–2.41 %. Average value of microhardness for samples produced with Cu/Ti multilayer, is equal to H = 4.340 GPa, and Young's modulus is E = 161.3 GPa.

Applicability of porous interlayers from nickel, cobalt and copper in nichrome welding was also studied (Figure 8). Welding was performed at temperature T = 1200 °C, pressure P = 40 MPa, soaking time t = 20 min.

It is found that application of cobalt-based interlayers leads to development of considerable porosity in the joint zone (Figure 8, *a*), and nonuniformity of element distribution (Figure 8, *b*). Content of chemical elements in the butt joint is equal to: 15.80 Ni; 6.47 Cr; 1.09 Fe; 76.64 Co, wt.%. Total width of JZ is equal to 35–38 μm. Depth of cobalt diffusion from interlayer into Ni–Cr alloy is equal to 7–10 μm, proceeding from element distribution (Figure 8, *b*). Average value of microhardness for samples, produced with porous interlayer from cobalt, is equal to H = = 3.244 GPa, and Young's modulus is E = 157.3 GPa.

At application of copper-based porous interlayers the line of contact of interlayer–Ni–Cr alloy disappears as a structural element during welding (Figure 8, *c*).

It should be noted that, as copper melting temperature is equal to 1083 °C, in this case welding was conducted in transient liquid phase diffusion bonding (TLDB) mode. Presence of liquid phase in the butt joint ensured activation of surfaces of blanks being welded and copper diffusion through the entire foil thickness.

Application of copper interlayers leads to a more uniform nature of element distribution in the butt joint (Figure 8, *d*) and minimal number of defects. Chemical element content in the butt joint is as follows: 68.46 Ni; 17.26 Cr; 0.99 Fe; 14.27 Cu, wt.%. Average value of microhardness for samples produced with porous copper interlayer, is equal to H = 2.258 GPa, and Young's modulus is E = 137.1 GPa.

In welded joints produced with application of porous nickel interlayer, formation of coarse-grained structure is observed in the joint zone. Width of the joint zone is equal to 20–25 μm (Figure 8, *e*). There are no defects in the joint zone.

However, a string of pores, located along the butt joint, is observed on the boundary of interlayer–Ni–Cr alloy. Chemical element content in the butt joint is equal to: 93.67 Ni; 4.96 Cr; 0.46 Al; 0.91 Fe, wt.%, that may be indicative of the fact that a nickel-based low alloy was formed in the butt joint.

Average value of microhardness of the joint zone of samples, produced using a porous nickel interlayer,

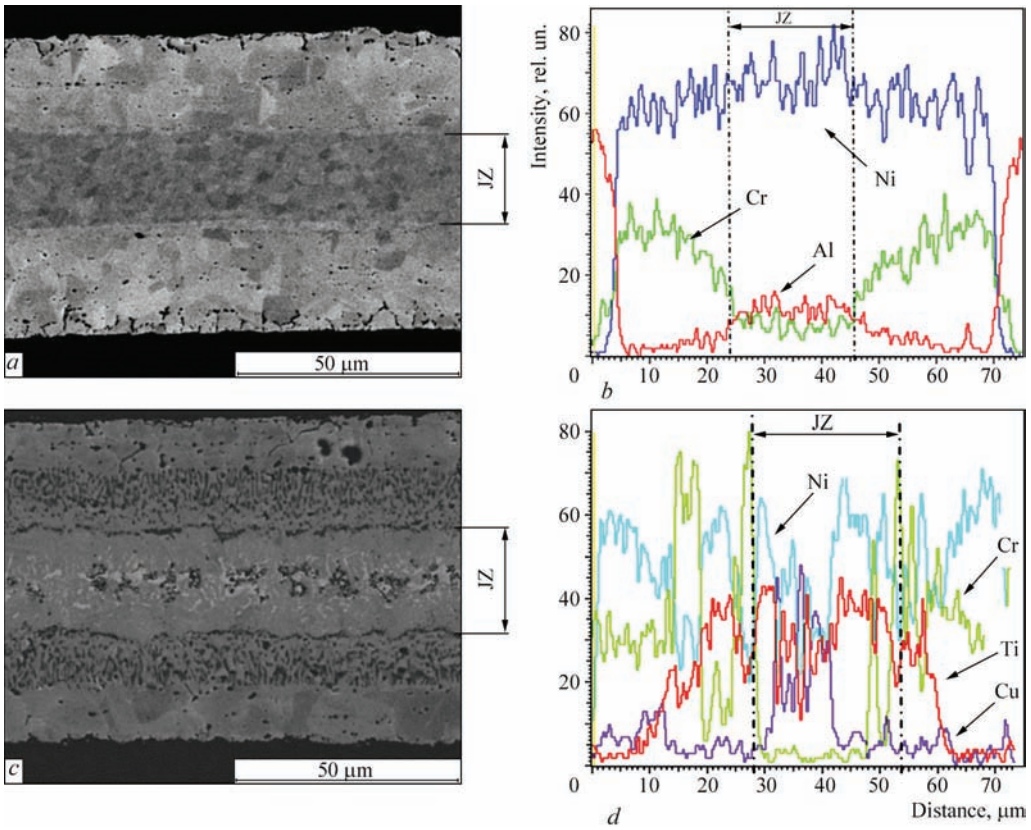

Figure 7. Microstructure and distribution of elements in joints produced with application of multilayers of Al/Ni (*a*, *b*) and Cu/Ti (*c*, *d*) systems

is equal to H = 2.119 GPa, and Young's modulus is E = 158.5 GPa.

Results of micromechanical studies of the initial material and welded joints are shown in Figure 9.

As is seen from the given data, foil microhardness (average value) after annealing decreases from 3.754 to 2.293 GPa. In welded joints produced using Al/Ni and Cu/Ti multilayer foils average values of microhardness in the joint zone are equal to 4.340 and 4.637 GPa, respectively, that, in our opinion, can be indicative of intermetallic phases formation in the butt joint. In joints, produced with application of porous foils from Cu and Ni, average values of microhardness in the butt joint (2.258 and 2.119 GPa, respectively), are close to microhardness values of Ni–Cr foil after annealing. In joints, produced with application of foil from cobalt, microhardness in the joint zone is equal to 3.224 GPa, that is higher than average microhardness values for as-annealed base material.

Mechanical properties of welded joints produced in vacuum diffusion welding of Ni–Cr alloy samples were studied. Sample length was 18 mm and width was 11 mm. Overlap was equal to 5 mm in sample welding. Results of tensile mechanical testing of welded joints are given in Table 2.

As is seen from Table 2, average strength of base metal of Ni–Cr alloy is equal to 405 MPa. Foil annealing leads to lowering of its strength level to 305 MPa. Application of multilayer foils of Cu/Ti and Al/Ni systems ensures average strength properties of the joints on the level of 161 and 100 MPa, respectively that, as was shown above, may be associated with considerable chemical inhomogeneity in the joint zone and increase of microhardness of individual structural elements in the butt joints.

Average strength of samples, made with application of porous cobalt interlayer, is equal to σ_t = = 223 MPa. Samples, produced with application of cobalt interlayer, are characterized by presence of defects in the joint zone, both in the form of pores, and as considerable chemical inhomogeneity of elements, namely Cr, Ni, Al. In our opinion, development of porosity in the butt can be associated with manifestation of Kirkendale effect.

Average strength of samples, produced with application of a porous nickel interlayer, is equal to σ_t = = 108 MPa. Proceeding from the results of metallographic studies, it can be assumed that the obtained results are associated both with formation of a zone in the butt joint which consists of low-alloyed nickel, as with the presence of pore stringers from two sides of the interlayer, that, probably, is what leads to lowering of welded joint strength.

Application of porous copper interlayer in welding Ni–Cr alloy allows producing joints with average value of strength σ_t = 317 MPa. Microstructural analysis of welded joints shows that in the case of application of porous copper interlayer and welding mode, which

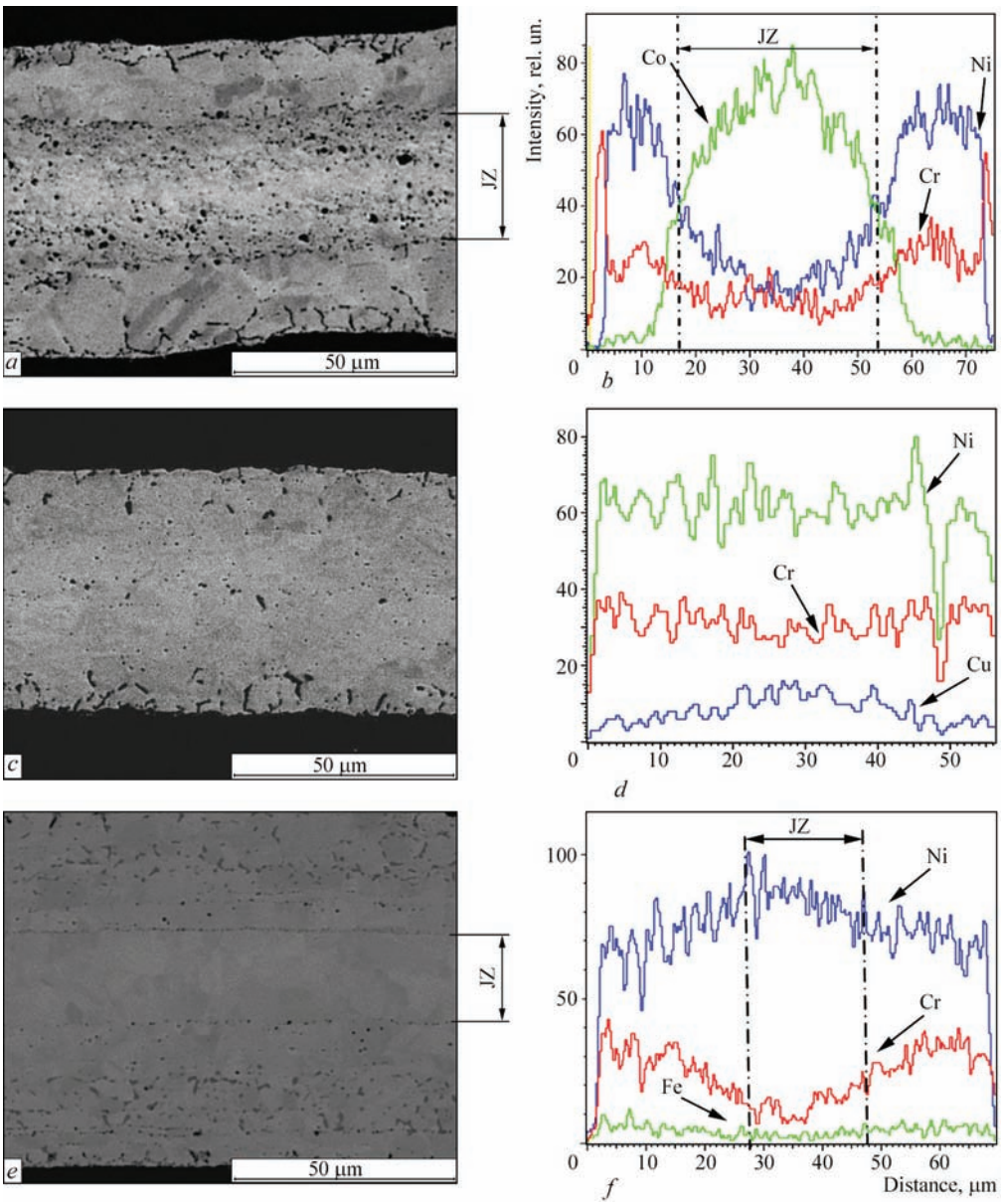

Figure 8. Microstructure and element distribution in joints produced with application of porous interlayers of Co (*a*, *b*); Cu (*c*, *d*) and Ni (*e*, *f*)

ensures running of intensive diffusion processes in the butt, the interlayer disappears as a structural element. Joint strength is on the level of that of base metal, subjected to heat treatment.

Conclusions

1. Vacuum diffusion welding of Ni–Cr powder alloy YuIPM-1200 (Ni–20Cr–3–4Fe–0.40–0.6Al–0.25–0.35Ti–0.5Y, wt.%) without application of interlayers results in formation of defects in the form of pores in the joint zone in all the studied temperature ranges of welding.

2. It is shown that annealing of Ni–Cr alloy foil in vacuum $B = 1.33 \cdot 10^{-3}$ Pa at temperature, corresponding to that of diffusion welding, is accompanied by oxidation of sample surface.

3. Application of Al/Ni and Ti/Cu multilayers in diffusion welding of Ni–Cr alloy, produced by the technology of electron beam evaporation and condensation in vacuum, promotes formation of defectfree joints. Diffusion zones with higher level of microhardness form in the joint zone.

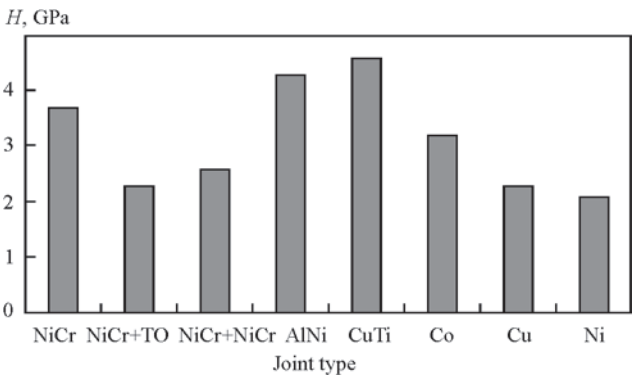

Figure 9. Microhardness values, produced for base metal and welded joints by the results of automatic indentation

Table 2. Results of mechanical tensile testing of welded joints

Sample number	Sample type	Type and thickness of interlayer, mm	Sample fracture location		σ_t, MPa	$\sigma_{t\,av}$, MPa
			Base metal	Joint zone		
1	BM	–	+	–	440	405
2			+	–	–	
3			+	–	370	
1	As-annealed BM	–	+	–	200	305
2			+	–	215	
3			+	–	500	
1	Welded joint	Cu/Ti, δ = 0.04	–	–	75	161
2			+	–	250	
3			+	–	160	
1	Same	Al/Ni	–	+	–	100
2			–	+	100	
3			–	+	–	
1	»	Ni, δ = 0.025	+	–	120	108
2			+	–	160	
3			–	+	45	
1	»	Cu, δ = 0.03	+	–	200	317
2			+	–	310	
3			+	–	360	
4			+	–	400	
1	»	Co, δ = 0.05	+	–	175	233
2			+	–	260	
3			–	+	–	
4			+	–	265	

4. Application of interlayers based on porous foil from nickel, copper and cobalt, ensures establishing of physical contact of surfaces being welded, promotes running of diffusion processes and welded joint formation. Copper-based interlayers in diffusion welding of Ni–Cr alloy, enable producing joints with the strength on the level of that of base metal after heat treatment.

1. Tumino, G. (2003) European development and qualification status and challenges in hot structures and thermal protection systems for space transportation concepts. In: *Proc. of the 4th European Workshop on Hot Structures and Thermal Protection Systems for Space Vehicles* (Palermo, Italy, 26–29 Nov. 2002). Paris: European Space Agency, 2003, 39–43.
2. *Multilayer thermal protection system of reusable space vehicle.* Pat. 91891 Ukraine. Int. Cl. B64G 1/58, B64C 1/38, B64C 3/36. Fill. 26.11.2013. Publ. 25.07.2014.
3. Frolov, G.A., Tsyganenko, V.S., Pasichny, V.V. (2010) Thermal tests of elements of rocket and space engineering products at radiation heating. *Aviatsionno-Kosmicheskaya Tekhnika i Tekhnologiya*, **10**, 28–32.
4. Gusarova, I.A., Parko, M., Potapov, A.M. et al. (2016) Evaluation of high temperature resistance of three-layer honeycomb panel produced from YuIPM-1200 alloy by vacuum diffusion welding. *The Paton Welding J.*, **12**, 29–33.
5. Medovar, B.I. (1966) *Welding of heat-resistant austenitic steels and alloys*. Moscow: Mashinostroenie.
6. Sporer, D., Fortuna, D. (2014) Selecting materials for brazing a honeycomb in turbine engines. *Welding J.*, 93(**2**), 44–48.
7. Atkinson, H.V. (1985) Review of the role of short-circuit diffusion in the oxidation of nickel, chromium and nickel-chromium alloys. *Oxidation of Metals*, 24(**3/4**), 177–197.
8. Musin, R.A., Antsiferov, V.N., Kvasnitsky, V.F. (1979) *Diffusion welding of heat-resistant alloys*. Moscow: Metallurgiya.
9. Stolyarov, V.N. (1971) Heat-resistant joints of nickel alloys made by diffusion welding and press braze-welding. *Svarochn. Proizvodstvo*, **1**, 26–29.
10. Lyushinsky, A.V. (2006) *Diffusion welding of dissimilar metals*. Moscow: Akademiya.
11. Musin, R.A., Lyamin, Ya.V. (1991) Application of perforated inserts in diffusion welding. *Svarochn. Proizvodstvo*, **2**, 2–4.
12. Falchenko, Yu.V., Muravejnik, A.N., Kharchenko, G.K. et al. (2010) Pressure welding of micro-dispersed composite material AMg5 + 27 % Al_2O_3 with application of rapidly solidified interlayer of eutectic alloy Al + 33 % Cu. *The Paton Welding J.*, **2**, 7–10.
13. Ustinov, A.I., Falchenko, Yu.V., Melnichenko, T.V. et al. (2015) Diffusion welding of steel to tin bronze through porous interlayers of nickel and copper. *Ibid.*, **9**, 13–19.
14. Kharchenko, G.K. et al. (2009) Examination of diffusion processes in welded joints of titanium aluminide (TiAl). *Visnyk ChDTU. Seriya Tekhn. Nauky*, **37**, 117–119.
15. Ustinov, A.I., Matvienko, Ya.I., Polishchuk, S.S. et al. (2009) Investigation of phase transformations and plastic deformation at continuous heating of Al/Cu multilayer foil. *The Paton Welding J.*, **10**, 23–27.
16. Firstov, S.A. et al. (2007) Indentation equation. *Dopovidi Nats. Akademii Nauk Ukrainy*, **12**, 100–106.
17. Davies, B.J., Stephenson, S. (1962) Diffusion bonding and pressure brazing of Nimonic 90 nickel-chromium-cobalt alloy. *British Welding J.*, Vol. 2, Issue 3, 139–148.
18. Akimov, V.V. et al. (2009) Influence of porosity on elastic properties of hard alloys TiC–TiN. *Prikl. Mekhanika i Tekhn. Fizika*, 50(**4**), 136–138.

Received 02.02.2017

doi.org/10.15407/tpwj2017.03.05

FORMATION OF NANODIMENSIONAL POLYGONIZATION SUBSTRUCTURE IN SPRAYED ELECTRIC ARC COATINGS

A.N. DUBOVOJ, A.A. KARPECHENKO, M.N. BOBROV and **Yu.E. NEDELKO**
National University of Ship Building named after Admiral Makarov
9 Geroyev Ukrainy Ave., 54025, Nikolayev, Ukraine. E-mail: laborantmtm@gmail.com

In the work the possibility of forming a thermally stable nanodimensional polygonization substructure in the sprayed electric arc coatings of Sv-08G2S and 12Kh18N10T wires was studied applying the additional deformation and pre-recrystallization heat treatment. It was shown that carrying out additional deformation of coatings allows 15–40 % increasing the duration of holding at heat treatment of up to 90–180 min without a significant deterioration in hardness due to decrease in the mobility of polygonization subboundaries. It was established that the size of the coherent scattering regions (CSR) of both deformed coatings, as well as coatings without deformation after performing the heat treatment (which provides the maximum hardness) is 1.5–3.0 times smaller than that in the state after spraying. With an increase in duration of holding the deformed coatings up to 150 min, the size of their CSR due to reduced mobility of subboundaries increases slightly, that is correlated with the slight decrease in hardness. As a result, carrying out the additional deformation by 40 and 15% and the subsequent heat treatment of the sprayed electric arc coatings of Sv-08G2S and 12Kh18N10T allows forming a thermally stable nanodimensional polygonization substructure, which provides an increased hardness as compared to the sprayed state by 75 and 54 %, respectively. 8 Ref., 1 Table, 2 Figures.

Keywords: *deformation, polygonization substructure, pre-recrystallization heat treatment, electric arc coatings*

The modern tendency of development of technology of thermal spraying mostly consists in increase in physical and mechanical properties of coatings applying nanostructuring. The methods for formation of nanostructures, such as spraying of ultra-dispersed powders [1, 2] and the powders produced using mechanical alloying and mechanical synthesis [3], transformation of amorphous phase into nanocrystalline ones [4] requiring special preparation of powder, are rather complex and labor-intensive and, as a result, expensive. The challenging is the application of pre-recrystallization heat treatment (PHT) of sprayed coatings [5, 6], which allows increasing their physical and mechanical properties due to producing a refined and nanodimensional polygonization substructure.

However, the produced polygonization substructure has a low thermal resistance (not more than 10 min) due to running the processes of collective polygonizaiton during a long holding at the elevated temperature which restrains the application of PHT for massive products.

The aim of this work is investigation of opportunity of forming a thermally stable nanodimensional polygonization substructure in the sprayed electric arc coatings.

For investigations the electric arc coatings were selected, as they are characterized by a high effect of increasing hardness after PHT and producing the nanodimensional substructure [5]. The coating was produced using the installation KDM-2 which is equipped with electric arc spraying device EM-14M at the following mode: arc voltage is 30 V, current is 110 A, pressure of compressed air is 0.4–0.6 MPa, distance of spraying is 100 mm. As a spraying material the welding wires of the grade Sv-08G2S and high-alloyed wires of steel 12Kh18N10T of 1.2 mm diameters were used. The optimization of the PHT mode of coatings was carried out by the values of hardness. The hardness on Vickers HV was determined in the device TP at the load to indenter of 5 kg (DSTU ISO 6507-4:2008). The heat treatment of specimens was carried out in the laboratory electric furnace SNOL-1.6.2.0.08/9-M1 at the temperature of 500 and 600 °C, respectively [6]. The additional deformation of coatings was performed by pressing at different levels of deformation. The results of measurement of hardness of deformed and heat-treated coatings are given in Figure 1.

According to the data given in Figure 1, *a*, the use of the following deformation of coatings provides a lower reduction in hardness at the increase in duration of holding at PHT to 90–180 min. Thus, for the coating of Sv-08G2S wire without deformation at the increase in duration of holding to more than 2 min (maximum hardness) to 90 min, the hardness is reduced by 30 %. Using the deformation of coating by 20, 30 and 40 % and increase in duration of holding from 5 min (maximum) to 90 min, the hardness is de-

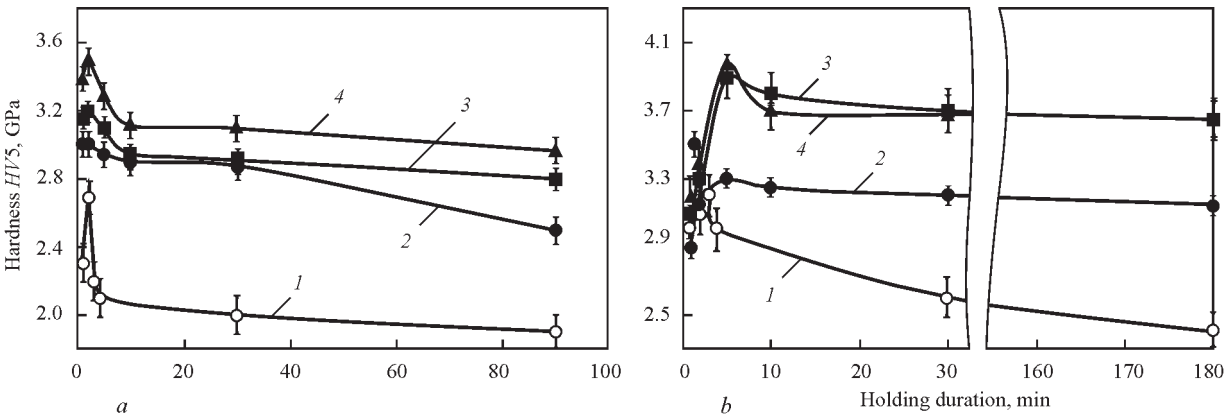

Figure 1. Dependence of hardness of electric arc coatings of the wires Sv-08G2S (*a*) and 12Kh18N10T (*b*) on the duration of holding at the heat treatment and the degree of additional deformation (curve *1* — without deformations); for a: *2* — 20; *3* — 30; *4* — 40 %; for *b*: *2* — 10; *3* — 15; *4* — 20 %

creased by 17, 12 and 16 %, respectively. The sufficient stability and high hardness of the polygonization substructure are provided by 40 % deformation.

The similar dependence is also observed for the coatings, produced of 12Kh18N10T wire (Figure 2, *b*). For the coating without deformation, at the increase in duration of holding time from 3 to 180 min, the hardness is reduced by 25 %. Using the additional deformation by 10, 15, 20 % and at the increase in the duration of holding from 5 to 180 min, the hardness decreases by 7, 5 and 8 %, respectively. In this case, the highest stability of the polygonization substructure is provided by the 15 % deformation.

This is explained by the fact that in the course of repeated deformation the dislocation interaction is finished by the appearance of dislocation barriers from 50 to 75 % (Hirt, Lomer–Cottrell), the rest ones participate in the formation of dislocation tangles. These dislocation barriers, which arise along the direction perpendicular to the axis of deformation, restrain the movement of dislocations and, as a result, reduce the mobility of polygonization subboundaries, and thus, provide a stabilizing effect by reducing the speed of polygonization processes [7].

The maximum 90 min duration of holding for Sv-08G2S wire and 150 min duration for 12Kh18N10T are provided by increase in hardness as compared to

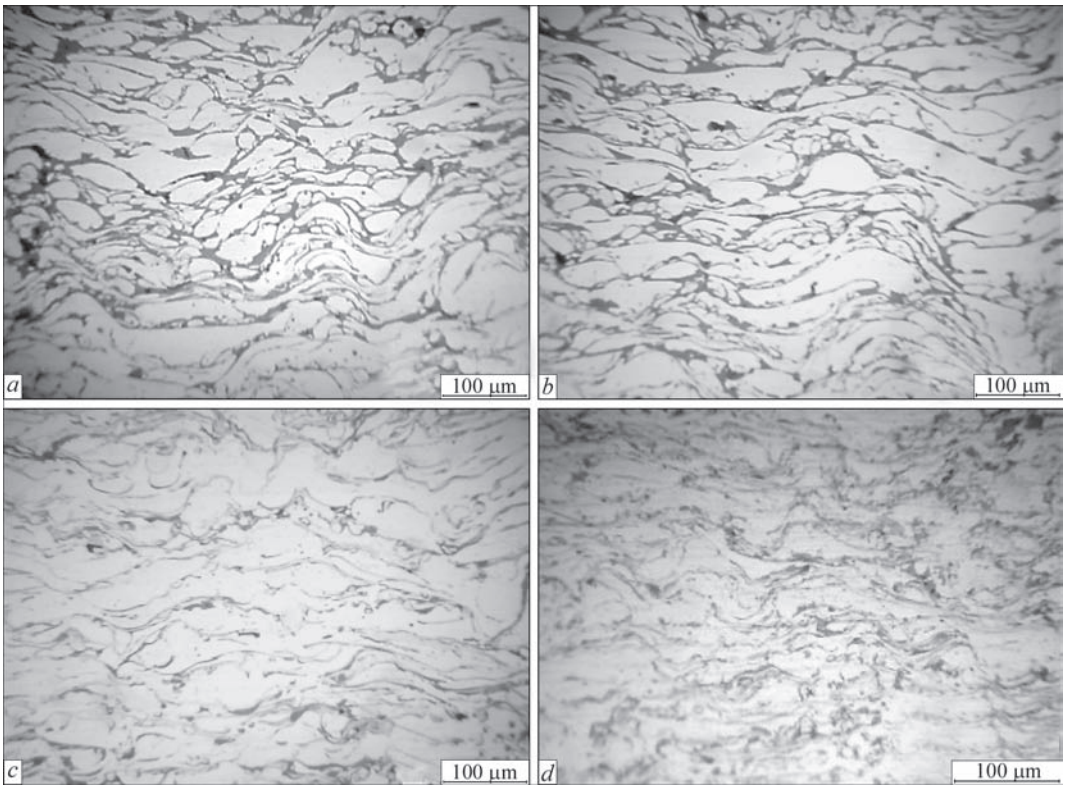

Figure 2. Microstructure of electric arc coatings of the wires Sv-08G2S (*a*, *b*) and 12Kh18N10T (*c*, *d*): *a*, *c* — after spraying; *b* — after PHT (3 min, 600 °C); *d* — after deformation at a load of 20 t

Dependence of CSR sizes of X-ray radiation of electric arc coatings on the type of treatment

Coating material	Type of treatment	CSR, nm
Св- Sv-08G2S	After spraying	200
	Spraying + PHT (2 min, 500 °C)	62
	Spraying + deformation by 30 %	163
	Spraying + deformation by 30 % + PHT (5 min, 500 °C)	82
	Spraying + deformation by 30 % + PHT (90 min, 500 °C)	111
12Kh18N10T	After spraying	200
	Spraying + PHT (3 min, 600 °C)	153
	Spraying + deformation by 15 %	164
	Spraying + deformation by 15 % + PHT (5 min, 600 °C)	87
	Spraying + deformation by 15 % + PHT (150 min, 600 °C)	138

the state after spraying by 75 % and 54 %, respectively due to increased thermal stability of the polygonization substructure as a result of deformation of coatings.

The microstructure of coatings was examined using the optical metallographic microscope MMU-3.

The investigation of microstructure of electric arc coatings of the wire 12Kh18N10T, given in Figure 2, showed that after PHT, as compared to the initial one, no changes were observed (Figure 2, *a*, *b*).

The coatings have a typical rippled microstructure. After spraying the average thickness of lamellas is about 14 μm (Figure 2, *c*), deformation using pressing to 15 % causes a decrease of this parameter to 11.9 μm (Figure 2, *d*).

The influence of deformation and PHT on the substructure of sprayed coatings was evaluated by changing the sizes of coherent scattering regions (CSR) of X-ray radiation applying the approximation method [8]. As the CSR corresponds to the internal ordering of the grain region and does not include the highly distorted boundaries, the size of CSR is identified with the average size of crystallites [8]. The X-ray diffraction analysis was carried out in the diffractometer DRON-3 in CuK_a-radiation ($\lambda = 0.154$ nm) using Ni of β filter. The rotation of specimens was carried out in the range of double angles from 30 to 100°, the scanning speed was 1 degree/min. The results of investigations are shown in Table.

According to the given data, the size of CSR subgrains of both deformed coatings, as well as coatings without deformation after performing PHT, which provides the maximum hardness, is 1.5–3.0 times smaller than in the state after spraying. With an increase in duration of holding to 90 and 150 min of the deformed coatings of Sv-08G2S and 12Kh18N10T due to decreased mobility of subboundaries the size of their CSR increases insignificantly, which correlates with a slight decrease in hardness (see Table). At somewhat shorter holding of 45 and 60 min, respectively, the CSR size for both coatings amounts to about 96 nm.

Thus, carrying out the additional deformation of 40 and 15 % and PHT of the sprayed electric arc coatings of Sv-08G2S and 12Kh18N10T allows forming a thermally stable nanodimensional polygonization substructure which provides an increased hardness as compared to the sprayed state by 75 and 54 %, respectively.

1. Kear, B.H. et al. (2000) Thermal sprayed nanostructured WC/Co hard coatings. *J. of Thermal Spray Technology*, **9**, 399–406.
2. Siegmann, S., Brandt, O., Drovak, D. (2004) Thermally sprayed wear resistant coatings with nanostructured hard phases. *Ibid.*, **3**, 37–43.
3. Borisov, Yu.S. et al. (2010) Producing of powders for thermal spray coatings by methods of mechanic alloying and mechanochemical synthesis. *Svarochn. Proizvodstvo*, **12**, 18–22.
4. Kalita, V.I. (2005) Physics, chemistry and mechanics of formation of coatings strengthened by nanosized phases. *Fizika i Khimiya Obrabotki Materialov*, **4**, 46–57.
5. Dubovy, O.M. et al. (2010) Influence of prerecrystallization of heat treatment on physical-mechanical properties of sprayed coatings and wrought metals and alloys. *Metaloznavstvo ta Obrobka Metaliv*, **3**, 7–11.
6. *Method of deposition of coatings*. Pat. 88755 Ukraine. Fill. 23.09.2009. Publ. 10.11.2009.
7. *Method of deformation-thermal treatment of electric arc coatings*. Pat. 10721 Ukraine. Fill. 03.11.15. Publ. 25.04.16.
8. Gorelik, S.S., Rastorguev, L.N., Skakov, Yu.A. (1970) *X-ray and electro-optical analysis*. Moscow: Metallurgiya.

Received 05. 01.2017

doi.org/10.15407/tpwj2017.03.06

STATE-OF-THE-ART AND PROSPECTS OF MANUFACTURING WELDED TANKS FOR OIL STORAGE IN UKRAINE (REVIEW)

Yu.P. BARVINKO, A.Yu. BARVINKO, A.N. YASHNIK and **D.V. TOKARSKY**
E.O. Paton Electric Welding Institute, NASU
11 Kazimir Malevich Str., 03680, Kiev, Ukraine. E-mail: office@paton.kiev.ua

The critical analysis of rationality of the further construction of vertical welded tanks for oil storage of 20–50 thous. m^3 capacity with the use of coiled sheet (blanks) panels is given. It is shown that the application of coiling method during erection of tanks of large capacity in 1970–1985 was largely dictated by the foreign economic circumstances. The production capacities for manufacture of coiled sheet panels, created in those years, continued to dictate the need for construction of coiled tanks also in the period of economic stability in the country. The drawbacks of coiled tanks and the proposed ways of their elimination are considered. After the collapse of the USSR the construction of tanks for oil storage of separate sheets began in the CIS countries. On the example of tanks with a protective wall the possibility of improving their reliability is shown applying the new steels of increased and high strength. The proposals for the constructive improvement of the separate elements of tanks of large capacity and the new grades of steels, recommended for them are given. 26 Ref., 1 Table, 5 Figures.

Keywords: *cylindrical tanks, coiled sheet panels, vertical site butts, low-cycle loading, restoration of wall serviceability, high-quality steels, sheet-by-sheet erection of wall*

In the recent years the periodic publications on welded steel structures deal with an active discussion regarding the rationality of applying the coiling method during construction of cylindrical steel tanks of a large capacity (V = 20–50 thous. m^3) and the search for optimal solutions for improvement of their geometrical shape [1]. A great part of coiled tanks was constructed in the USSR in the 1970–1985 years. The construction of tanks was closely connected with transportation of large volumes of Syberian oil to the European territory of the Soviet Union. Those were the years of military and economic struggle of two world systems, the years when the time was one of the most important factors in development of the country economy. The state needed to construct the main oil pipelines with the tank parks of large capacity in the shortest term in order to supply the Syberian oil to constructing objects of large oil chemistry and to the world market for filling the country budget. Under those conditions the problems of construction quality and the guaranteed service life of tanks were often sidelined.

Before discovery of the Syberian oil, during oil production of about 50 million tons per year, there was no demand for the tanks of more than 10 thous. m^3 capacity in the country. Under those conditions the quality of coiled tanks at $V \leq 5$ thous. m^3 completely satisfied the consumers. At the same time to satisfy a high demand for oil, there was a mass construction of tanks of 50–100 thous. m^3 capacity at a high technical level in the countries of Europe and in Japan. The oil was transported by tankers with displacement ranging from 50 to 150 thous. m^3 and that fact dictated namely a large capacity of tanks.

By 1970 in the system of the Ministry of Assembly and Special Construction Works the technical capacities were created allowing manufacturing the coiled sheet panels for more than 20 tanks VST (vertical steel tank) of 50 thous. m^3 per year only in one mill [2]. Under the conditions of urgent need in creating tank parks of large capacity there was no time for study and mastering foreign experience. Also from the point of view of the present time it should be confessed, that application of coiling method under that situation provided realization of an important state task, though with a rather low quality and the service life of not more than 20 years.

At the same time, even when that problem was no longer urgent, the construction of tanks of 20–50 thous. m^3 capacity with a considerably low quality was persistently continued [3]. However, that fact has its explanation as well: the Ministry of Erection and Special Construction Works established full monopoly for the whole cycle of tanks manufacture. The mentioned agency worked out the norms on erection of coiled tanks, the tanks were manufactured at the plants of the Ministry and erected by the own organizations. Already at the stage of designing the steel structures of tanks there was a necessary requirement for providing the possibility of applying the coiling method during their manufacture and erection [4]. Beginning from 1965, all the tanks with the capacity of not more than 20 thous. m^3 were constructed of coiled sheet panels. The intention of the Ministry-monopo-

list is natural and understandable. At its enterprises the large, highly-specialized production capacities were created intended only for manufacture of coiled panels. No one supports the refuse from manufacture of tanks applying coiled panels. The experience just convinced [3, 5] that it was rational to apply them for tanks with a wall thickness of not more than 8 mm. In practice, these are the vessels with the capacity of not more than 3 thous. m^3. Regarding the refuse from shop automatic welding, we should note that in the recent years for the walls and bottoms of tanks of large capacity the sheets of sizes of up to 2.5×8.0 m at the thickness of 8–30 mm are used. The sheets are welded using automatic and mechanized welding, which allows producing high-quality welded butt joints of the wall at an acceptable welding speed.

Throughout 1992–2011 the associates of the PWI carried out an evaluation of the technical condition of more than 200 coiled tanks with a capacity of 3–50 thous. m^3 at the oil parks in Ukraine. The inspection showed that after 15–20 years of service they completely exhausted their service life and required a complex capital repair [6]. Only the condition of separate tanks of the capacity of not more than 5 thous. m^3 was evaluated as satisfactory. The main reason was the presence of a large angular deformation f in the vertical welded site joints of the wall (f = 30–50 mm on base of 500 mm) and the presence of horizontal corrugations and dents in the middle and upper parts of the wall surface (Figure 1). For over 60 years the attempts of site workers to find an acceptable way to impart a design curvature to the end sections at the wall thickness of 10–18 mm, were not successful.

The cause for formation of corrugations on the wall during uncoiling the coil was considered by the authors in the publication [7]. It was shown on the concrete tank that with the difference in marks of any points of the outer contour of the bottom from the horizontal by 30–40 mm, which are accepted in the norms [8], the formation of corrugations on the middle and upper wall areas is inevitable. The panel, welded of separate sheets, represents a rectangle with dimensions of about 18×30 m, where 18 m is the height of the wall. As is observed in practice, it is impossible to impart a profile of the outer contour of the bottom with a difference in the marks of the circumferential basement of up to 40 mm without fractures arising on the thinner upper girths of the wall.

To improve the serviceability of vertical site butts of the wall of coiled tanks it was important to establish the scientifically grounded tolerances for angular deformations in them. The accepted tolerances had to ensure that welded joints would work out the designed service life in the conditions, which exclude the appearance of low-cycle fatigue in them. In 1987 at the PWI a special composite specimen for a low-cycle testing of welded joints applying angular

Figure 1. Formation of corrugations and dents on the wall after deployment of coils. 5 thous. m^3 tank with a vertical wall

deformation was developed (Figure 2). The tests of specimens of steels 16G2AF, 09G2S and VSt3sp [9] with different value of angular deformation allowed obtaining the dependence of N_{cr} on value of angular deformation in the extended range of values f. N_{cr} is the number of loading cycles of specimen before arising a visually observed crack of 3–4 mm length in the welded joint. However, the tolerances for angular deformations, developed at the PWI, were included into the new norms for erection of tanks [10] as the recommended ones. Such a record allowed the project developers to take those values f, which were easily reached by site workers. As a result, in the norms [8, 11], the recommended values for vertical site butts of the wall were excluded. In the norms a new record appeared that the value f was accepted according to the requirements of the project «Metal Structures» (MS) of the standard [12], which allows the construction of coiled tanks with a service life of not more than 15–20 years. In the standard, one tolerance for the value of angular deformation f = 1/2 inch on the 1 m long template was accepted.

At the presence of fatigue cracks in the vertical site joints of wall of the majority of coiled tanks of 10–50 thous. m^3 capacity (Figure 3, *a*) an urgent need for their repair appeared. All the specialists understood that this is a rejection of coiled technology in construction and the angular deformation (Figure 3, *b*), can not be eliminated by repair of the weld. At the initial stage of service of tanks with angular deformations, the proposals on repair were reduced to local unloading of welded joint from the circumferential forces by mounting the rigid horizontal stiffeners in the weld zone [13]. Such a solution resulted in an additional concentration of stresses in the welded

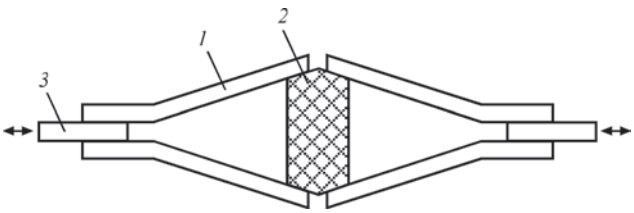

Figure 2. Scheme of composite specimen for low-cycle testing of welded joints with angular deformation: *1* — elements being tested; *2* — damper; *3* — element for fixing in the pulsator

Figure 3. 10 thous. m^3 tank with a vertical wall: fatigue cracks along the weld fusion zone (*a*); angular deformations in the vertical butt welded joint of the wall (*b*)

joint and after one or two years of service near the end regions of stiffener welds the fatigue cracks began to appear. In a number of cases several repairs of welded joints were performed by means of their partial (in girths) cutting out and welding-in of special inserts [14]. In the process of works the inadmissible deviations of geometric shape were formed on the adjacent areas of the wall. To eliminate them, a system of horizontal and vertical stiffeners with tension bars was mounted on the wall, which significantly reduced the serviceability of the wall (Figure 4).

The obtained results showed that to eliminate or reduce the local deformation of the wall after welding-in inserts, it is necessary to know the stressed state of inserts and the adjacent regions of the wall. The evaluation of stressed state of a wall area of the tank during replacement of a site butt on it with separate inserts was carried out at the PWI [15]. The calculation was carried out for the tank of the capacity of 50 thous. m^3, the project of the Central Research and Design Institute of Metal Structures named after N.P. Melnikov (Moscow), the metal of the wall was steel

Figure 4. Improvement of geometric shape of the wall of the coiled 20 thous. m^3 capacity vertical wall tank with a fixed roof applying local air holes

16G2AF, taking into account the specific technology of welding-in of inserts. The evaluation of risk of buckling of a flexible plate was performed using an approximate energy method, according to which the risk of buckling will be high, if $E = U + W < 0$, where E is the total energy of the elastic system; U is the potential bending energy for the given region; W is the work of membrane welding stresses.

The obtained diagrams of residual stresses are given in the work [15]. The calculation results allowed evaluating the probability of wall buckling in the repair area. Based on the obtained results, a special technology for replacing a vertical butt with inserts in one line along the girths with the scatter of vertical welds was developed at the PWI. The technology was tested many times in practice, as for example in vertical steel tanks of 50 thous. m^3 with floating roof at the oil refinery in Mozyr at the linear production-dispatching station «Lisichansk», when the replacement of all site butts was performed; in the vertical steel tanks of 20 thous. m^3 with fixed roof at the oil pumping stations of Kremenchug, «Snigirevka», «Avgustovka» and many other. After repair all the tanks were put into operation with a project level of loading and the service life of at least 20 years.

After more than 30 years of unsuccessful experience in construction of tanks of 20–50 thous. m^3 capacity of coiled sheet panels, the proposals of some authors [16, 17] regarding the possibility of applying the coiling method also in future, while using their inventions, are rather questionable. However, the proposals to improve the serviceability of the wall are based on significant

local violations of its rigidity, geometric shape, changes in the laminar flow of the force flow of circumferential stresses. Finely, this will lead to the appearance of new zones of stress concentration, fracture nuclei and propagation of fatigue cracks on the wall.

Since 1991, the dictate on construction of tanks under the standard projects was cancelled. The main figure then was the customer, and the main requirements for the tanks were the quality of erection, the designed service life of at least 40–50 years and the increased environmental safety. Since 2001, in the CIS countries, the tanks of large capacity began to be constructed everywhere using the sheet-by-sheet method and with the designed service life of at least 40 years (Figure 5). In Russia, the tanks were constructed «on a turn-key basis» by foreign companies [18]. In the Republic of Belarus on the Druzhba oil pipeline, two capacities of $V = 75$ thous. m^3 were constructed by the Polish company, and six capacities of $V = 50$ thous. m^3 were made by Belarusian erecting organizations [19]. The project of MS of the tank and the author's supervision were carried out by the PWI specialists. The construction coincided with the beginning of a wide application of tanks with a protective wall and a double bottom. Replacing the traditional fire dike with a protective wall provided a significant increase in the capacity of the oil park at the same areas, and a double bottom had to prevent oil from spilling to the environment. The presence of additional requirements to the tanks with a protective wall for prevention of the avalanche fractures of the main tank wall in the standards [8, 11] demanded for a scientific confirmation of the fact that new steels applied for the wall would guarantee the fulfillment of the standard requirements. With this aim, at the PWI the experimental investigations on resistance to propagation of tough fatigue crack of welded butt joints of steels of C390 strength class: 06GB and 09G2SYuch-U [20, 21] (having $KCV_{-40} \geq$ ≥ 170 J/cm^2) were carried out. On the full-scale specimens under the conditions of cyclic loading, the process of initiation and propagation of a fatigue crack from the initial notch along the fusion line was investigated. It was shown that at the final critical stage of its propagation the formed through crack had a small area of a stable (predictable) state. The length of that area by a number of cycles Nz = 300 and the periodicity of loading of tanks equal to a one loading during three days, provides a guaranteed detection of a crack by the oil spot during visual inspection of the wall in accordance with the requirement of the acting regulations on service of tanks [14]. The detection of fatigue cracks in vertical welded butt joints of the wall at the subcritical stage of their propagation almost prevents the extended fractures and full opening of the wall. This provides a clear specification of the functional purpose of a main (inner) and a protective wall of the tank. The main wall: providing static strength and prevention of extended tough fractures, the protective wall: providing static strength of the tank during its filling with oil, poured from the main tank.

Figure 5. Erection of wall of 50 thous. m^3 vertical wall tank with a floating roof applying sheets of 2.5×8.0 m

The issue of the hard contour conditions influencing the tough properties (KCV_{-40}) of the circumferential welded joints of branch pipes and manholes during their cutting-in to the first girth of the wall was also investigated. This mainly relates to the sheet rolled metal of the lower girths of the wall, which are supplied in the state after hardening with tempering: steel 06GB 390 and 06GB 355 [22] and normalized steel 09G2SYuch-U [26]. The steels 06GB390 and 06GB355 are attractive by a low carbon content and high standard values of $KCV_{-40} \geq 120$ J/cm^2 (in fact 300 J/cm^2 and more in the thicknesses of up to 50 mm). There were expectations that high tough properties of sheet metal largely compensate the increased welding deformations in the metal of circumferential weld, which arise during welding in hard contour. The branch pipes were welded-in with preheating of edges applying the electrodes OK Autrod 12.51. However, after the branch pipes with a diameter of 400 mm were welded-in into a 26 mm thick wall girth, in the circumferential welds the cold cracks appeared. To eliminate them, a rather complicated welding technology was applied, including preheating of edges, pinning of initial passes and post-weld heating of welded joint. It should be noted that the sheet rolled metal of steels supplied in the state after hardening with tempering, according to the technical conditions, has $\sigma_y/\sigma_t \leq 0.85$ for the thicknesses of 25 mm and more, and ≤ 0.90 for the thicknesses smaller than 25 mm. In accordance with the requirement of standards [8, 12], the ratio σ_y/σ_t should not exceed 0.75. In the steels proposed in these standards, the required ratio is fulfilled only for the normalized sheet steels at the present time.

For a more complete evaluation of influence of hard contour on the values of impact toughness of weld metal and the fusion zone of steels 09G2SYuch-U and 06GB, the additional investigations were carried out. Imitating the welded joint of the wall with the branch pipe and the conditions of hard contour, the plates of these steels of 26 mm thick were welded applying the electrodes LB-52U of 3.2 mm diameter. One plate was heat-treated: tempering at the temperature of 620 °C with one hour holding. The specimens were manufactured of each plate for testing on KCV_{-40} along the fusion line and weld metal. The details of the test results are considered in the work [21]. The Table given the final test results. The test results show that a high tempering of insert assembles, in accordance with the standards for wall thickness exceeding 25 mm, reduces the value of impact toughness KCV_{-40} for these steels to 10 %. This gives grounds to suggest that while obtaining a larger number of statistic data the issue of application of heat treatment at the wall thickness of 30 mm and more for the considered steels, as is accepted for pressure vessels, can be relevant [23].

The obtained results provide a determined scientific grounding for the tendency prevailed in the recent years, that for the tanks of large capacity the normalized sheet rolled metal of steels of strength class C350–420 at actual values of KCV_{-40} ≥150 J/cm^2 with the content of carbon of 0.14–0.18 % and sulfur of less than 0.01 % should be applied. The presence of higher carbon somewhat complicates and increases the cost of welding technology applied for these steels. The welded joints of wall of these steels are made using welding wire of the type OK Autrod 13/28 ESAB with a nickel content of 2.4 %. In this regard, the more attractive are the sheet normalized rolled metal 09G2SYuch-U and 09KhG2SYuch-U of the steel class C 355–420 with a reduced content of carbon (0.10–0.13 %), increased content of manganese (1.9–2.2 %) and microalloying with cerium (0.001–0.050 %), developed at the PWI [24].

With the use of the sheet normalized steel 09G2SYuch-U390 in accordance with the project and at the supervision of the PWI specialists, in the Republic of Belarus two vertical steel tanks of 50 thous. m^3 with a floating roof were constructed with a protective wall (Figure 5). In the main tank the first (l = 26 mm) and the second (l = 22 mm) wall girths, and in the protective tank the first one (l = 21 mm) were made of this steel. In accordance with the factory certificates for the sheet l = 26 mm, the value of impact toughness was KCV_{-40} = 173–204 J/cm^2. The application of preheating of edges and mechanized shielded-gas welding (Ar + 20 % CO_2) with the solid wire EMK 6 ER 70 S-6 eliminated the occurrence of cold cracks in welded joints of the wall and in the welds after welding-in of branch pipes and manholes. After additional investigations of welded joints taking into account the presence of hard contour, the solution was taken to refuse from a high tempering of insert assembles and manholes. The assembly of the bottom hatch was subjected to heat treatment, as was envisaged [12].

The author's supervision of erection of four tanks of 50 thous. m^3 capacity, having a protective wall [19], revealed a number of significant drawbacks regarding the design and serviceability of the two-layered central part of the bottom. The two-layer bottom was used at the request of the customer. The assembly and welding of one sealed compartment of the bottom per one shift, provided by the project to prevent moisture from entering the compartment, was often an unreal task. Having ten compartments on the bottom, it was almost impossible to succeed in ten dry days at the construction area. Therefore, the ends of the compartments remained open until the moisture evaporated completely during solar heating of the upper bottom. It was necessary to refuse also the control of sealing the compartments by vacuum. When the tank is filled the vacuum does not react to the presence of leakage in the upper bottom. In winter, in the interlayer space, the moisture condenses, which leads to a sharp drop in vacuum. Therefore, to check sealing the sensors with a response to the presence of hydrocarbon vapors were mounted into the signal pipes.

The analysis of assembly of the double bottom showed that its structure is very metal-consuming and labor-intensive in manufacture. The total design thickness of the bottom of tanks was 8 + 11 = 19 mm (vertical wall tanks of 75 and 50 thous. m^3 with a floating roof [19]) at the thickness of the outer, contour, bottom (edges) was 20 mm. There is a clear disregard of the principle of maximum concentration of metal in one element. With leakage of the sealed compartment, the removal of oil and its vapors from it is complicated. The experience, gained over 20 years in service of tanks of a capacity of 20 thous. m^3 with a thickness of edges of 9 mm [25], convincingly showed that such thickness in the presence of anticorrosion coating is quite sufficient to maintain its impermeability over 40 years. This is confirmed also by the norms of the

Influence of hard contour conditions on the value of toughness of welded butt joints of 06Gb and 09G2SYuch-U steels of 26 mm thickness

Welding conditions	Heat treatment presence	KCV_{-40}, J/cm^2	
		09G2SYuch-U	06GB
In free state	Absent	317.1–416.9 351.7×3	338.5–342.2 350.7×3
	High tempering	303.4–329.3 316.1×3	341.1–339.3 340.2×3
Hard contour	Absent	338.3–337.5 338.3×3	340.1–339.2 340.6×3
	High tempering	338.7–273.4 308.1×3	343.3–248.2 311.3×3

Note. Notch location is fusion line.

OJSC «AK Transneft» [26], where the thickness of the edge and the central part of the bottom of tanks of a large capacity is accepted as equal to 9 mm.

On agreement with the customer, in two similar tanks of the third stage of construction, the bottoms were accepted as single-layer of 12 mm thickness [19]. The application of a single-layer thickened central part of the bottom significantly reduced the metal consumption and the volume of site works and increased its reliability. Taking into account the experience gained in the construction of tanks in the Republic of Belarus, the PWI realized the projects of vertical 50 thous. m^3 tank with a floating roof for its construction at the linear production-dispatching station «Brody», the vertical 20 thous. m^3 tank with a floating roof at the oil pumping station «Avgustovka» (the customer is PJSC «Ukrtransneft»), for capital repair of the vertical 50 thous. m^3 tank with a floating roof (PJSC «Ukrtatnafta», Kremenchug). In all the mentioned objects the application of the new tested steels and design solutions was provided.

Based on the mentioned analysis of the performed works for evaluation of technical condition of the coiled tanks of the capacity of 5–50 thous. m^3 after their service during 15–20 years and proposals on construction of tanks with a protective wall and a guaranteed service life of at least 40 years, the following conclusions can be made:

- tanks for storage of oil and oil products with the thickness of lower girth of wall of 10 mm and more, assembled of coiled sheet panels, do not meet the requirements of existing standards as to the geometric shape of wall and the estimated service life of 20 years;
- application of coiled sheet panels during erection of wall of tanks should be limited in the standard of Ukraine by a thickness of the lower girth of not more than 8 mm;
- in the standard of Ukraine ([8], Table 13), it is necessary to state clearly the requirements to the local angular deformations of vertical welds of the wall. The admissible value of deflection f on the 500 mm base for the entire wall should be indicated not in the project of MS, but in the standard;
- the list of steel grades recommended in the standard of Ukraine (DSTU B V.2.6-183:2011, Table 7) should be supplemented with the new steels of strength class C355–440: 06GB355; 06GB390 (delivery in the state of hardening with tempering); 09G2SYuch-U390; 09KhG2SYuch-U440 (delivery in the as-normalized state).

1. Barvinko, A.Yu. et al. (2016) Application of sheet quality steel of higher strength in oil storage tanks. *Montazhn. i Spets. Raboty v Stroitelstve*, **1**, 2–8.
2. Biletsky, S.M., Golinko, V.M. (1983) *Industrial manufacture of oversized welded sheet structures*. Kiev: Naukova Dumka.
3. Kupreishvili, S.M. (2013) Vertical cylindrical tanks with floating roofs. *Montazhn. i Spets. Raboty v Stroitelstve*, **2**, 2–16.
4. *SNiP 2.09.03–85*: Construction of industrial enterprises, 33.
5. Barvinko, Yu.P., Golinko, V.M. (2009) To the 60th anniversary of industrial application of the technology of manufacturing cylindrical tanks from coiled blanks. *The Paton Welding J.*, **2**, 26–28.
6. Barvinko, Yu.P., Barvinko, A.Yu., Kargin, A.Yu. (2006) Restoration of tanks for oil storage with walls from coiled blanks of 20 thous. m^3 and 50 thous. m^3 capacity. *Montazhn. i Spets. Raboty v Stroitelstve*, **10**, 5–13.
7. Barvinko, Yu.P., Barvinko, A.Yu. (2013) On possibility of application of coiled blanks in modern tank building. *Ibid.*, **11**, 2–7.
8. *DSTUB V.2.6-183.2011*: Vertical cylindrical steel tanks for oil and oil products, 77.
9. Biletsky, S.M. et al. (1992) Improvement of resistance to low-cycle fatigue of vertical welded butt walls of cylindrical tanks with angle deformations. *Avtomatich. Svarka*, **7/8**, 41–46.
10. *VSN 311–89:* Assembly of vertical cylindrical steel tanks for storage of oil of 100 to 50000 m^3 volume. 33–37, 60.
11. *GOST R 52910–2008*: Vertical cylindrical steel tanks for oil and oil products, 52.
12. (2007) *API STANDARD 650*: Welded steel tanks for storage of oil products, 410.
13. Popovsky, B.V., Ritchik, G.A. (1986) Ensuring of geometric shape of coiled tank walls in zones of site welds. *Montazhn. i Spets. Raboty v Stroitelstve*, **11**, 12–15.
14. (1988) *Operating rules of tanks and instructions for their repair*. Moscow: Nedra.
15. Makhnenko, V.I., Barvinko, A.Yu., Barvinko, Yu.P. et al. (2002) Estimation of stressed state of the wall of coiled vertical cylindrical tanks in welding-in of insert plates. *The Paton Welding J.*, **5**, 2–6.
16. Kupreishvili, S.M. (2015) Oil production and state-of-the-art of modern tank building. *Montazhn. i Spets. Raboty v Stroitelstve*, **10**, 2–11.
17. Doroshenko, F.E. (2016) Problems of ensuring of geometric accuracy of vertical steel tank bodies. *Ibid.*, **5**, 2–7.
18. Kupreishvili, S.M. (2016) Classical vertical cylindrical tank. *Montazhn. i Spets. Raboty v Stroitelstve*, **7**, 2–11.
19. Chernikov, O.P. et al. (2014) Modern tank building in Belarus Republic. *Ibid.*, **12**, 9–13.
20. Barvinko, A.Yu., Barvinko, Yu.P. (2016) On possibility of prevention of avalanche fractures of wall of cylindrical tanks for oil storage using steel sheets with higher values of impact toughness. *Tekhn. Diagnostika i Nerazruch. Kontrol*, **2**, 44–49.
21. Poznyakov, V.D., Barvinko, A.Yu., Barvinko, Yu.P. et al. (2012) Cold resistance and lamellar fracture resistance of welded joints on steel 06GB-390. *The Paton Welding J.*, **3**, 35–39.
22. *TU U 27.1-05416923-085:2006*: Sheet products being welded from quality steel of 355-590 strength classes for machine building. Term of validity 12-31–2016, 11.
23. *OST 26 291*: Welded steel vessels and apparatuses. General specifications.
24. *TU 14-1-5065–2006*. Modification 1. Thick plates of low-alloy steel of grades 09G2SYuch; 09G2SYuch-U; 09KhG2SYuch; 09KhG2SYuch-U.
25. *Typical project TP 704-1-70*: Vertical cylindrical steel tank for oil and oil products of 20000 m^3 capacity. Moscow: TsNII PSK, 1972.
26. *RD 16.01-60.30.00-KTN-026-1–04:* Codes of design of vertical steel tanks for oil storage of 1000–50000 m^3 capacity. Moscow.

Received 18.01.2017

doi.org/10.15407/tpwj2017.03.07

STATE-OF-THE-ART OF METHODS FOR IMPROVEMENT OF CORROSION RESISTANCE AND CORROSION FATIGUE RESISTANCE OF WELDED JOINTS (REVIEW)

S.A. SOLOVEJ
E.O. Paton Electric Welding Institute, NASU
11 Kazimir Malevich Str., 03680, Kiev, Ukraine. E-mail: office@paton.kiev.ua

To improve the service reliability of products and welded structures in the conditions of corrosive environment, the methods of surface plastic deformation of metal are applied, which impart the physical-mechanical properties to the hardened layer, differed from the base metal. The technical progress contributes not only to the development of new methods of surface plastic deformation (for example, surface fusion using a nanopulsed laser), but also to the continuous improvement of conventional methods (shot blasting, pressure treatment, etc.), the efficiency of which was proved in practice. The aim of this review is to evaluate the current state of use of surface plastic deformation methods to increase the corrosion fatigue resistance and durability of steels and welded joints. The analysis of literature data showed that the experimental investigations of recent years are mainly devoted to the determination of efficiency of hardening the stainless steels and their joints applying these methods for subsequent application in such areas as medicine (implants), nuclear power engineering (reactors) and shipbuilding. For the treatment of welded metal structures, the most promising is ultrasonic impact treatment due to compactness and mobility of the equipment, ecological compatibility of the technological process, high efficiency, capability of strengthening the welded joints in any spatial positions in the field conditions. 37 Ref., 4 Figures.

Keywords: *welded joint, corrosion, surface plastic deformation, ultrasonic impact treatment, corrosion fatigue, corrosion resistance*

The service life of a large part of welded metal structures (bridges, overpasses, stationary offshore platforms, antenna-mast constructions, cranes, frames of rolling stock carriages, etc.) is determined by the fatigue resistance of their welded assemblies and components. The corrosive effect from the environment leads to a decrease in the characteristics of fatigue resistance of the base metal and welded joints, and, as a result, promotes a premature corrosion-fatigue fracture. To improve the service reliability of products and structures, the advanced welding technologies are introduced, new welding materials are applied, modern coatings are used, etc. The application of these measures, as a rule, is not sufficient for a significant increase in their service life, therefore, in practice, to increase the fatigue resistance of base metal and welded joints under the influence of corrosive environment the different methods of surface plastic deformation (SPD) of the metal are applied. The SPD methods, such as shot blasting, running-in by balls and rollers, pneumatic hammer treatment, hydraulic shot blasting, inertial-dynamic hardening, explosion treatment, etc. have proved to be efficient. Despite the considerable volume of publications on the establishment of efficiency in application of SPD methods and the experience of their use in practice [1–4], the world research centers continue to carry out investigations on this topic. This is associated with the fact that a constant improvement of technologies (equipment, consumables) and the materials, which are subjected to hardening, expands the scope of application for SPD methods.

Increase in corrosion resistance and resistance to corrosion fatigue of metals and alloys applying SPD methods. Over the years in the course of investigations it was established that SPD methods contribute to change in the structure of the surface layer of metal, increase in hardness and wear resistance, inducing the residual compressive stresses, increase in resistance to corrosion fatigue and change in roughness of the surface. The publications of the recent years are devoted to investigation of efficiency of conventional SPD methods (shot blasting, grinding and treatment by a pneumatic hammer) depending on technological parameters of surface hardening, as well as on investigation of quite new technologies (for example, surface fusion using a nanopulsed laser or high-power pulsating electron beam) [5–17].

In the works [6–9] the results of investigations of shot blasting treatment (ST) of the surface of specimens of base metal of stainless steels are given for

increase of their corrosion resistance. The results of investigations of corrosion resistance of hardened specimens are given depending on technological parameters of treatment: type of shot (steel, ceramic) and size of shot (from 125 to 850 μm), working air pressure, treatment time, number of surface treatments (one or two) and intensity of treatment. It was established that ST improves the hardness and wear resistance of specimens, but, as a rule, it leads to decrease in corrosion resistance of stainless steels. This is connected with increase in the effective surface area of corrosion-mechanical losses of the material due to increase in surface roughness after ST. In order to increase the corrosion resistance of base metal, it is proposed to apply the additional measures for the surface passivation: deposition of a thin hydroxyapatite film, nitriding, grinding to the depth of 10–15 μm. It was shown that application of ST leads to increase in resistance to corrosion fatigue. In the work [6] it was established that the limit of the endurance margin based on $2 \cdot 10^7$ cycles of stress changes in specimens of steel AISI316L in Ringer's solution after ST is 4 % lower than that after compression (deformation) in hot state, but it is 55 % higher than in the initial state (Figure 1). The deposition of a hydroxyapatite film additionally increases the limit of the endurance margin of specimens in Ringer's solution by 4.4 % after ST and by 6.3 % after deformation in a hot state.

In the works [9–11] the data of corrosion resistance of specimens of stainless steels after application of the technology of high-frequency mechanical peening (HMP), known as ultrasonic impact treatment (UIT) in the foreign literature, are given. It was established that UIT improves their corrosion resistance due to structural changes in the surface layer of the metal, increase in microhardness and formation of a uniform oxide film enriched in chromium. It is shown that as a result of UIT of steel AISI321 the refining of structure to nanosizes occurs in a thin surface layer of metal: in the course of deepening to 30 μm from the surface being treated, the grain size increases gradually from 10 to 60 nm. It is noted that despite a more significant increase in martensite after UIT, and, consequently, the increase in galvanic effect between austenite and martensite in stainless steels, the resistance of general and localized corrosion of specimens after UIT is higher as compared to the base metal and specimens, hardened applying ST.

In the work [12] the efficiency of applying surface mechanical grinding (SMG) for increasing the corrosion resistance of specimens of stainless steel AISI304 was investigated depending on such technological parameters of treatment as diameter of the balls (2, 5 and 8 mm), and the time of treatment (15, 30 and 45 min).

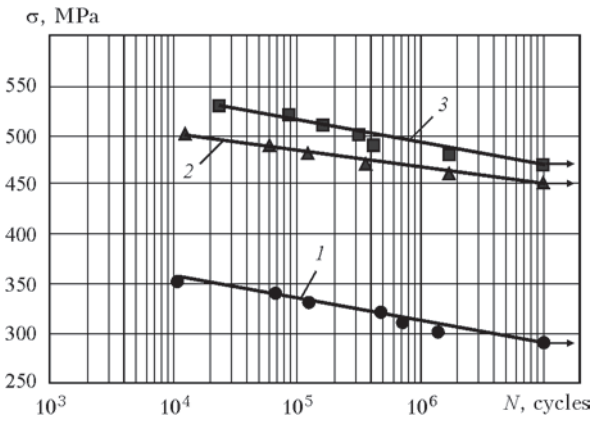

Figure 1. Fatigue curves of specimens of steel AIS1316L in Ringer's solution: *1* — in initial state; *2* — after hardening by shot blasting treatment; *3* — after compression (deforming) in a hot state [6]

The SMG technology represents a mechanical surface treatment with steel balls over the preset time in the special vacuum chamber mounted on the vibrating table. It was shown that roughness of specimen surface after SMG increases with increase in diameter of the applied balls and almost does not depend on the time of treatment. It was found that only during treatment with balls of 2 mm diameter, the corrosion resistance of specimens hardened applying SMG in NaCl solution negligibly exceeds the strength of unhardened specimens.

In the work [13] the results of experimental investigations of efficiency of application of quartz shot blasting (in fact sandblasting) and polishing to improve the corrosion resistance of specimens of stainless steel AISI316LVM, widely used in medicine, are presented. It is shown that a higher corrosion resistance is in the specimens after polishing and passivation of the surface during 60 min holding in 20 % solution of NHO_3. It was found that, despite the maximum roughness, the corrosion resistance of specimens after quartz shot blasting during 120 s and the subsequent passivation of the surface is almost not inferior to the specimens after polishing and passivation. High roughness and corrosion resistance make this treatment promising for using in medicine to improve the corrosion resistance of implants of steel AISI316LVM.

In the works [14, 15] the influence of plastic deformation (pressure treatment) on corrosion resistance of stainless steels was investigated. It was established that with increase in the deformation degree (reduction in thickness) of the rolled products from 17 to 47 %, the hardness, yield strength and corrosion resistance are increased. The authors of the work [15] showed that during manufacture of pipes according to the conventional technology (hot-rolled products, deformation degree is 68 %), the rate of pitting corro-

sion is 3–4 times higher than after the proposed technology of hardening (cold-rolled metal, deformation degree is 75–78 %). The drawbacks of the standard document ASTM G-48, which regulates the tests on resistance to pitting corrosion at the temperature of 40 °C, were mentioned. It is shown that increase in temperature from 40 to 50 °C increases the rate of corrosion by hundreds of times. It is noted that the subsequent sand blasting does not lead to change in mechanical properties, but it significantly reduces the corrosion resistance of the material due to increase in roughness of the surface.

In the work [16], the efficiency of the fusion of steel AISI304L surface using nanopulsed laser was investigated. It was established that this treatment leads to increase in surface roughness (due to spatter of molten metal from pulsating laser), formation of an oxide film with high chromium content, the replacement of martensite with δ-iron and stretching of grains towards the treatment surface. The abovementioned changes in the surface layer of metal contribute to increase in corrosion resistance.

In the work [17], the use of pulsating high power electron beam (PHPEB) was investigated with the aim of increasing the corrosion and wear resistance of steel FV520B (chromium content is 13.0–14.5 %). The parameters of equipment for PHPEB are the following: voltage is 27 kV, maximum current is up to 10 kA, pulse time is 2.5 μs. It is shown that with increase in the number of pulses from 1 to 25, the average grain size in the surface layer of metal does not exceed 2 μm, but the thickness of this layer is only 4 μm. After treatment by 25 pulses, the corrosion rate decreases significantly, and the wear resistance three times increases.

Improvement of corrosion resistance and resistance to corrosion fatigue of welded joints of metal structures applying SPD methods. The application of sufficiently new SPD methods (high-power pulsed electron beam and surface fusion using nanopulsed laser) for treatment of welded joints of engineering metal structures is not possible at this stage of their development. During hardening of the structures, the preference is given to the SPD methods, which allow performing treatment of welded elements of a complex geometric shape, treatment of longitudinal welds, as well as site welds in the field conditions. The most effective among them are the methods which provide the maximum reduction in stress concentration at the transition from the weld metal to the base metal, the substantial relaxation of residual welding tensile stresses and inducing the residual compressive stresses: grinding, ST, treatment with pneumatic hammer and UIT.

In the works [18, 19], the experimental data are presented on increase in the characteristics of fatigue resistance of welded joints applying grinding the fusion line in the air and under water, respectively. The authors of the work [18] established that grinding of the fusion line increases the limit of endurance margin of welded joints of stainless steels on the basis of 10^7 cycles of stress changes by 109 % (from 110 to 230 MPa) and by 63 % (from 86 to 140 MPa), respectively, in air and in 3 % solution of NaCl. Moreover, the cyclic life of welded joints increases in air by up to 50 times, and by up to 10 times in the corrosive environment. In the work [19] it was shown that the limit of endurance margin of welded joints of low-alloyed steel on the basis of $2 \cdot 10^6$ cycles of stress changes is increased by 20 % after grinding of the fusion line, by 35 % after UIT, and by 61 % after grinding with subsequent UIT. It is noted that the level of induced residual compressive stresses after UIT is 3 times higher than after grinding.

In the works [20, 21] the efficiency of applying ST to increase the resistance of butt welded joints of stainless steels to pitting corrosion and stress corrosion cracking, respectively, is considered. In the work [20], the welded joints were produced both by the electric arc welding (EAW), as well as by the laser welding (LW). The tests on corrosion resistance were carried out in the salt fog chamber (5 % NaCl solution) with a periodic inspection after 24, 48, 72, 120, 240, 480, 720 and 1000 hours. It is shown that in the joints produced by EAW, the pitting corrosion occurs most intensively in the heat-affected zone (HAZ), the depth of pittings reaches 20–40 μm. After ST hardening, the depth of pittings does not exceed 5–10 μm. In the joints produced by LW, the pittings were formed along the fusion line, reaching 30 μm in depth. After application of ST, the pittings were not revealed even at 1000 h of exposure in 5 % solution of NaCl, i.e. the complete protection against corrosion (R_p10) was achieved in accordance with PN-EN ISO 10289:2002. In the work [21], the resistance to stress corrosion cracking of specimens produced by plasma welding was evaluated according to the corrosion susceptibility coefficient of welded joints on the basis of comparing the areas of diagrams of specimens tension (by the value of the spent work) in the air and in 3.5 % solution of NaCl. It was established that the highest resistance is in welded joints after shot blasting at the air pressure of 0.4 MPa. It is shown that with decrease or increase in air pressure, the corrosion resistance of the joints deteriorates.

In the work [22] it is proposed to increase the characteristics of resistance to corrosion fatigue of welded T-joints of steel 12Kh18N10T using a pneumatic

hammer with a ball-pin hardener (BPH). It was established that in hardening of weld and HAZ of up to 15 mm width, the limit of endurance margin of welded joints on the basis of 10^7 cycles of stress changes is increased by 25 and 27 %, respectively, in air and in the synthetic sea water. It is shown that sea water reduces the limit of endurance margin of welded joints based on 10^7 cycles as compared to the air tests by 16.7 and 15.3 %, respectively, in the initial and hardened states (Figure 2).

In foreign and domestic papers of the recent years, the influence of UIT on corrosion resistance and corrosion fatigue of welded joints is ever increasingly investigated [19, 23–27]. At first, this is connected with the fact that within many years of investigations the basic regularities of improvement of the fatigue characteristics of welded joints in air (without influence of corrosive environment) depending on the strength class of steel, type of welded joint, characteristics of the loading cycle, etc. applying the UIT technology [28–35] have been already established. Secondly, this is facilitated by the compactness and mobility of equipment, environmental cleanness of the technological process of treatment (as compared to grinding, sandblasting and shot blasting), ability to perform hardening of welded joints in any spatial positions, in the field conditions and in some cases under water as well [19].

Thus, in the work [23], the results of fatigue tests of pipe steel welded joints in air and in corrosive environment (10 % solution of NaCl + 10^{-3}–10^{-2} M $Na_2S_2O_3$) in the initial state and after UIT are given. It is shown that as a result of UIT, the radius of transition from weld to HAZ is increased by 1550 %, the angle of weld inclination is reduced by 50 %, the microhardness is increased by 33 %, the structure is refined, the level of residual welding tensile stresses is reduced. In the corrosive environment these factors contribute to twice increase in the cyclic life of welded joints.

In the work [24] the efficiency of application of UIT and laser treatment was evaluated to improve the resistance of corrosion fatigue of butt welded joints of steel 15G2FB. To UIT hardening the fusion line and HAZ of 10–15 mm width were subjected. It is shown that sea water reduces the limit of endurance margin based on $2 \cdot 10^7$ cycles of stress changes of welded joints in the initial state by 42.8 %, and in the hardened state — by 41.2 %. It was established that the limit of endurance margin of welded joints based on $2 \cdot 10^7$ cycles of stress changes as a result of UIT in air is increased by 20 % (from 140 to 170 MPa), and in synthetic sea water by 25 % (from 80 to 100 MPa). The laser treatment did not lead to increase in characteristics of fatigue resistance of welded joints. It is noted that fracture of the hardened UIT specimens in sea water occurred far from the fusion line.

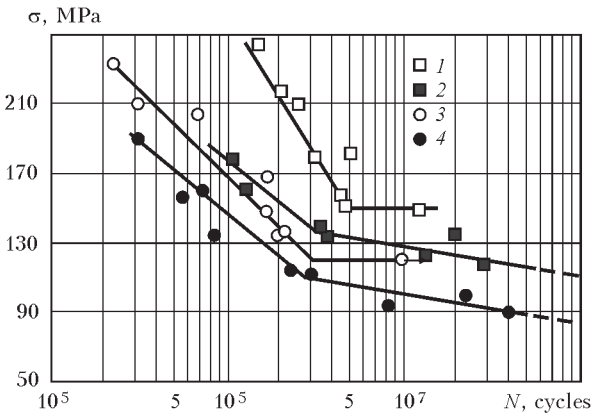

Figure 2. Fatigue curves of welded T-joints of steel 12Kh18N10T: *1, 2* — after applying BPH in air and in synthetic sea water, respectively; *3, 4* — in initial state after welding in air and in synthetic sea water, respectively [22]

In the work [25] the possibility of applying UIT to improve the characteristics of fatigue resistance, microhardness and corrosion resistance of specimens of butt welded joints of stainless steel 304 were investigated. It was established that the limit of endurance margin of butt welded joints based on of $4 \cdot 10^5$ cycles as a result of UIT, is increased by 29 % (from 225 to 290 MPa). In this case, the depth of the plastically deformed metal layer (visible change in the grain structure) does not exceed 100 μm. It is shown that hardening by UIT twice increases the hardness of the metal of the fusion line. It was established that corrosion resistance in solution of 3.5 % NaCl of the welded joints, hardened applying UIT, is higher than that of unhardened joints and it is at the base metal level. The corrosion rate of the joints, hardened applying UIT, (0.0033–0.0061 mm/year) is at the level of the base metal (0.0038 mm/year), which is significantly lower than the corrosion rate of welded joints in the initial state (0. 0118–0.0323 mm/year).

In the work [26], the efficiency of hardening of transverse welds of 127 mm diameter pipes of low-alloyed steel A106-B operating in the range of temperatures of 25–300 °C, applying UIT, was investigated [26].

It is shown that as a result of UIT, the microhardness of the fusion line metal was increased by 24 %, the residual welding tensile stresses decreased by 66 % and the corrosion rate in the 10 % solution of NaCl + 10^{-3}–10^{-2} M $Na_2S_2O_3$ decreased by 46 %. Reduction in the corrosion rate of the fusion line metal after UIT as compared to the base metal and weld metal is associated with the bainitic structure, improvement of grains and reduction of residual welding stresses. The increase in the cyclic life of specimens cutout from the preliminary hardened pipe was not observed. This

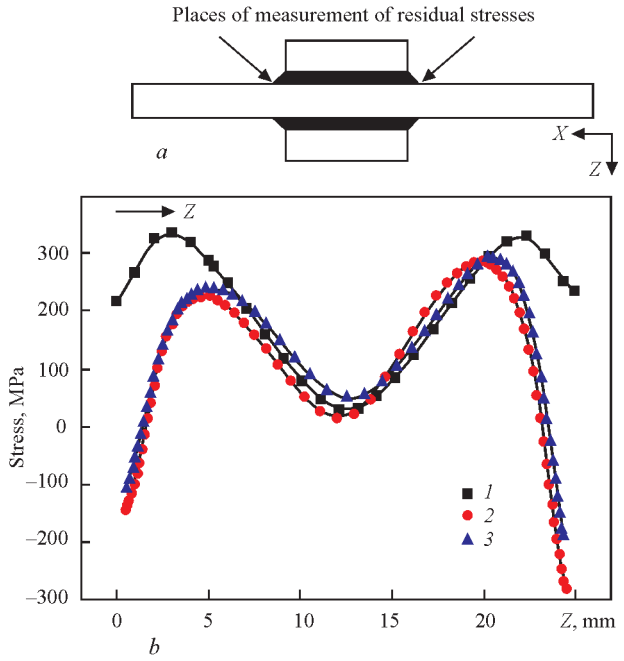

Figure 3. Schematics of measuring points (*a*) and diagrams of distribution of residual stresses in thickness (*b*) in welded specimen with longitudinal stiffeners welded-on on both sides: *1* — in initial state after welding; *2* — after UIT and holding in corrosion environment [36]

is connected with the hardening of welded joint only on one (outer) side of the pipe and redistribution of stresses as a result of cutting.

In the work [27] the results of tests of T-welded joints of low-alloyed steel 10KhSND (σ_y = 390 MPa) in air and in corrosive environment (3 % solution of NaCl) in the initial state after welding and after hardening applying UIT are given. It was established that the corrosive environment reduces the limit of endurance margin based on $2 \cdot 10^6$ cycles of stress changes of welded joints in the initial state by 15 % (from 124 to 10^5 MPa), and by 29 % (from 260 to 185 MPa in the hardened state applying UIT). It is shown that the application of HMP is expedient, since it increases the limit of the endurance margin of welded joints in 3 % solution of NaCl by 76 % (from 105 to 185 MPa) and increases the cyclic life by 3.5 times. It is noted that fracture of hardened specimens applying UIT in the corrosive environment occurs along the base metal far from fusion line.

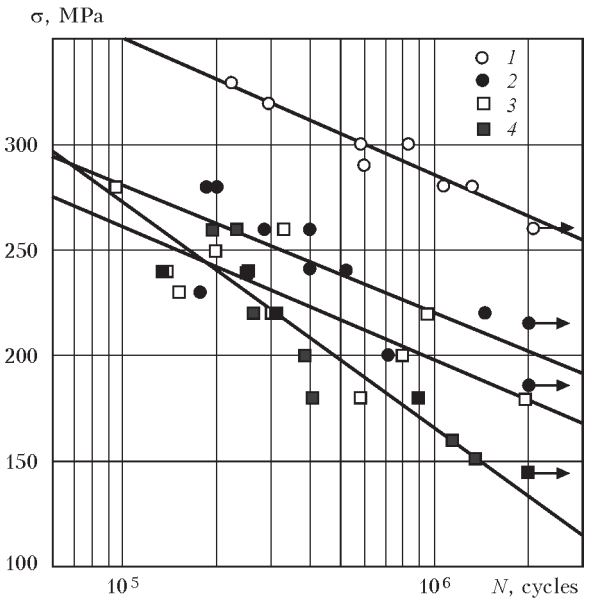

Figure 4. Fatigue curves welded T-joints of steel 15KhSND: *1, 3* — in states hardened and unhardened by HMP in air, respectively; *2, 4* — in states hardened and unhardened by HMP after effect of neutral salt fog during 1200 h, respectively [37]

All the literature data on efficiency of hardening welded joints by applying SPD (including UIT) methods considered above, which are susceptible to influence of corrosive environment, are associated with the experimental determination of corrosion fatigue characteristics of joints during their hardening in the as-welded state. It should be noted that during tests on corrosion fatigue in the solutions of NaCl, the time of staying welded specimens in the corrosive environment was from 10 to 200 hours. The works are being appeared devoted to long-term effect of aggressive environment on the state of plastically-deformed metal layer of welded joints hardened applying UIT, and, therefore, on the level of the induced residual compressive stresses and fatigue resistance characteristics [36, 37].

In the work [36], the residual stress fields of welded joints in the initial state, after hardening applying UIT and after hardening applying UIT followed by holding in the corrosive environment were investigated. The specimens of welded joints were manufactured of shipbuilding steel DH36 by its welding-in to the 25 mm thick plate on both sides of longitudinal stiffeners of 15 mm thickness. The holding of specimens in the corrosive environment (in synthetic sea water) was equivalent to 7.5 years of the structure service. The measurement of residual stresses in the surface layer of metal was carried out by X-ray and neutron non-destructive methods as well as by measuring the displacements after cutting the specimens by electroerosion method. It was established that application of UIT technology leads to inducing of residual compressive stresses in the near-surface layer of metal to the depth of more than 1 mm. It is shown that during holding in the corrosive environment, the corrosion-mechanical losses of surface layer of the specimen metal occurs. While comparing the weld metal to the base metal, the minimum losses (up to 1 mm) after holding in the corrosive environment along the hardened fusion line were recorded. It was established that despite the significant reduction in the maximum level of induced compressive stresses on the surface,

due to the partial loss of the hardened metal layer, they were almost unchanged in depth (Figure 3).

In the work [37] the influence of long-term action of the corrosive environment on the efficiency of improvement of characteristics of the fatigue resistance of welded joints of steel 15KhSND applying UIT was investigated. It was shown that in holding of welded joints, hardened applying UIT technologies, in the chamber of neutral salt fog during 1200 hours leads to formation of complex corrosion damages in the plastically deformed layer of metal: caverns transforming into pittings and corrosion cracks passing into caverns. It was found that in spite of partial damage to the hardened metal layer, the cyclic life of the joints is increased by 2–5 times depending on the levels of applied stresses, and the limit of endurance margin on the base of $2 \cdot 10^6$ cycles of stress changes is increased by 48 % (Figure 4). The fracture of specimens, hardened applying UIT, occurs along the base metal far from the weld and HAZ.

It is important to note that in this research direction there are no works devoted to the problems of establishing the efficiency of application of SPD methods to the in-service metal structures, the welded elements of which have a certain level of corrosion-fatigue damages.

Conclusions

1. The experimental investigations of the recent years are devoted mainly to the establishment of efficiency of application of both conventional (shot blasting, pressure treatment, etc.) as well as rather new methods of surface plastic deformation of metal (pulsating high power electron beam, fusion of surface using nanopulsed laser) to increase the corrosion fatigue resistance and corrosion resistance of base metal and welded joints.

2. Almost all the SPD methods (except of grinding) increase the roughness of the treated surface and, consequently, the effective surface area, which facilitates the increase in the corrosion rate of the metal. To increase the corrosion resistance of the surface layer of metal hardened by SPD methods, resulting in increase of surface roughness, it is advisable to apply additional measures for passivation of the surface (deposition of a thin hydroxyapatite film, nitriding, grinding to a depth of 10–15 μm, holding in 20 % solution NHO_3, etc.).

3. The SPD methods contribute to an increase in the corrosion resistance of welded joints, which is initially lower than the base metal, following the change in the structure of the surface layer metal and the substantial relaxation of the residual tensile stresses (or inducing the residual compressive stresses). For the treatment of welded metal structures, ultrasonic impact treatment (UIT) is the most promising due to the compactness and mobility of the equipment, the good ecology of technological process, high efficiency, ability of hardening the welded joints in any spatial positions in the field conditions.

4. Hardening of welded joints of stainless steels applying UIT technology, in addition to grinding the structure of the metal to nanosizes, increasing hardness and wear resistance, leads to formation of oxide film with an increased chromium content on the surface. Hardening of stainless steels specimens should be performed after preliminary determination of optimal technological parameters, since the amount of martensite increases with the treatment time increase (correspondingly, the galvanic effect between austenite and martensite increases), which leads to a decrease in corrosion resistance.

5. The corrosive environment reduces the efficiency of hardening the welded joints applying SPD methods to improve the resistance to fatigue as compared with the air tests. However, the application of SPD methods is reasonable, since it allows a significant increase in the cyclic life and the limit of endurance margin of welded joints under the influence of corrosive environment as compared to the unhardened joints.

6. At the long-time effect of corrosive environments on welded joints, hardened by SPD methods, a partial corrosion-mechanical and mechanical losses of the plastic deformed surface layer of metal, the formation of defects in the form of caverns, pittings, etc., occur. This leads to a significant decrease in the maximum level of induced compressive stresses on the surface, but in depth they practically do not change. At the same time, the characteristics of the fatigue resistance of welded joints with the damaged hardened metal layer remain higher than in the initial state.

7. There are no works devoted to the problems of establishing the efficiency of application of SPD methods to the in-service metal structures, the welded elements of which have a certain level of fatigue and corrosion damages.

1. Chaevsky, M.I., Shatinsky, V.F. (1970) *Increase of serviceability of steels in aggressive media under cyclic loading*. Kiev: Naukova Dumka.
2. Pokhmursky, V.I. (1974) *Corrosion-fatigue strength of steels and methods of its improvement*. Kiev: Ibid.
3. (1982) Corrosion fatigue of metals. In: *Proc. of 1st Soviet-Engl. Seminar*. Ed. by Ya.M. Korotyrkin. Kiev: Ibid.
4. Pokhmursky, V.I., Khoma, M.S. (2008) *Corrosion fatigue of metals and alloys*. Lviv: SPOLOM.
5. Chausov, M. et al. (2016) Enhancing plasticity of high-strength titanium alloys VT22 under impact-oscillatory loading. *Philosophical Magazine*, Vol. 97, 389–399.

6. Aymen, A. Ahmed et al. (2014) Effect of surface and bulk plastic deformations on the corrosion resistance and corrosion fatigue performance of AISI316L. *Surface & Coating Technology*, Vol. 259, 448–455.
7. Hashemi, B., Rezaee, M., Yazdi, Azar V. (2011) The wear and corrosion resistance of shot peened-nitrided 316L austenitic stainless steel. *Materials & Design*, **32**, 3287–3292.
8. Aymen, A. Ahmed et al. (2015) Effect of shot peening parameters and hydroxyapatite coating on surface properties and corrosion behavior of medical grade AISI316L stainless steel. *Surface & Coating Technology*, Vol. 280, 347–358.
9. Hang-sang Lee et al. (2009) Influence of peening on the corrosion properties of AISI304 stainless steel. *Corrosion Sci.*, Vol. 51, 2826–2830.
10. Mordyuk, B.N. et al. (2007) Effect of structure evolution induced by ultrasonic peening on the corrosion behavior of AISI321 stainless steel. *Mater. Sci. and Engineering A*, Vol. 458, 253–261.
11. Dong, Z. et al. (2015) Effect of ultrasonic impact peening on the corrosion of ferritic-martensitic steels in supercritical water. *J. of Nuclear Materials*, **457**, 266–272.
12. Balusamy, T. et al. (2013) Influence of surface mechanical attrition treatment (SMAT) on the corrosion behavior of AISI304 stainless steel. *Corrosion Sci.*, Vol. 74, 332–344.
13. Pereda, M.D. et al. (2012) Impact of surface treatment on the corrosion resistance of ASTM F138-F139 stainless steel for biomedical applications. *Procedia Materials Sci.*, Vol. 1, 446–453.
14. Suyitno, Arifvianto, B., Widolo, T.D. et al. (2012) Effect of cold working and sandblasting on the microhardness, tensile strength and corrosion resistance of AISI316L stainless steel. *Int. J. of Minerals, Metallurgy and Materials*, 19(**12**), 1093–1099.
15. Shepel, G.G. et al. (2009) Improving the corrosion resistance and reliability of austenitic and austenitic-ferritic steel pipe. *Steel in Translation*, Vol. 39, 1107–1110.
16. Pacquentin, W., Caron, N., Oltra, R. (2015) Effect of microstructure and chemical composition on localized corrosion resistance of a AISI304L stainless steel after nanopulsed-laser surface melting. *Appl. Surface Sci.*, Vol. 356, 561–573.
17. Hao, S. et al. (2015) Improving corrosion and wear resistance of FV520B steel by high current pulsed electron beam surface treatment. *Nuclear Instruments and Methods in Physics Research B: Beam Interactions with Materials and Atoms*, Vol. 356–357, 12–16.
18. Baptista, R., Infante, V., Branco, C.M. (2008) Study of the behavior in welded joints of stainless steels treated by weld toe grinding and subjected to salt water corrosion. *Int. J. of Fatigue*, Vol. 30, 453–462.
19. *Wenbin Gao* et al. (2015) Enhancement of the fatigue strength of underwater wet welds by grinding and ultrasonic impact treatment. *J. of Materials Processing Technology*, Vol. 223, 305–312.
20. Nasilowska, B., Bogdanowicz, Z., Wojucki, M. (2015) Shot peening effect on 904 L welds corrosion resistance. *J. of Construct. Steel Research*, Vol. 115, 276–282.
21. Zhiming, L. et al. (2015) Effect of high energy shot peening pressure on the stress corrosion cracking of the weld joint of 304 austenitic stainless steel. *Materials Science and Engineering: A*, Vol. 637, 170–174.
22. Kolomijtsev, E.V. (2012) Corrosion-fatigue strength of 12Kh18N10T steel T-joints and methods of its improvement. *The Paton Welding J.*, **12**, 36–38.
23. Daavari, M., Sadough Vanini, S.A. (2015) Corrosion fatigue enhancement of welded steel pipes by ultrasonic impact treatment. *Materials Letters*, Vol. 139, 462–466.
24. Kolomijtsev, E.V., Serenko, A.N. (1990) Effect of ultrasonic and laser treatment on fatigue resistance of butt welded joints in air and corrosion media. *Avtomatich. Svarka*, **11**, 13–15.
25. Abdulah, A., Malaki, M., Eskandari, A. (2012) Strength enhancement of the welded structures by ultrasonic peening. *Materials & Design*, Vol. 38, 7–18.
26. Daavari, M., Sadough Vanini, S.A. (2015) The effect of ultrasonic peening on service life of the butt-welded high-temperature steel pipes. *J. Mater. Eng. and Performance*, Vol. 24, 3658–3665.
27. Knysh, V.V., Valteris, I.I., Kuzmenko, A.Z. et al. (2008) Corrosion fatigue resistance of welded joints strengthened by high-frequency mechanical peening. *The Paton Welding J.*, **4**, 2–4.
28. Zhao, X., Wang, D., Huo, L. (2011) Analysis of the S-N curves of welded joints enhanced by ultrasonic peening treatment. *Materials & Design*, 32(**1**), 88–96.
29. Abston, S. (2010) The technology and applications of ultrasonic impact technology. *Austral. Welding J.*, Vol. 55, 20–21.
30. Yin, D. et al. (2010) The effects of ultrasonic peening treatment on the ultra-long life fatigue behavior of welded joints. *Materials & Design*, 31(**7**), 3299–3307.
31. Marquis, G. (2010) Failure modes and fatigue strength of improved HSS welds. *Engineering Fracture Mechanics*, Vol. 77, 2051–2062.
32. Wang, T. et al. (2009) Discussion on fatigue design of welded joints enhanced by ultrasonic peening treatment (UPT). *Int. J. of Fatigue*, 31(**4**), 644–650.
33. Kudryavtsev, Y. et al. (2007) Rehabilitation and repair of welded elements and structures by ultrasonic peening. *Welding in the World*, 51(**7/8**), 47–53.
34. Kuhlmann, U. et al. (2005) Verlaengerung der lebensdauer von Schweisskonstruktion aus hoeher festen baustaehlen durch Anwendung der UIT-technologie. *Schweissen und Schneiden*, 57(**8**), 384–391.
35. Yang, X., Ling, X., Zhou, J. (2014) Optimization of the fatigue resistance of AISI304 stainless steel by ultrasonic impact treatment. *Int. J. of Fatigue*, 61(**4**), 28–38.
36. Ahmad, B., Fitzpatrick, M.E. (2015) Effect of ultrasonic peening and accelerated corrosion exposure on residual stress distribution in welded marine steel. *Metallurg. and Mater. Transact. A*, Vol. 46, 1214–1226.
37. Knysh, V.V., Solovej, S.A., Nyrkova, L.I. et al. (2016) Influence of corrosion damage on cyclic fatigue life of tee welded joints treated by high-frequency mechanical peening. *The Paton Welding J.*, **9**, 42–46.

Received 01.02.2017

doi.org/10.15407/tpwj2017.03.08

FORWARD INVERTER SOURCE WITH INCREASED POWER FACTOR

V.V. BURLAKA, S.V. GULAKOV and **S.K. PODNEBENNAYA**
Pryazovskyi State Technical University
7 Universitetskaya Str., 875000, Mariupol, Ukraine. E-mail: office@pstu.edu

A paper proposes a circuit design of single-phase forward inverter source with increased power factor. A peculiarity of the source is absence of additional power inductive components, reduced capacity of storage capacitor in direct current circuit and simplified limit circuit of its charging current. The source has increased open circuit voltage, which does not depend on mains voltage and allows providing easier arc ignition in manual arc welding. Current consumed from mains is 30–45 % lower than in «classical» inverter sources without power factor corrector due to increased power factor. 11 Ref., 1 Figure.

Keywords: *power factor, welding, welding inverter, source, arc ignition, arc burning stabilizing, open circuit voltage*

Inverter sources have gained wide distribution for solution of the problems of automatic and manual arc welding, plasma cutting, plasma and electric arc spraying as well as concurrent processes. At that inverter sources for manual and semi-automatic welding acquired the widest distribution. They provide due to their mass and dimension parameters, ease of work, high mobility of welder and possibility of formation of special type output VAC and their regulation in welding for ensuring optimum conditions of electrode metal transfer and decrease of spattering.

Sources for welding and related processes, widely applying electric arc, are nonlinear loads, i.e. generators of mains current higher harmonics. Work of such equipment in electric mains can result in the problems of electromagnetic compatibility with other technical means.

It should be noted that development of inverter welding sources is aimed at obtaining of high specific power, high efficiency, flexible formation of output VAC etc., but electromagnetic compatibility of source with mains is of extremely low attention. The electromagnetic compatibility implies a harmonic factor and consumption current unbalance factor (for three-phase sources), power factor (calculated in accordance with IEEE1459-2010 standard), level of high-frequency noises and etc. It is not quite correct to refer welding sources to energy-saving equipment [1–7] due to high harmonic factor in consumption current and on data of [8] electric welding equipment makes 65 % of potential sources of electromagnetic noises.

High-frequency energy conversion [9] is used for efficiency increase and improvement of mass and dimension parameters of welding sources. It results in decrease of weight and dimensions of source (up to 70 % according to [10]), reduction of energy losses in source, increase of performance and rise of range of output parameters regulation. Regardless obvious advantages of the inverter sources on weight and dimension characteristics and efficiency, developers do not pay enough attention to problems of increase of their power factor. Thus, testing of single-phase inverter source SELMA ARC-160 at consumption power 1.1 and 3 kW showed that its power factor varies from 0.652 (1.1 kW) to 0.702 (3 kW) and cosφ on the first harmonic makes from 0.992 (1.1 kW) to 0.998 (3kW).

Low power factor in inverter sourses is explained by high content of the harmonics in consumption current (harmonic factor is more than 100 %). This results in rise of energy losses in mains (these losses to a first approximation depend on square of true power factor) and distortion of mains voltage form. Appearance of voltage surges in mains is also possible due to resonances on higher harmonic frequencies at welding source operation, moreover voltage amplitude can reach 800 V [11].

High harmonic factor of consumption current of considered inverter welding source is explained by design of its power part, namely scheme of alternating to direct voltage converter. In SELMA ARC-160 source such a converter is a single-phase diode bridge with smoothing high-capacity capacitor (around 2000 μF) at the output. Besides, it is known fact, that electrolytic capacitors, especially operating under heavy conditions (increased current and temperature), have limited service life and require periodic replacement due to

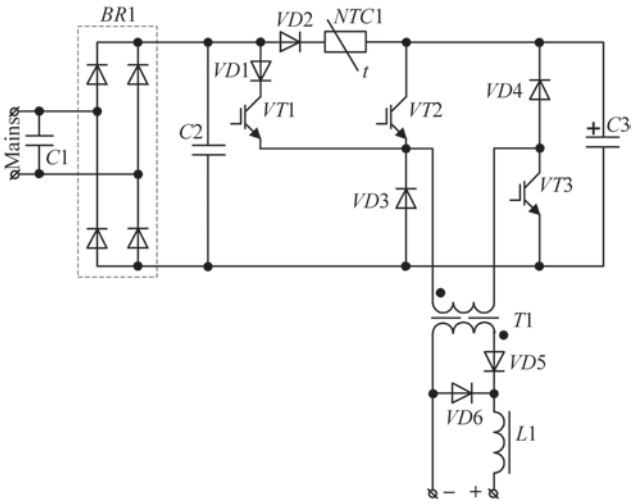

Scheme of power part of developed welding source

capacity loss and growth of internal resistance. This fact somewhat reduces reliability of inverter welding sources, power circuits of which have capacitor storages of large energy intensity.

Most of currently manufactured inverter welding sources do not have adjustment of power factor and do not satisfy standard requirements on electromagnetic compatibility of technical means (DSTU IEC 61000-3-2:2004, DSTU EN 61000-3-12:2014) in the whole possible range of working modes.

Authors developed an inverter welding source with increased power factor. The source is made based on forward converter, in which magnetization and demagnetization circuits of transformer are split and one power key is added. A circuit of power part of the source is given in the Figure.

*VT*2, *VD*3, *VT*3, *VD*4, *C*3, *T*1, *VD*5, *VD*6 and *L*1 elements form classical forward converter. Capacitor *C*3 has relatively small capacity, which allowed limitating its charging current when switching on the source using single thermistor NTC1. Mains voltage is rectified with input rectifier, formed by diode bridge *BR*1. Blocking capacitors *C*1 and *C*2 loose entry of high-frequency noises in the mains.

The peculiarity of developed source is *VD*1, *VT*1 and *VD*2 elements introduced in the circuit. Presence of *VT*1 key allows supplying rectified, but not smoothed mains voltage on power transformer primary winding. Diode *VD*2, at that, prevents discharge of storage capacitor *C*3 on T1 winding. Diode *VD*1 protects transistor *VT*1 from backward voltage at open *VT*2. Such design of power part allows limited control of shape of current consumed from the mains.

The source operates in the following way. The basic power keys are *VT*1 and *VT*3, they are synchronously regulated. Forward running of the source is started at their simultaneous opening.

If rectified mains voltage at bridge BR1 output is enough for load current keeping, then a control system sets forward running pulse duration in such a way as to provide average (for key switching period) mains consumption current proportional to rectified mains voltage. This guarantees significant increase of source power factor.

If voltage on BR1 bridge output is not enough for load current keeping, then key *VT*2 is opened and voltage from storage capacitor *C*3 is supplied on primary winding *T*1 (on *C*3–*VT*2–*T*1–*VT*3–*C*3 circuit). Since this voltage virtually equals the amplitude of mains voltage, it is enough for load charging, i.e. welding arc. Thus, at small absolute value of mains voltage the source comes in a mode of pilot arc maintaining due to energy stored in *C*3.

Backward running of the source is started from the moment of closure of all power keys (*VT*1–*VT*3). Energy, accumulated in a magnetic field of T1 transformer, is discharged into storage capacitor C3. Current, at that, passes on *T*1–*VD*4–*C*3–*VD*3–*T*1 circuit. Diode *VD*5 is closed in the secondary circuit, load current (current of choke *L*1) is locked via *VD*6.

Voltage of capacitor *C*3 can be stabilized at a level not lower that mains voltage amplitude due to discharge of *T*1 field energy into it. This allows stabilizing source open-circuit voltage and makes it independent on mains voltage.

Besides, since demagnetization (backward running) of the transformer takes place at increased voltage (on capacitor *C*3) and forward running occurs at lower voltage (rectified mains voltage), there is a possibility of converter work with relative pulse duration more than 0,5, i.e. duration of forward running can exceed half of the switching period.

Developed source uses the principle of forward conversion, therefore load power is changed with double mains frequency. However, it does not have critical importance for welding purpose due to thermal inertia of weld pool. Deionization of arc gap at mains voltage zero crossing is prevented due to transfer in a mode of «pilot» arc with small capacity (see above).

Experimental source, designed on given circuit, has power factor not less than 0.9. Thanks to this root-mean-square current consumed from mains is 30–45 % lower than in «classical» inverter sources without power factor corrector.

Application of proposed inverter welding source allows reducing losses of electric energy in a distributing network due to decrease of acting current and rise of quality of mains voltage as a result of reduction of harmonic factor.

1. Korotynsky, A.E. (2002) State-of-the-art, tendencies and prospects of development of high-frequency welding converters (Review). *The Paton Welding J*., **7**, 44.
2. Pentegov, I.V. et al. (2012) Electromagnetic compatibility of electric arc power sources. *Elektrotekhnika i Elektromekhanika*, **3**, 34–40.
3. Rymar, S.V., Zhernosekov, A.M., Sydorets, V.N. (2011) Influence of welding power sources on three-phase mains. *The Paton Welding J*., **10**, 40–45.
4. Lebedev, V.K. (1995) Tendencies of development of arc welding power sources. *Avtomatich. Svarka*, **5**, 3–6.
5. Zaruba, I.I., Andreev, V.V., Stepakhno, V.I. et al. (2011) Ways of increasing the technological efficiency of rectifiers for mechanized welding and surfacing (Review). *The Paton Welding J*., **11**, 37–40.
6. Lebedev, A.V. (2012) Transistor power sources for electric arc welding (Review). *Ibid*., **9**, 30–36.
7. Lebedev, V.K. (2004) Tendencies in development of power sources and control systems (based on materials of US patents). *Ibid*., 1, 37–45.
8. Galperin, V., Kolesnik, D. (2008) Ensuring of electromagnetic compatibility of industrial processing equipment. *Elektrooborudovanie: Ekspluatatsiya i Remont*, **7**, 8–12.
9. Rozanov, Yu.K. (1987) *Semiconductor converters with higher frequency link*. Moscow: Energoatomizdat.
10. Galvery, W.L., Marlow, F.M. (2006) *Welding essentials: Questions & answers*. Industrial Press.
11. Potapievsky, A.G., Saraev, Yu.N., Chinakhov, D.A. (2012) Consumable electrode gas-shielded welding of steels. In: *Engineering and technology of future*. Tomsk: TPU.

Received 19.01.2017

PATON PUBLISHING HOUSE

www.patonpublishinghouse.com

SUBSCRIPTION

«The Paton Welding Journal» is Published Monthly Since 2000 in English, ISSN 0957-798X.

«Avtomaticheskaya Svarka» Journal (Automatic Welding) is Published Monthly Since 1948 in Russian, ISSN 005-111X.

«The Paton Welding Journal» is Cover-to-Cover Translation of Avtomaticheskaya Svarka» Journal into English.

If You are interested in making subscription directly via Editorial Board, fill, please, the coupon and send application by Fax or E-mail.

The cost of annual subscription via Editorial Board is $348 for «The Paton Welding Journal» and $180 for «Avtomaticheskaya Svarka» Journal.

«The Paton Welding Journal» can be also subscribed worldwide from catalogues subscription agency EBSO.

SUBSCRIPTION COUPON

Address for journal delivery _____

_____

Term of subscription since _____ **20** **till** **20** _____

Name, initials _____

Affiliation _____

Position _____

Tel., Fax, E-mail _____

We offer the subscription all issues of the Journal in pdf format, starting from 2009.

The archives for 2009–2014 are free of charge on *www.patonpublishinghouse.com* site.

ADVERTISEMENT

in «Avtomaticheskaya Svarka» and «The Paton Welding Journal»

External cover, fully-colored:
First page of cover (190×190 mm) — $700
Second page of cover (200×290 mm) — $550
Third page of cover (200×290 mm) — $500
Fourth page of cover (200×290 mm) — $600

Internal cover, fully-colored:
First/second/third/fourth page of cover (200×290 mm) — $400

Internal insert:
Fully-colored (200×290 mm) — $340
Fully-colored (double page A3) (400×290 mm) — $500

- Article in the form of advertising is 50 % of the cost of advertising area
- When the sum of advertising contracts exceeds $1001, a flexible system of discounts is envisaged

Size of journal after cutting is 200×290 mm

Editorial Board of Journal «Avtomaticheskaya Svarka» and «The Paton Welding Journal»
E.O. Paton Electric Welding Institute of the NAS of Ukraine
International Association «Welding»
11 Kazimir Malevich Str. (former Bozhenko Str.), 03680, Kiev, Ukraine
Tel.: (38044) 200 60 16, 200 82 77; Fax: (38044) 200 82 77, 200 81 45
E-mail: journal@paton.kiev.ua; www.patonpublishinghouse.com